

Dissertation

zur Erlangung des akademischen Grades eines
Doktors der Naturwissenschaften
der Fakultät für Chemie und Chemische Biologie
der Technischen Universität Dortmund

**Investigation of
Acyl Protein Thioesterase activity
at the membrane**

Vorgelegt von
Kathrin Estel
aus Bochum

1. Gutachter : Prof. Dr. Stefan Raunser
2. Gutachter : Prof. Dr. Andrea Musacchio
Eingereicht am : 21. Dezember 2018

Die vorliegende Arbeit wurde im Zeitraum von November 2014 bis Dezember 2018 in der Abteilung für Mechanistische Zellbiologie des Max-Planck-Instituts für molekulare Physiologie unter der Leitung von Dr. I. Vetter durchgeführt.

Eingereicht am : 21.12.2018

Tag der mündlichen Prüfung : 11.02.2019

Prüfungskommission:

Erstgutachter : Prof. Dr. S. Raunser

Zweitgutachter : Prof. Dr. A. Musacchio

Vorsitzender : Prof. Dr. S. Kast

Ein Hoch auf die Wissenschaft, sie verändert die Welt! (Eleor, MasK and Music Musical 2015)

Contents

List of Figures	VII
List of Tables	IX
List of Abbreviations	X
1 Kurzfassung	XIV
2 Abstract	XVI
3 Introduction	1
3.1 Lipid modification of proteins	1
3.1.1 Protein S-palmitoylation	1
3.2 Small GTPase Ras	2
3.3 Acyl Protein Thioesterase (APT) 1 and 2	5
3.3.1 Acyl Protein Thioesterase 1 and 2 are classified as α, β -Hydrolases	5
3.3.2 General knowledge about Acyl Protein Thioesterases	5
3.3.3 Structural characteristics of human Acyl Protein Thioesterases	8
3.4 The cell cycle and APTs role in this	9
3.4.1 APT's function in asymmetric cell division	9
3.4.2 The Golgi and its disassembly and reassembly during mitosis	12
4 Objectives	13
5 Material and Methods	14
5.1 Materials	14
5.1.1 Buffers	14
5.1.2 Phospholipids and Reagents	14
5.1.3 Kits	15
5.1.4 Enzymes	15
5.1.5 Antibiotics	15
5.1.6 Antibodies	16
5.1.7 Plasmids for mammalian expression	16
5.1.8 Bacterial strains and media	16
5.1.9 Cell lines	17
5.1.10 Software	17
5.1.11 Instruments	18
5.2 Methods	18
5.2.1 Cloning, Expression and Purification of Proteins	18
5.2.1.1 Polymerase Chain Reaction (PCR)	19
5.2.1.2 Determination of DNA concentration	19
5.2.1.3 Transformation of DNA into chemically competent bacteria cells	19

5.2.1.4	Plasmid isolation from bacteria cells	20
5.2.1.5	Agarose gelelectrophoresis	20
5.2.1.6	DNA sequencing	20
5.2.1.7	Protein expression and purification	21
5.2.1.8	SDS-PAGE and coomassie blue staining	22
5.2.1.9	Determination of protein concentration	23
5.2.2	Cell biological methods	23
5.2.2.1	Cell culture and transfections	23
5.2.2.2	Thawing cells	23
5.2.2.3	Freezing cells	23
5.2.2.4	PC12 cell differentiation assay	23
5.2.2.5	Determination of the mitotic index and preparation of mitotic gallery	24
5.2.2.6	Immunofluorescence staining	25
5.2.2.7	Electroporation	25
5.2.3	Vesicle assays	26
5.2.3.1	Preparation of Large Unilamellar Vesicles (LUVs)	26
5.2.3.2	Preparation and imaging of Giant Unilamellar Vesicles (GUVs)	26
5.2.3.3	FRET measurements	27
5.2.3.4	Ambient Stopped-Flow Fluorescence Spectroscopy	27
5.2.4	Electron spray ionization - mass spectrometry (ESI-MS)	28
5.2.4.1	Protein ESI	28
5.2.4.2	Detection of APT activity on palmitoylated substrates	28
5.2.5	Sortase ligation	29
5.2.6	DTNB assay	29
5.2.7	OPTS assay	29
5.2.8	Crystallization	30
6	Results	31
6.1	Development of an assay for physiological APT substrates	31
6.1.1	DTNB assay for colorimetric detection of free thiol groups	31
6.1.2	ESI-MS measurements for physiological APT substrates	39
6.2	A FRET-based system to study the activity of human APTs on a membrane bound substrate	43
6.2.1	Determination of the association and dissociation rate of the palmitoylated N-terminal hAPT1 peptide to model membranes	45
6.2.2	Steady state FRET assay for APT catalytic activity on palmitoylated peptides in DOPC vesicles	51
6.2.2.1	APT activity on the palmitoylated N-terminal APT1-peptide in DOPC vesicles	51
6.2.2.2	APT activity on a palmitoylated H-Ras peptide in DOPC vesicles	55
6.3	Investigation of hAPT's membrane affinity <i>in vitro</i>	58
6.4	Microscope assay to investigate the APT activity on a palmitoylated N-terminal APT1 peptide associated to giant unilamellar vesicles (GUV)	64
6.5	<i>In vitro</i> reconstitution of a mono-palmitoylated H-Ras by a sortase mediated ligation	67
6.6	PC12 cell neuronal differentiation assay to investigate the <i>in vivo</i> activity of new APT inhibitors	69
6.7	<i>In vivo</i> localization of APT	76
6.7.1	Localization of APT in HeLa cells	76
6.7.2	Localization of electroporated hAPTmCherry proteins in HeLa cells	78

6.8	APT's function in mitosis	80
6.8.1	<i>In vivo</i> localization of APT during mitosis	80
6.8.2	Effect of hAPT1/2 inhibition on the mitotic index	81
7	Discussion	84
7.1	Development of an assay for physiological APT substrates	84
7.2	APT's activity on palmitoylated peptides in presence or absence of model membranes	87
7.3	Investigation of APT's membrane affinity <i>in vitro</i> and <i>in vivo</i>	89
7.4	<i>In vivo</i> effects of APT inhibition	90
7.4.1	PC12 cell neuronal differentiation assay to investigate the efficiency of new APT inhibitors	90
7.4.2	The effect of APT inhibition on the mitotic index	91
A	Appendix	93
	Bibliography	97
	Acknowledgments	105
	Affidavit	107

List of Figures

3.1	Activation cycle of Ras.	2
3.2	Ras structure and isoform specific post-translational lipid modifications.	3
3.3	Acylation cycle of Ras.	4
3.4	hAPT1 and hAPT2 crystal structures.	6
3.5	<i>In vivo</i> localization of APT.	7
3.6	Human APT1 structure.	8
3.7	The electrostatic surface of APT1 and predicted membrane insertion of hAPT1.	9
3.8	The cell cycle and its phases.	10
3.9	The different phases of mitosis and cytokinesis.	11
3.10	Disassembly and reassembly of the Golgi during mitosis.	12
5.1	Assembled electroformation chamber.	26
6.1	Two different artificial substrates to measure the thioesterase activity of APT.	31
6.2	Mechanism of the DTNB assay.	32
6.3	Crystal structure of hAPT (green). A fatty acid (blue) from xenopus APT1 is superimposed to indicate the active site and adjacent binding tunnel. Five cysteine residues that can be potentially modified with TNB are shown in purple.	33
6.4	DTNB assay to investigate the activity of hAPT1 on Acetyl-CoA.	33
6.5	Scheme of how DTNB could bind to the cysteine residues of APT.	34
6.6	Masses of hAPT1 after incubation with DTNB.	34
6.7	DTNB concentration and time dependend cysteine modification of hAPT1.	35
6.8	OPTS activity assay of hAPT1 after 15 min incubation with different DTNB concentrations.	36
6.9	Reaction velocities of hAPT1 hydrolysis on OPTS with different DTNB concentrations.	37
6.10	OPTS activity assay of hAPT1 after incubation with different concentrations of DTNB.	38
6.11	Results of the ESI-MS measurements after hAPT1 incubation with DTNB in different concentrations.	38
6.12	Chemical structures of three different physiological substrates of hAPT.	40
6.13	ESI-MS measurements to investigate the activity of human APT isoforms on different substrates.	41
6.14	Chemical structure of the N-terminal APT1 peptide.	44
6.15	Fluorescence spectra of fluoresceine and rhodamine.	44
6.16	Scheme of the FRET-based assay to determine the association and dissociation rate of the APT1 peptide to DOPC vesicles.	46
6.17	Representative association curve of 0.2 μ M hAPT1-peptide to DOPC vesicles.	47
6.18	Association curves of 0.2 μ M FITC-labeled, palmitoylated hAPT1-peptide to rhodamine DOPC vesicles.	47
6.19	Amplitudes of the association curves.	48
6.20	Observed rate constanst of the association curves.	49
6.21	Dissociation curve of FITC labeled hAPT1-peptide localized on rhodamine labeled DOPC to unlabeled DOPC vesicles.	50

6.22	Association and dissociation process of the APT1-peptide to DOPC vesicles.	51
6.23	Measuring the APT activity on vesicle bound palmitoylated peptide.	52
6.24	Stopped-flow measurement indicating the catalytic activity of hAPTs on the vesicle bound APT1-peptide.	53
6.25	Chemical structure of the C-terminal H-Ras peptide.	55
6.26	Measuring the APT activity on vesicle bound palmitoylated H-Ras peptide.	56
6.27	DOPC vesicle with palmitoylated H-Ras peptide.	56
6.28	Prediction of how APT1 could be oriented within the cell membrane.	58
6.29	Scheme of APT binding to the membrane.	59
6.30	Chemical structures of DOPC, DOPG and DOGS-Ni-NTA.	60
6.31	Scheme of GUV electroformation.	60
6.32	Experiment to investigate if hAPT1/hAPT2 can bind to model membranes.	61
6.33	Control experiment to test if APT1 can be anchored to vesicles.	62
6.34	Experiment to investigate if hAPT1 can bind to negatively charged model membranes.	63
6.35	Time series of FITC intensities around DOPC vesicles after addition of hAPT1, hAPT2, and buffer.	65
6.36	Integrated and normalized FITC intensities around the DOPC vesicles.	66
6.37	Mechanism of the <i>in vitro</i> reconstitution of H-Ras by a sortase mediated ligation.	67
6.38	SDS-gel of the <i>in vitro</i> reconstitution of H-Ras by a sortase mediated ligation.	68
6.39	PC12 cell differentiation after stimulation with NGF.	72
6.40	Percentage of differentiated PC12 cells with and without APT inhibitors.	73
6.41	Fluorescent image of PC12 cell differentiation, 48 h after transfection with HRasG12V-mCitrine.	74
6.42	Percentage of PC12 cells with neurite outgrowth after transfection with a plasmid containing the constitutively active HRasG12V, with and without inhibitors.	75
6.43	Localization of hAPT1 in HeLa cells.	77
6.44	Electroporation of APT1/2mCherry proteins into HeLa cells.	79
6.45	Mitotic gallery depicting localization of human APTs during mitosis.	81
6.46	Specific hAPT inhibitors.	82
6.47	Mitotic index after combined hAPT1/2 inhibition.	82
7.1	APT structure with DTNB in the binding pocket.	86
7.2	Scheme how APT depalmitoylates its membrane bound substrates.	88
A.1	Bleaching test of DOPC vesicles labeled with rhodamine-phosphoethanolamine-lipids.	93
A.2	Integrated and normalized rhodamine intensities of the DOPC vesicles.	93
A.3	ML348 and ML349 precipitates in the cell culturing medium.	94
A.4	Electroporation of recombinant APT1mCherry proteins into HeLa cells without a cell compartment marker.	95

List of Tables

5.1	Phospholipids and Reagents.	14
5.2	Kits.	15
5.3	Enzymes.	15
5.4	Antibiotics for bacteria.	15
5.5	Antibiotics for mammalian cells.	15
5.6	Primary antibodies.	16
5.7	Secondary antibodies.	16
5.8	Components of the used media.	17
5.9	Cell lines.	17
5.10	Software.	17
5.11	Instruments.	18
5.12	Standard PCR program for Pfu- or Phusion-polymerase.	19
5.13	Standard PCR program DNA sequencing.	20
6.1	Calculated (apparent) k_{cat} values for hAPT1 and hAPT2 hydrolyzing the APT1-peptide, lyso-PPC and DPPC.	42
6.2	Total amplitudes and observed rate constants for the different DOPC concentrations of the association experiment.	48
6.3	Measured k_{obs} values and calculated (apparent) k_{cat} values for hAPT1 and hAPT2 hydrolyzing the APT1-peptide.	54
6.4	Structures and inhibition constants for non-covalent APT1 and APT2 inhibitors	70
A.1	Crystallographic statistics of the co-crystal structure of hAPT1 and DTNB.	96

List of Abbreviations

A	Absorption
ABPP	Activity-based protein profiling
AcCoA/Acetyl-CoA	Acetyl-CoenzymeA
Akt	Protein kinase B
APT	Acyl protein thioesterase
APS	Ammonium persulfate
Asp	Aspartic acid
Bodipy FL C₁₂	4,4-Difluoro-5,7-Dimethyl-4-Bora-3a,4a-Diaza-s-Indacene-3-Dodecanoic Acid
BSA	Bovine serum albumin
Cdc	Cell division control protein
CHAPS	3-[(3-cholamidopropyl)dimethylammonio]-1-propanesulfonate
CMC	Critical micelle concentration
Cys	Cysteine
Da	Dalton
DiFMUO	6,8-difluoro-4-methylumbelliferyl octanoate
DMSO	Dimethyl sulfoxide
DNA	Deoxyribonucleic acid
dNTP	Deoxynucleotide
DOGS-Ni-NTA	1,2-dioleoyl-sn-glycero-3-[(N-(5-amino-1-carboxypentyl)iminodiacetic-acid)succinyl](nickel-salt)
DOPC	1,2-dioleoyl-sn-glycero-3-phosphocholine
DOPG	1,2-dioleoyl-sn-glycero-3-phospho-(1'-rac-glycerol) sodium salt
DPPC	1,2-dipalmitoyl-sn-glycero-3-phosphocholine
DTE	Dithioerythritol
DTNB	5,5'-dithiobis-(2-nitrobenzoic acid)
EDTA	Ethylenediaminetetraacetic acid
eNOS	Endothelial nitric oxide synthase
ER	Endoplasmic reticulum

ESC	European Screening Centre
ESI-MS	Electrospray ionization mass spectrometry
FITC	Fluorescein isothiocyanate
FKBP12	FK506 binding protein 2
FP	Fluorescence Polarization
FRET	Fluorescence resonance energy transfer
G-proteins	Guanine nucleotide-binding proteins
GAP	GTPase activating protein
GalT	1,4-galactosyltransferase
GEF	Guanine nucleotide exchange factor
GFP	Green fluorescent protein
GDP	Guanosine diphosphate
GSH	Glutathione
GST	Glutathione S-transferase
GTP	Guanosine triphosphate
GUV	Giant unilamellar vesicles
HeLa	Human cell line taken from cervical cancer from Henrietta Lacks
His	Histidine
HPLC	High-performance liquid chromatography
HPTS	8-hydroxypyrene-1,3,6-trisulfonic acid
HVR	Hypervariable region
IPTG	Isopropyl β -D-1-thiogalactopyranoside
ITO	Indium tin oxide
k	Rate
k_{ass}	Association rate
k_{cat}	Turnover number
K_d	Dissociation constant
k_{diss}	Dissociation rate
K_i	Inhibition constant
k_{obs}	Observation rate
λ	Wavelength
LB	Luria-Bertani medium
LC-MS	Liquid chromatography–mass spectrometry

LMV	Large multilamellar vesicles
LUV	Large unilamellar vesicles
LYPLA1/2	Lysophospholipase 1/2
Lyso-PPC	1-palmitoyl-2-hydroxy-sn-glycero-3-phosphocholine
M	Mitosis phase
MAP-kinase	Mitogen-activated protein kinase
MDCK	Madin-Darby Canine Kidney cells
MEK	Mitogen-activated protein kinase kinase
MeOH	Methanol
ML348	N-[2-Chloro-5-(trifluoromethyl)phenyl]-2-[4-(2-furoyl)-1-piperazinyl]acetamide
ML349	(5,5-Dioxo-4H-thieno[4,5-c]thiochromen-2-yl)-[4-(4-methoxyphenyl)piperazin-1-yl]methanone
N-Rh DHPE	N-(lissamine rhodamine B sulfonyl)-1,2-dihexadecanoyl-snglycero-3-phosphoethanolamine triethylammonium salt
NGF	Neuronal growth factor
Ni	Nickel
Ni-NTA	Nickel-Nitrilotriacetic acid
OD	Optical density
OPTS	1-octanoyloxypyrene-3,6,8-trisulfonic acid trisodium salt
PAT	Palmitoyl acyltransferases
PBS	Phosphate-buffered saline
PBST	Phosphate-buffered saline with tween
PC12	Rat pheochromocytoma cells
PCR	Polymerase Chain Reaction
PFA	Paraformaldehyde
PI3K	Phosphatidylinositol 3-kinases
PMSF	Phenylmethylsulfonyl fluoride
pNP	Para-nitrophenol
PPTS	1-palmitoyloxypyrene-3,6,8-trisulfonic acid trisodium salt
Rab	Ras-related protein in brain
Ras	Rat sarcoma
RGS4	Regulator of G protein signaling 4
RO3306	5-(6-Quinolinylmethylene)-2-[(2-thienylmethyl)amino]-4(5H)-thiazolone
S-phase	Synthesis phase

S-palmitoylation	Thioester palmitoylation
SDS	Sodium dodecyl sulfate
Ser	Serine
SNAP-23	Synaptosomal-associated protein 23
TagBFP	Monomeric blue fluorescent protein
TCEP	Tris(2-carboxyethyl)phosphine
TEMED	Tetramethylethylenediamine
TFA	Trifluoroacetic acid
TNB	5-thio-2-nitrobenzoic acid
Tris	Tris(hydroxymethyl)aminomethane
TrkA	Tropomyosin receptor kinase A
U2 OS	Human Bone Osteosarcoma Epithelial Cells

1 Kurzfassung

Die Enzyme Acyl Protein Thioesterase 1 und 2 (APT1 und APT2) spielen eine wichtige Rolle bei der Depalmitoylierung verschiedener Proteine in der Zelle, unter anderem deacylieren sie das Protoonkogen Ras. Damit verhindern sie die fehlerhafte Lokalisierung von Ras an internen Membranen, was die Signalweiterleitung von extraellulären Botenstoffen durch das Ras Protein an der Plasmamembran ermöglicht. Die Repalmitoylierung von Ras erfolgt am Golgi-Apparat. Die Inhibierung von APT kann diesen Zyklus unterbrechen, so dass das von Ras vermittelte Proliferationssignal, z.B. in Krebszellen, unterbrochen werden kann. Somit ist APT ein potentielles Ziel von Anti-Tumor-Medikamenten.

APT selbst kann reversibel an einem N-terminalen Cystein palmitoyliert sein, was eine erhöhte Membranaffinität zur Folge hat. Bis heute ist der Effekt verschiedener Membrantypen auf APT und dessen Substrate sowie der Einfluss der physiologischen Membranumgebung auf die APT-Aktivität unbekannt. Weiterhin ist unklar, ob APT die Substrate aktiv aus der Membran extrahieren kann bzw. direkten Zugriff auf membrangebundene Substrate hat, und/oder ob die Palmitoylierung am N-terminalen Cystein einen Einfluss auf die Effizienz der Substratextraktion oder –depalmitoylierung hat.

Ein Ziel dieser Arbeit war es daher, herauszufinden, ob APT ein membrangebundenes Substrat depalmitoylieren kann und wo dieser Prozess stattfindet (an der Membran oder im Cytosol). Dazu wurde ein FRET-System mit Fluoreszenz-Markern an palmitoylierten Peptiden sowie an Vesikeln am Plattenleser und an der Stopped-Flow etabliert. Als Peptide wurden ein Nonapeptid entsprechend dem N-Terminus von hAPT1 sowie ein längeres Peptid entsprechend dem C-Terminus von H-Ras gewählt. Es wurde gezeigt, dass sowohl hAPT1 als auch hAPT2 beide Vesikel-gebundenen Peptide hydrolysieren können, wobei hAPT2 etwas effizienter als hAPT1 war, und das H-Ras-Peptid etwa schneller gespalten wurde als das hAPT1-Peptid. Dies deutet auf Wechselwirkungen des Ras-Peptids ausserhalb des aktiven Zentrums und des Palmitat-Bindungstunnels hin. Jedoch wurde auch gezeigt, dass APT die Peptide nicht aktiv aus der Membran extrahiert, sondern dass die Dissoziationsrate der palmitoylierten Peptide, zumindest beim hAPT1-Peptid, ratenlimitierend ist. Weiterhin wurde die Membranaffinität von APT in vitro mittels konfokal Mikroskopie an „Giant Unilamellar Vesicles“ (GUVs), die durch Elektroformation erzeugt wurden, sowie in vivo mittels Lokalisationsstudien in HeLa-Zellen mit transfiziertem und elektroporiertem APT Protein untersucht. APTs besitzen prominente hydrophobe Bereiche, die nahelegten, dass APTs in Membranen insertieren können, unabhängig von der Palmitoylierung. In dieser Arbeit konnte gezeigt werden, dass die hydrophoben Bereiche nicht ausreichend zur Membranlokalisierung sind, wohingegen die N-terminale Palmitoylierung essentiell für eine Membran-

bindung in der Zelle ist. In den Zellstudien wurde gezeigt, dass palmitoylierte APT an den Golgi Membranen lokalisiert ist und dass die Zellen in der Lage waren ein rekombinantes elektroporiertes APT Protein zu palmitoylieren.

Für die weitere Untersuchung der Funktion von APTs, insbesondere des Einflusses von potentiellen Helfer-Proteinen wie FKBP12, ist es wichtig, ein palmitoyliertes Ras-Protein von voller Länge zur Verfügung zu haben. In dieser Arbeit konnte ein einfach-palmitoyliertes H-Ras Protein durch Sortase-Ligation eines palmitoylierten Peptids mit einem entsprechen mutieren H-Ras-Konstrukt erfolgreich dargestellt werden.

Die Forschung an APT Inhibitoren wurde intensiviert, nachdem entdeckt wurde, dass die APT-Inhibierung mit dem kovalenten Inhibitor Palmostatin Auswirkungen auf die Lokalisierung und Signalweiterleitung von Ras hat. Ein PC12-Differenzierungsassay, bei dem die Entwicklung von neuronalen Ausläufern von der Signalweiterleitung durch Ras abhängt, wurde verwendet, um die in vivo Effizienz von APT Inhibitoren zu analysieren. Es wurde gezeigt, dass die spezifischen APT1 und APT2 Inhibitoren ML348 und ML349 keinen signifikanten Effekt auf die Differenzierung haben, wohingegen der in einer Kollaboration mit der European Lead Factory (ELF) entwickelte APT2-spezifische Inhibitor ESC1000595 die Differenzierung stark verringert. Das Grundgerüst dieses Inhibitors kann zudem im Gegensatz zum ML349-Inhibitor chemisch modifiziert werden, um die APT2-Bindung und Spezifität zu steigern.

Da wenig über die Lokalisation von APT und dessen Aktivität während der Mitose bekannt ist, wurden Lokalisierungsstudien mit transient transfizierten APTs durchgeführt. In den frühen mitotischen Phasen ist APT zytosolisch verteilt, während es in den späteren Phasen am Flemming-Körper und partiell an der Plasmamembran zu finden ist. Aufgrund der veränderten APT Lokalisierung während der Mitose wurde untersucht, ob eine APT- Inhibierung den mitotischen Index beeinflusst. Tatsächlich hatten Zellen, die mit APT1- und APT2- spezifischen Inhibitoren behandelt wurden, einen höheren mitotischen Index und brauchten dementsprechend länger für das Durchlaufen der Mitose.

Eine weiteres Ziel dieser Arbeit war es, ein Assay zu entwickeln, mit dem die APT-Aktivität auf biologische Substrate untersucht werden kann, da bisher nur Assays für artifizielle Substrate beschrieben sind. Hierfür wurde die Elektrosprayionisation-Massenspektrometrie (ESI-MS) bzw. ein DTNB(5,5'-Dithiobis-2-nitrobenzoesäure)-basiertes Assay verwendet. Mit Hilfe der ESI-MS Methode war es möglich, die Aktivität von APT auf (Lyso-)-Phospholipide sowie auf palmitoylierte Peptide zu untersuchen. Mit dieser Methode konnte gezeigt werden, dass sowohl APT1 als auch APT2 Lyso-Phospholipide und palmitoylierte Peptide hydrolysieren können, wobei die Peptide um 4-5 Größenordnungen effizienter gespalten werden. Das DTNB-Assay ist ein kolorimetrisches Verfahren, welches freie Thiol-Gruppen nachweist. Es stellte sich heraus, dass DTNB in hohen Konzentrationen, die für das Assay nötig sind, an alle fünf Cysteine von APT bindet, und dadurch zur Entfaltung und entsprechend zur Inaktivität führt. Interessanterweise fungiert DTNB in niedrigen Konzentrationen, bei denen APT nicht kovalent modifiziert wird, als kompetitiver Inhibitor mit einem K_i -Wert von 350 nM. Dementsprechend konnte aus dem DTNB-Assay ein neues Inhibitor Gerüst identifiziert werden.

2 Abstract

The enzymes Acyl Protein Thioesterase 1 and 2 (APT1 and APT2) were described to depalmitoylate the proto-oncogen Ras. This depalmitoylation is assumed to prevent mislocalization of Ras on internal membranes, thus ensuring its predominant localization at the plasma membrane, where Ras can translate extracellular signals into cellular responses. Repalmitoylation takes place at the Golgi. Inhibition of APT can disturb the acylation cycle, leading to a weaker Ras mediated proliferation signal in cancer cells, making APT a potential anti-cancer target.

APT itself undergoes a dynamic palmitoylation at an N-terminal cysteine to achieve a steady state membrane localization. To date, the effect of different membrane types on APT and its target proteins as well as the mechanism by which the physiological membrane environment influences APT activity still remains unclear. Furthermore, it also remains unknown if APT can extract and depalmitoylate its palmitoylated target proteins by itself and/ or if APT1/2 palmitoylation at Cys2 has an effect on substrate extraction/depalmitoylation.

One aim of this thesis was the investigation of APT's activity on membrane bound substrates and where this process takes place (at the membrane or in cytosol). Therefore, a FRET approach (in a plate reader and a stopped-flow machine) was used with fluorescently labeled vesicles and fluorescently labeled palmitoylated peptides. It was shown that APT can depalmitoylate vesicle-bound peptides (both a peptide with the sequence of APT's N-terminus and a peptide with the C-terminal sequence of H-Ras), but APT can not actively extract the peptide from the membrane. The kinetic constants of the association and dissociation reaction of the peptides were measured, and apparent k_{cat} values showed that hAPT2 seems to be slightly more active on those substrates compared to hAPT1.

Moreover, the membrane affinity of APT was analyzed *in vitro* via fluorescence confocal microscopy localization studies on giant unilamellar vesicles, and *in vivo* via localization studies of transfected and electroporated APT constructs. It was shown in the literature that APT is recruited to membranes if it is palmitoylated at Cys2, but APT also features prominent hydrophobic patches, that were predicted to confer to membrane affinity. This work revealed that a membrane anchor (palmitoylation at Cys2) is essential for APT to bind to membranes and that the hydrophobic patches are not sufficient for a membrane localization. For those studies giant unilamellar vesicles were prepared with the method of electroformation. In the cell studies it was demonstrated that APT is located with the palmitoylated Cys2 to the Golgi membranes and the cells are able to palmitoylate a recombinant electroporated APT protein.

To further investigate the function of APTs, particularly the influence of potential helper proteins such as FKBP12, it is important to have a full-length palmitoylated Ras protein available. In this work, a mono palmitoylated H-Ras protein could be successfully synthesized by sortase ligation of a palmitoylated peptide to a H-Ras construct.

As mentioned above, the research on APT inhibitors was intensified after discovering that APT inhibition with Palmostatin affects Ras localization and signaling, making APT a potential anti-cancer target. A PC12 differentiation assay, where neuronal outgrowth is dependent on the Ras downstream cascade, was used to analyze the *in vivo* efficiency of APT inhibitors. It was shown that the specific APT1 and APT2 inhibitors, ML348 and ML349, have no significant effect on the differentiation, whereas the novel APT2 specific inhibitor ESC1000595, designed in collaboration with the European Lead Factory (ELF), can significantly reduce the neuronal outgrowth similar to the commonly used MEK inhibitor U0126. In addition ESC1000595 is a modifiable precursor which can be further improved by the addition of functional groups to enhance the APT2 inhibition.

As little is known about the function of APT in mitosis, localization studies with transiently transfected APTs were performed. In early mitotic phases, APT is cytosolically distributed and in the later phases it is located at the midbody and partially to the plasma membrane. Based on the altered localization of APT in mitosis it was further investigated if APT inhibition influences the mitotic index. Indeed the cells treated with APT1 and APT2 specific inhibitors have a higher mitotic index, meaning that the cells have a delayed mitosis, although there are no obvious chromosomal defects.

Several assays are established to monitor APT's activity on artificial substrates. In this thesis one aim was the development of an assay to investigate APT's activity on biological substrates, using either an Electrospray ionization mass spectrometry (ESI-MS) approach or a DTNB (5,5'-dithiobis-(2-nitrobenzoic acid)) assay. With the ESI-MS assay the hydrolyzation activity of APT on phospholipids and on a palmitoylated peptide was analyzed. It was shown that both APT1 and APT2 are able to depalmitoylate lyso-phospholipids, and both are 4-5 orders of magnitude more efficient in cleaving a palmitoylated peptide.

The DTNB assay, is a colorimetric assay, that can detect free thiol groups. No APT activity on Acetyl-CoA could be detected in this assay. It turned out that in high DTNB concentrations (which are required for the assay) it can modify all five APT's cysteines, resulting in an unfolded and therefore inactive APT protein. At low concentrations, DTNB can surprisingly function as a non-covalent inhibitor with a K_i of 350 nM, leading to the inactivation of the enzyme. Thus from the DTNB assay a new inhibitor scaffold was identified.

3 Introduction

3.1 Lipid modification of proteins

It is of great importance that cells are able to communicate with their environment in order to react to external stimuli, however, the lipids of the plasma membrane create a layer around the cells separating it from the external environment. Cellular communication with the extra-cellular environment (e.g. cell signaling and membrane trafficking) and between cellular membrane components depends on proteins that are either secreted into the environment, embedded in cellular membranes, or reversibly associated with membranes [1]. These membrane-associated proteins are predominantly kinases or GTPases that can interact with downstream effectors, leading to an intracellular signaling cascade that can trigger different cellular responses. Among these responses are cellular differentiation or proliferation, membrane trafficking, protein secretion, signal transduction, and, apoptosis [1], [2]. The interaction of these membrane-associated proteins with the membrane are often controlled and regulated by the binding or attachment of lipids to proteins. This can occur via two processes: On the one hand, proteins can specifically bind to certain lipid molecules, ensuring these complexes are recruited to membrane. On the other hand, many proteins are post-translationally modified with lipid molecules. Among these protein lipidations are cysteine prenylation, N-terminal glycine myristoylation, cysteine palmitoylation, and serine and lysine fatty acylation. As a result, these modifications can regulate protein–membrane interactions, protein–protein interactions, protein stability and enzymatic activities [1].

If one of the signaling cascades regulated by the membrane-associated protein becomes dysfunctional (e.g. overexpression or mutation in proteins) this can lead to an uncontrolled cell growth or prevention of apoptosis. Thus, these disorders where these proteins have been mutated or are over-expressed are linked to diseases including cancer. Hence, targeting these malfunctions provides an opportunity for the development of potential anti-cancer therapeutics [2].

3.1.1 Protein S-palmitoylation

An important, reversible posttranslational modification is the cysteine palmitoylation. During cysteine palmitoylation a 16-carbon palmitoyl group is coupled by a thioester bond to a cysteine residue. Proteins are in most instances palmitoylated close to either a transmembrane domain or another membrane targeting post-translational modification such as another prenylated cysteine or myristoylated glycines [1].

Due to the reversibility of the thioester bond formation, the level of palmitoylated proteins can be controlled in the cell without protein destruction, in contrast to the irreversible farnesylation. The regulation of cysteine palmitoylation is conducted by two classes of enzymes: the addition of a palmitate to a protein is implemented by palmitoyltransferases, while depalmitoyltransferases can remove the palmitoyl residues [3]. One prominent small GTPase protein that is regulated by the palmitoyltransferase/ depalmitoyltransferase mechanism is the Ras protein.

3.2 Small GTPase Ras

One of the key proteins in cancer research is the Ras-Protein (Rat sarcoma). Oncogenic mutations in Ras can be found in 20-30 % of all human tumors, making Ras and its pathway a potential target for cancer therapy [4]. As a member of the GTPase family, Ras (21 kDa) officiates as a molecular switch in many signal transduction cascades, cycling between a GDP-bound OFF and a GTP-bound ON state (Figure 3.1). Ras can translate extracellular signals into a variety of cellular responses.

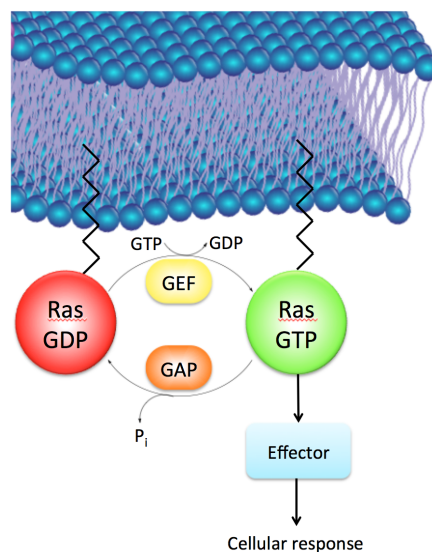


Figure 3.1: Activation cycle of Ras. Ras cycles between a GDP-bound inactive and a GTP-bound active states. The Ras guanine nucleotide exchange factor (GEF) facilitates the dissociation of the bound GDP and replacement by GTP. Active Ras proteins can interact with specific effectors leading to a downstream pathways with cellular responses such as proliferation, differentiation or apoptosis. The Guanosine triphosphate hydrolysis is accelerated by the GTPase activating protein, GAP, allowing a rapid inactivation of Ras.

Activation of Ras itself is regulated by the Ras guanine nucleotide exchange factor (GEF) that facilitates the dissociation of the bound GDP so that it can be replaced by the intracellular GTP that is in excess of GDP [5]. The exchange of GDP to GTP induces a structural change in the protein, whereby an interaction site for the downstream effector proteins is formed [6]. The interaction of active Ras with specific effector proteins leads to a signaling cascade that causes cellular

responses such as proliferation, differentiation, or apoptosis [7]. Although Ras has a slow intrinsic GTPase activity, the hydrolysis of GTP is accelerated by the GTPase activating protein, GAP, allowing for the rapid inactivation of Ras [5]. A single point mutation in Ras at amino acid G12, G13, or Q61 prevents Ras from hydrolyzing GTP. Then, Ras is unable to return to its inactive state and consequently remains in the active conformation, causing uncontrolled cell proliferation in what is known as Ras mediated cancer.

There are four human Ras isoforms, denoted H-Ras, N-Ras, K-Ras4A and K-Ras4B. All Ras proteins have a catalytic G-domain (amino acid: 1-166) that can be divided into an N-terminal effector domain (sequence identity: 100 %) and a C-terminal region (sequence identity: 90 %) [8]. The main sequence difference between the isoforms is in the hypervariable region (HVR) at the C-terminus starting at amino acid 167. The HVR region consist of a linker region and an isoform specific membrane anchor region. The latter is responsible for membrane binding as well as for the isoform specific cellular localization (Figure 3.2) as it is the interaction of this region with different effector proteins that leads to the isoform specific cellular responses [9], [10]. The membrane anchor region of Ras proteins can be posttranslationally lipidated: The cysteine of the C-terminal CAAX box motif can be irreversibly farnesylated by the farnesyltransferase, resulting in a relatively weak membrane affinity. The farnesylated Ras diffuses to the ER where the tripeptide AAX is cleaved and the new C-terminus is methylated. In addition to the farnesylation, H-Ras, N-Ras and K-Ras4A are reversibly palmitoylated at the Golgi, whereas K-Ras4B contains a polybasic region that enhances its membrane affinity for the negatively charged plasma membrane (Figure 3.2). From the Golgi the palmitoylated proteins are transported to the plasma membrane by the secretory pathway [9], [11]. At the plasma membrane Ras can convert extracellular signals into cellular responses, via activating the MAP kinase pathway, which leads to cell proliferation.

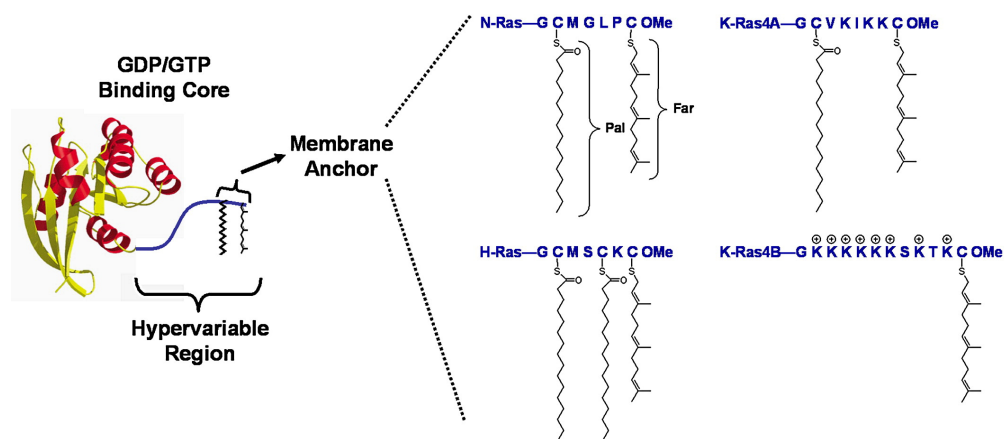


Figure 3.2: Ras structure and isoform specific post-translational lipid modifications. All isoforms share the catalytic G-domain but exhibit differences at the hypervariable region (HVR). All isoforms are farnesylated, and N-Ras and K-Ras4A are additionally palmitoylated at a second cysteine close to the farnesylation site. H-Ras is even palmitoylated twice, whereas K-Ras has an additional polybasic stretch [12].

The reversibility of palmitoylation allows Ras to be spatially regulated via a reaction-diffusion mechanism known as the “acylation cycle” (Figure 3.3 A). This mechanism ensures an enrichment of Ras at the plasma membrane and prevents mislocalizations on other intracellular membranes [13]. In the acylation cycle, H- and N-Ras are palmitoylated at the Golgi by protein-acyl transferases (PATs). The increase of the membrane affinity leads to a trapping of the Ras proteins at the Golgi membranes. From the Golgi, the Ras proteins are transferred to the plasma membrane in vesicles via the secretory transport pathway, resulting in a non-equilibrium enrichment of Ras at the plasma membrane [13]. Due to membrane dynamics like endocytosis and membrane mixing, Ras can be mislocalized to endomembranes and become trapped there via the palmitoyl modification that confers a high membrane affinity. Thioesterases such as Acyl protein thioesterase 1 (APT1) can correct Ras mislocalizations by depalmitoylating the protein. The resulting decrease in membrane affinity allows Ras to diffuse rapidly in the cell, allowing it to be repalmitoylated at the Golgi by PAT's and then "pumped" back to the plasma membrane, completing the acylation cycle [13].

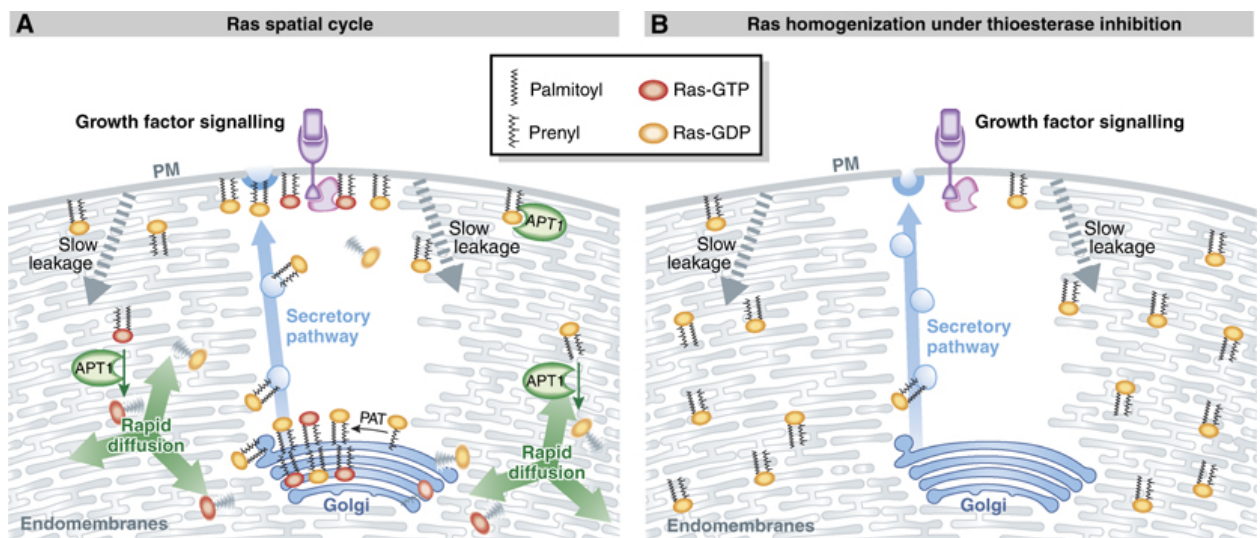


Figure 3.3: Acylation cycle of Ras. A): If Ras is mislocalized at inner cellular membranes, it is ubiquitously depalmitoylated by APT, then rapidly diffuses to the Golgi apparatus where it gets repalmitoylated by palmitoyl acyltransferases (PAT) and transferred back to the plasma membrane via vesicular transport. B) If APT is inhibited, Ras is not depalmitoylated, thus it sticks to the endomembranes and can not be transported to its proper plasma membrane localization, leading to a reduced Ras mediated signaling [14].

It has been postulated that APT's function is to prevent mislocalization of H- and N-Ras to endomembranes by completing the acylation cycle and reestablish the physiological plasma membrane localization of Ras proteins. Inhibition of APT would block the acylation cycle meaning Ras would remain distributed within endomembranes. The absence of Ras from the plasma membrane would lead to weaker Ras mediated proliferation signal [15]. Therefore, in the context of cancer, inhibition of APT could lead to a downregulation of the oncogenic Ras signal, making APT a potential anti-cancer target.

3.3 Acyl Protein Thioesterase (APT) 1 and 2

Investigation of Acyl protein thioesterase 1 and 2 intensified when they were discovered to depalmitoylate oncogenic Ras proteins [15]. Attempts to inhibit Ras have been unsuccessful until now [16], therefore other approaches have been developed to suppress Ras mediated tumor growth. Inhibition of APT is one of these indirect approaches developed to reduce the Ras induced proliferation signal (see section 3.2). Consequently, investigation into the function of APT, its mechanism of action in Ras depalmitoylation mechanism as well as APT inhibitors has become of great interest.

3.3.1 Acyl Protein Thioesterase 1 and 2 are classified as α , β -Hydrolases

APT1 and APT2 are members of the family of α , β - hydrolase protein family, which comprises diverse proteins such as lipases, peptidases, esterases, thioesterases and amidases with a serine as catalytic residue [17]. All α , β - hydrolases contain a three-layered (a/b/a) core with a central element of eight β -sheets, connected and surrounded by six α -helices [18]. The serine hydrolases have a conserved catalytical triad at their catalytic centers, which is formed by the three amino acids Ser-His-Asp [19]. Many of the serine hydrolase enzymes are drug targets for diseases like type 2 diabetes, Alzheimer as well as infectious diseases [19]. Therefore, many serine hydrolases are well studied; however, several enzymes in this group remain poorly characterized in terms of their biological function and substrate binding activity [17].

3.3.2 General knowledge about Acyl Protein Thioesterases

In 1988 the two Acyl Protein Thioesterases were discovered as lysophospholipases in a mouse cell line and subsequently named Lysophospholipase 1 (LYPLA1) and Lysophospholipase 2 (LYPLA2) [20]. LYPLA1 was found to hydrolyze a range of lysophospholipids and other long-chain mono-acyl glycerol esters [21]. Besides the mentioned *in vitro* studies, LYPLA1 was shown to depalmitoylate various proteins in cells, including depalmitoylation of G α [22]. Later on, it was shown that they have a preferred substrate specificity for palmitoylated proteins, thus the proteins were subsequently renamed acyl protein thioesterases (APT) [23]. Mainly only vertebrates express the APT1 homologue depalmitoylase APT2 (68% sequence identity to APT1) [24]. A superimposition of the crystal structures highlighting the high structural sequence identity is shown in Figure 3.4. Similar to APT1, APT2 is able to hydrolyze lysophospholipids [25]. However, APT2 can additionally hydrolyze prostaglandin glycerol esters [26]. Many substrates were characterized *in vitro* for APT1, among them were Ras [23], various heterotrimeric G protein α subunits [23], [27], eNOS [28], RGS4 [23] and SNAP-23 [29].

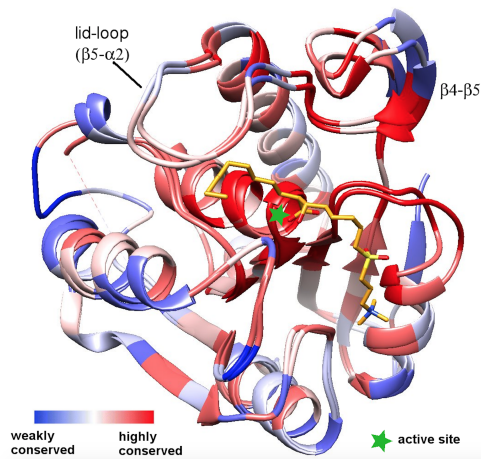


Figure 3.4: Superimposed crystal structures of hAPT1 and hAPT2 with Palmostatin M in the active site (green star), adapted from [30]. Blue regions display the weakly conserved regions of the protein, whereas the red regions are highly conserved regions found in both proteins.

Both APT proteins are expressed and active in nearly all tissue types [31] and can efficiently depalmitoylate proteins *in vitro* [32]. Furthermore, APT1/2 were shown to regulate S-palmitoylation and trafficking of peripheral membrane proteins in cells [24]. Still it remains unclear if APT1 and APT2 are functionally redundant or if they are able to hydrolyze different substrates [24].

Both proteins contain a cysteine at the second position, which can be palmitoylated [33], [34], increasing membrane affinity [35]. Studies on APT1 or APT2 localization in the cell have been performed with GFP or other fluorescent APT fusion proteins [34], [33]. As shown in Figure 3.5 both APTs are found diffusely in the cytoplasm, and enriched at internal Golgi membranes [34], and also at the plasma membrane [33]. The membrane affinity with just one palmitoylation site is relatively weak and Vartak *et al.* postulated that its life time is too short to survive the secretory pathway to the plasma membrane [34], thus it is more likely that APT is located to the Golgi membranes. When the cysteine at amino acid 2 was mutated, APT no longer had correct membrane localization but was largely cytosolic distributed. Moreover, it has been postulated that APT1 can depalmitoylate other APT1 proteins and APT2, but that, in contrast, APT2 is unable to depalmitoylate APT1 [33]. Due to the reversible palmitoylation APT itself undergo an acylation cycle [33], [34]. The biological function of APT's palmitoylation is still unknown. Either the palmitoylation increases the membrane affinity, thus bringing APTs closer to membrane bound substrates, or it could be mediating direct interactions of APT with cofactors or substrates.

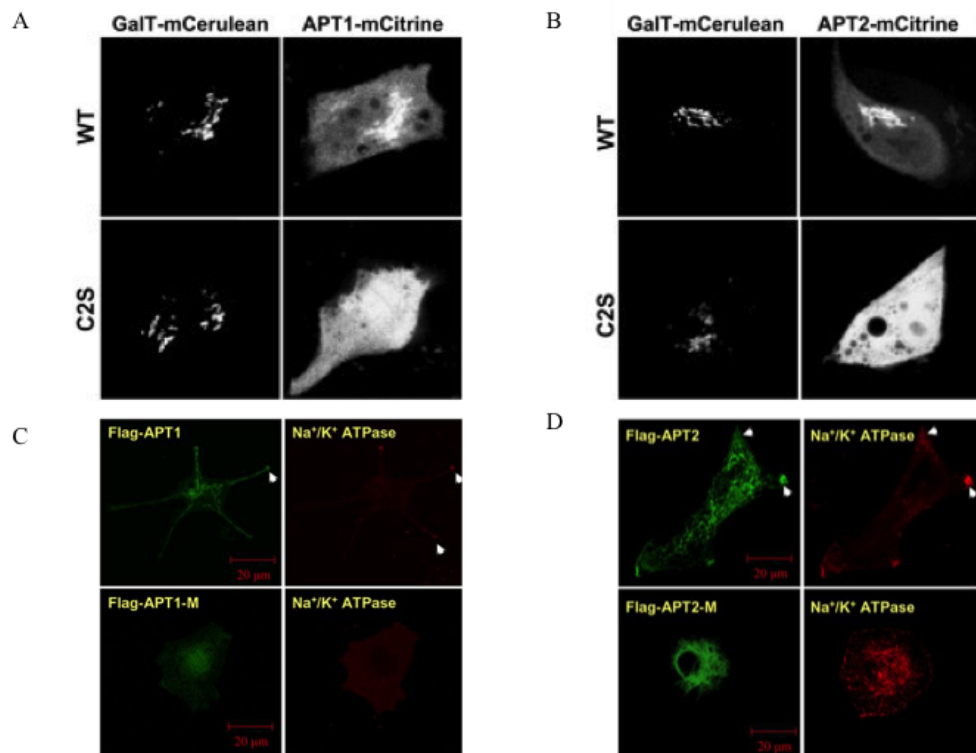


Figure 3.5: *In vivo* localization of APT according to Vartak [34] and Kong [33]. The upper row shows that full length APT1-mCitrine (A, left) and APT2-mCitrine (B, right) localized in the cytosol and also at the Golgi membrane (GalT-mCerulean was used as a Golgi marker). The C2S mutant, which cannot be palmitoylated, is localized in the cytosol [34]. The two lower rows show localization of hAPT1 (C, left) and hAPT2 (D, right) at the plasma membrane, colocalizing with the plasma membrane marker Na⁺/K⁺ ATPase stained in red. The C2S mutant (Flag-APT1-M and Flag-APT2-M), which cannot be palmitoylated, is localized in the cytosol [33].

Ever since it has been shown that inhibition of APT can influence the localization of membrane bound proteins, especially the mislocalization of N-Ras away from the plasma membrane [36], some inhibitors of APT have been synthesized. Covalent binding inhibitors of both APT1 and APT2 include the β -lactone mechanism-based inhibitor Palmostatin B and the related choline-derivative, Palmostatin M (Figure 3.4) [32]. There are limitations to the utility of Palmostatin inhibitors such as non-specific inhibition of numerous other serine hydrolases due to its covalent binding mode [37]. Further, Palmostatin and its derivatives are unstable in serum [22], even so these inhibitors were used in many studies to investigate APT function.

More specific inhibitors of APT1 and APT2 have been discovered in recent years. The APT1 specific inhibitor ML348 ($K_i=304$ nM, shown in Figure 6.46 a) and the APT2 specific inhibitor ML349 ($K_i=230$ nM, shown in Figure 6.46 b) were found by high throughput screening [38], [39]. In contrast to Palmostatin, these specific inhibitors show *in vivo* inhibition of APT in all major tissues at low micromolar concentrations [40], [41].

3.3.3 Structural characteristics of human Acyl Protein Thioesterases

The first published crystal structure of hAPT1 was solved in 2000 [42], with the structure of hAPT2 being published in 2016 [43]. Human APT1/2 contain an α/β serine hydrolase fold with a catalytical triad comprising Ser114, Asp169, and His203, similar to lipases and carboxylesterases [44], [45]. Compared to other serine hydrolases, APT is one of the smallest and lacks the first β strand in the canonical fold. The fourth α helix has been replaced by a shorter α helix that was named G3 because of the 3_{10} helix fold [42]. The structure of hAPT1 is shown in Figure 3.6.

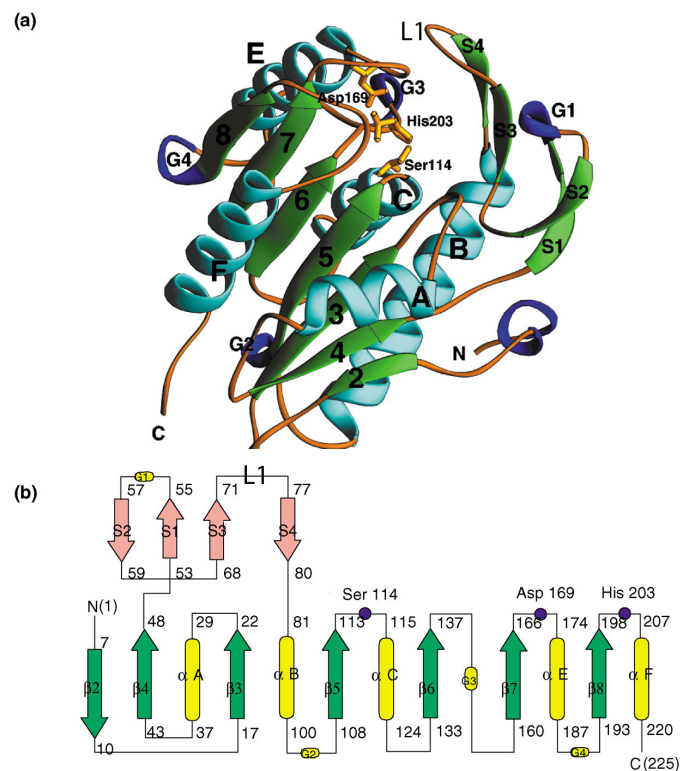


Figure 3.6: Human APT1 structure. Figure a) shows APT's tertiary structure in a ribbon diagram. The seven β strands are displayed as green arrows and are numbered 2-8 because the first β strand of the canonical α/β hydrolase fold is missing. Additionally, the four short β strands are labeled S1-S4. The five α helices are displayed in blue and are labeled from A to F, with a shorter $\alpha 4$ than in the canonical fold. In dark blue the four 3_{10} -helices are shown and are named G1-G4. The residues of the catalytical triad (blue dots), Ser114, Asp169, and His210, are colored in gold. b) The topology model of the secondary hAPT1 structure is displayed. The green arrows present the eight β strands, which are labeled $\beta 2$ - $\beta 8$, and the six helices are shown in yellow, αA - αF . Additional β sheets are found within two regions: S1-S2 and the loop region L1 that connects the two strands S3 and S4) [42].

Furthermore, APTs contain an insertion, connecting the short $\beta 4$ - $\beta 5$ sheet with the $\beta 5$ - $\alpha 2$ loop (L1 in Figure 3.6). This loop covers the catalytic triad and forms a binding tunnel to which substrates can bind [24], hence, it is referred to as the "lid-loop" in this thesis. The binding tunnel has slightly different conformations in the two isoforms, which is thought to affect substrate specificity [30]. Investigation of the polar surface of APT1 shows that it has pronounced hydrophobic patches that are usually buried, due to forming a dimer in the observed crystal structures [30], [46]. However, the real function of this hydrophobic patch is still unknown. It could form a non-polar binding site for membrane insertion (as a membrane insertion was predicted by a membrane-protein-prediction server, Figure 3.7). The fact APT can be palmitoylated at cysteine2 suggests that APT activity is directly related to its membrane localization. The position next to the membrane may also influence the hydrophobic channel orientation and engagement of APT's substrates. [24].

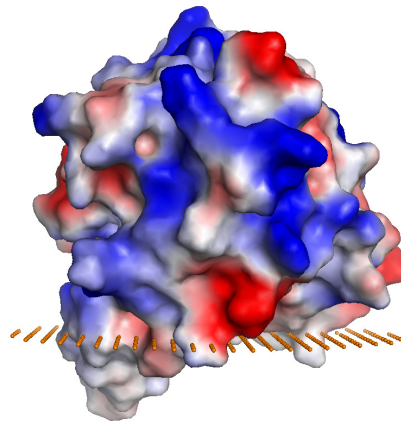


Figure 3.7: The polar surface and predicted cell membrane position (orange plane). The negatively and the positively charged regions of the protein are shown in red and blue, respectively. The white regions correspond to the non-polar surface. Membrane-prediction server: <http://opm.phar.umich.edu/server.php>.

3.4 The cell cycle and APTs role in this

3.4.1 APT's function in asymmetric cell division

Little is known about the potential function of APTs in the cell cycle. Recently it was reported that the depalmitoylation activity of APT1 has an effect on the asymmetric partitioning of the cell fate determinants Numb and β -catenin during cell division of U2 OS tumor cells [47]. APT1 itself is asymmetrically localized in dividing U2OS cells, and APT's catalytic activity seems to be necessary for the asymmetric localization of Notch, the antagonist of Numb, and the Wnt signalling mediator β -catenin, of which both are palmitoylated [47]. Furthermore, it was shown that the interaction of APT1 with the palmitoylated small GTPase CDC42 supported the asymmetric localization of Numb and β -catenin to the plasma membrane [47].

Since APTs have also been implicated in the regulation of some aspects of cell division, some fundamentals are introduced in the following.

The cell cycle, in which an eukaryotic cell is duplicated, is a fundamental biological process, where replicated chromosomes are separated into two identical resulting daughter cells. The cell cycle can be broken down into four stages (shown in Figure 3.8) based on morphological changes the cell undergoes, which includes duplicating and separating its entire genome.

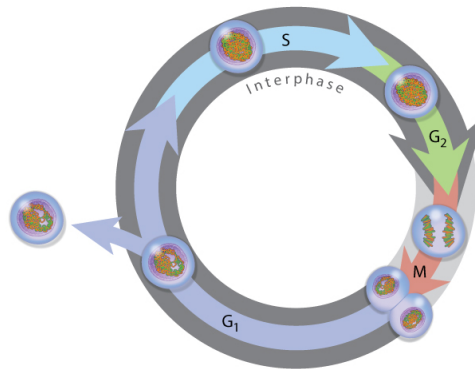


Figure 3.8: In a dividing cell, the mitosis (M) phase is preceded by a growth phase, interphase. Interphase is comprised of three stages; Gap 1 (G₁), followed by Synthesis (S) phase during which the cells duplicates its chromosomes, and finally Gap 2 (G₂) phase. Subsequently, the cell enters mitosis where it divides into two genetically identical daughter cells [48], [49].

During Gap 1 (G₁) phase the cells investigates the surrounding environment. If conditions are suitable, if there is sufficient nutrients for example, then cell division proceeds. If the conditions are unsuitable for a cell division (like in starvation conditions), the cell escapes the cycle. Upon proceeding into the cell cycle, the cell enters the S-phase (synthesis phase). Here, the chromosomal DNA is duplicated, with the newly synthesized daughter strands recruiting additional histones and other proteins to form the so called "sister chromatids". At the end of the S-phase there is a mitotic checkpoint that controls progression into the next step of the cell cycle, meaning if the chromosomes have been successfully copied the cell can move into the next phase Gap 2 (G₂). Gap 2 phase is where the cell is prepared for mitosis (M-Phase). Mitosis itself can be divided into five phases as shown in Figure 3.9 [48], [49], [50].

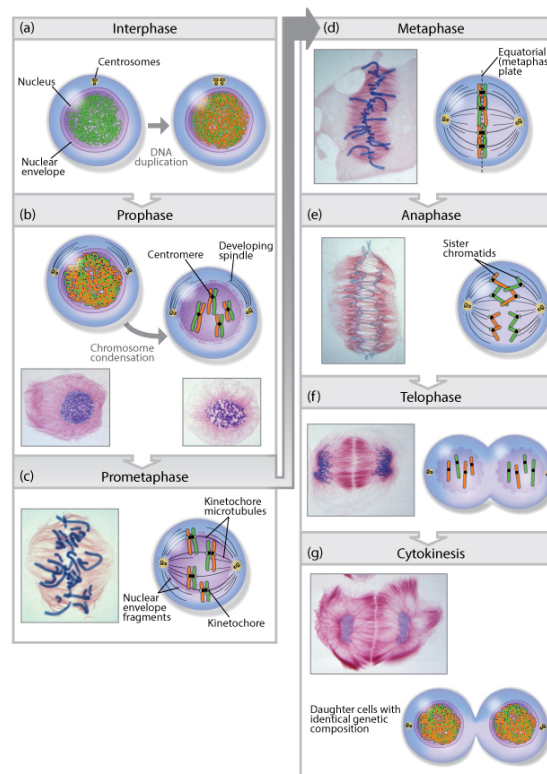


Figure 3.9: The different phases of mitosis and cytokinesis. Before mitosis, the cell duplicated its chromosomes in S-phase, in mitosis those chromosomes will be equally divided into two daughter cells. Mitosis itself can be divided into five phases: prophase, prometaphase, metaphase, anaphase, and telophase, where the chromosomes have been separated. The complete separation of the two daughter cells follows in cytokinesis [48], [49].

Mitosis begins with prophase (Figure 3.9 b). Here, the chromosomes condense and the mitotic spindle starts to form with the centromeres moving to opposite poles, from which microtubules starts to polymerize. Next, prometaphase follows (Figure 3.9 c). Prometaphase starts with the abrupt fragmentation of the nuclear envelope into small vesicles, allowing the spindle fibres to attach to the sister chromatids, via a large protein assembly at the centromere of each chromosome, called the kinetochore. In metaphase (Figure 3.9 d) the chromosomes align along the metaphase plate in the middle of the mitotic cell. In order to be equally separated the two sister chromatids attach to microtubules originating from opposite spindle poles. Attachment to microtubules is highly regulated in order to ensure each sister goes to an opposing pole. During anaphase (Figure 3.9 e) the sister chromatids are separated by the microtubules attached to the centromeres depolymerizing pulling the sister chromatids in opposite directions. In the subsequent telophase (Figure 3.9 f) a new nuclear envelope is constituted, surrounding each set of the separated sister chromatids. Thus two identical daughter nuclei are formed, in which chromosomes begin to decondense, completing the process of DNA separation. Finally, during cytokinesis (Figure 3.9 g) the cytoplasm is divided as a contractile ring is formed in in middle of the two daughter cells [48], [49], [50].

3.4.2 The Golgi and its disassembly and reassembly during mitosis

The Golgi apparatus can be described as a manufacturing, storage, dispatching, and sorting factory. The Golgi is made up of a stacks of disc shaped cavities surrounded by membranes. Often, a cell contains several of these stacks, called Dictyosomes, which are connected among each other. Multiple transport vesicles that are required for the exchange of substances between the Golgi and other cellular components surround the Golgi. There is a defined polarity to the Golgi, with different structures and functions being carried out on the convex and the concave sides. The convex cis-site faces the endoplasmic reticulum (ER) and absorbs proteins and substances synthesized in the ER. Conversely, the concave trans-site faces the plasma membrane and is from where cargo leaves the Golgi via vesicular transport [49]. Importantly, the Golgi is a renowned platform for palmitoylation of multiple proteins with different cellular functions, among these are heterotrimeric G proteins, phosphatidylinositol 3-kinase, N-Ras, eNOS, tankyrase, cyclin B2, and Cdc42 [51].

In comparison to nuclear division, the division of cytoplasmic components is less specific. Many organelles including the endoplasmic reticulum (ER) and the mitochondria, stay unchanged and intact during mitosis. In contrast, the Golgi disassembles during mitosis. There are two hypotheses as to why the Golgi disassembles. One hypothesis is that the disassembly serves as a mechanism for the simultaneous implementation of the connected Golgi membrane system into the new daughter cells. The second hypothesis is that disassembly ensures the regulation of the activity and the localization of signal or effector molecules that are associated with Golgi membranes during interphase. During mitosis the Golgi is broken down and reassembled (shown in Figure 3.10) in the following steps. First, in prophase (Figure 3.10 1), a lateral stretch of the Golgi ribbon forms around the nuclear envelope. In prometaphase (Figure 3.10 2), the Golgi is separated into fragments, followed by metaphase where a partial or complete dispersal flat discs that are normally found in stacks, occurs (Figure 3.10 3). Subsequently, the reassembly of the Golgi starts in the telophase (Figure 3.10 4) with the reappearance of small fragments. Finally, in cytokinesis (Figure 3.10 5), the fragments coalesce into a complete new Golgi for each daughter cells [51].

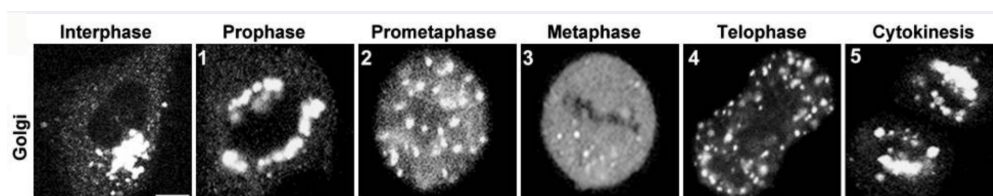


Figure 3.10: Confocal images of the disassembly and reassembly of the Golgi during mitosis. Synchronized NRK cells expressing GalT-YFP as a Golgi marker [51].

4 Objectives

Protein palmitoylation is a reversible posttranslational modification of a cysteine residue with a 16-carbon palmitoyl group coupled via a thioester bond. Due to the reversibility of this reaction, the level of palmitoylated proteins can be controlled in the cell. This regulation is conducted by two classes of enzymes: the addition of a palmitate to a protein is implemented by palmitoyltransferases. In contrast, depalmitoyltransferases can remove the palmitoyl residues. The hydrolysis that removes the palmitoyl residue seems to be mainly catalyzed by acyl protein thioesterase enzymes (APT).

The two human APT isoforms were firstly described as a lysophospholipases, but later, biochemical assays revealed a strong depalmitoylating activity on several S-palmitoylated proteins. Among these protein substrates is the cancer protein Ras, which is mutated in 20-30 % of all human tumors. It was shown that the inhibition of APT leads to a weaker signalling via Ras mediated pathways in cancer cells. Thus APT became a potential anti-cancer target and the research into the structure and function of APTs as well as the development of specific APT inhibitors was stepped up.

APT itself undergoes a dynamic palmitoylation to achieve a steady state membrane localization. To date, the effect of different membrane types on APT and its target proteins as well as the mechanism by which the physiological membrane environment influences APT activity still remains unclear. Furthermore, it also remains unclear if APT can extract and depalmitoylate its palmitoylated target proteins by itself, if APT1/2 palmitoylation at Cys2 has an effect on substrate extraction/depalmitoylation, and if helper proteins (for instance FKBP12, which was described as a cofactor in Ras depalmitoylation) are required to extract membrane bound substrates.

In this thesis, biophysical- and *in vivo* methods were used to investigate the effect of APT palmitoylation. Specifically, how membrane localization influences the activity of APTs and its cellular localization. In order to accomplish this, depalmitoylation activity of APT on a membrane bound substrate was analyzed by fluorescence spectroscopy and fluorescence microscopy. Notably, an *in vitro* assay for biological substrates was implemented by ESI-mass spectroscopy, since only activity assays with artificial APT substrates were available until now. A thiol group detection assay was investigated for the suitability as assay for activity of APTs on natural substrates. The effect of APT's cysteine palmitoylation on the *in vivo* localization was analyzed using the methods of electroporation and transient transfection. As little is known about the localization of APT and its activity during mitosis, localization studies with transiently transfected APTs were performed. Further, the changes caused to the mitotic index and to the differentiation of PC12 cells upon APT inhibition was determined.

5 Material and Methods

5.1 Materials

All chemicals and buffer ingredients were purchased in the highest available purity from Fluka (Neu-Ulm), GE (Freiburg), Merck (Darmstadt), Qiagen (Hilden), Roche (Mannheim), Roth (Karlsruhe), Serva (Heidelberg), Pan Biotech (Aidenbach) and Sigma-Aldrich (Deisenhofen). Protein- and DNA-ladders were purchased from MBI Fermentas, BioRad and Thermo Scientific.

5.1.1 Buffers

The used buffers are described in the corresponding method.

5.1.2 Phospholipids and Reagents

Phospholipids and reagents used in this study are listed in table 5.1.

Table 5.1: Phospholipids and Reagents.

Products	Manufacturer
DOPC	Avanti Polar Lipids (USA)
DOPG	Avanti Polar Lipids (USA)
DOGS-Ni-NTA	Avanti Polar Lipids (USA)
Lyso-PPC	Avanti Polar Lipids (USA)
DPPC	Avanti Polar Lipids (USA)
<i>N</i> -Rh DHPE	Thermo Fisher (Darmstadt)
Bodipy FL C ₁₂	Life Technologies (Carlsbad)
Chloroform	Sigma Aldrich (Darmstadt)
Ammoniumcarbonat	Sigma Aldrich (Darmstadt)

5.1.3 Kits

Kits used in this study are listed in table 5.2.

Table 5.2: Kits.

Kits	Manufacturer
QIAprep Spin Miniprep Kit	Qiagen (Hilden)
QIAGEN Plasmid Maxi Kit	Qiagen (Hilden)
Roti-Prep Plasmid MINI	Carl Roth (Karlsruhe)

5.1.4 Enzymes

Commercially available enzymes used in this study are listed in table 5.3.

Table 5.3: Enzymes.

Enzymes	Manufacturer
BSA	Sigma (Deisenhofen)
Dnase I	Roche (Mannheim)
PreScission protease	GE Healthcare (Freiburg)
Restriction enzymes	New England Biolabs (Schwalbach)
T4 DNA ligase	New England Biolabs (Schwalbach)

5.1.5 Antibiotics

Antibiotics were added to the culturing media with the following final concentrations (Table 5.4 and Table 5.5).

Table 5.4: Antibiotics for bacteria.

Antibiotic	Concentration
Ampicillin	100 µg/mL
Kanamycin	50 µg/ mL
Tetracyclin	7 µg/ mL
Chloramphenicol	25 µg/ mL

Table 5.5: Antibiotics for mammalian cells.

Enzymes	Manufacturer
Penicillin	100 µg/mL
Streptomycin	0.1 mg/mL

5.1.6 Antibodies

All used primary and secondary antibodies are listed in table 5.6 and table 5.7.

Table 5.6: Primary antibodies.

Antigen	Origin	Dilution	Manufacturer
CREST	human	1:200	Antibodies Inc.
Tubulin	mouse	1:4000	Sigma
APT1 (ab91606)	goat	1:100 (IF)	Abcam
APT2 (ab151578)	goat	1:100 (IF)	Abcam

Table 5.7: Secondary antibodies.

Antigen	Origin	Dilution	Fluorophor	Manufacturer
IgG α -human	goat	1:200	Alexa647	Jackson Immuno Research
IgG α -mouse	goat	1:200	Rhodamine Red	Jackson Immuno Research
IgG α -goat	donkey	1:200	Rhodamine Red	Jackson Immuno Research

5.1.7 Plasmids for mammalian expression

The mCitrine APTs and GalT-TagBFP plasmids were a kind gift from Philippe Bastiaens, Department of systemic cell biology Max Planck Institute for Molecular Physiology, Dortmund, Germany. The plasmids and cloning protocols are described in [34].

5.1.8 Bacterial strains and media

For transformations the bacterial strain *Escherichia coli* DH5 α F⁻ ϕ 80dlacZ Δ M15 Δ (lacZYA-argF) U169 recA1 endA1 λ -hsdR12(rK⁻, mK⁺) supE44, thi-1 gyrA, relA1 and for protein expression the strain BL21 (DE3) codon + RIL *E. coli* B F⁻ dcm ompT hsdS(rB-mB-) gal λ (DE3) was used.

For amplifying the plasmids the strain *Escherichia coli* Omnimax F⁻ mcrA Δ (mrr-hsdRMS-mcrBC) ϕ 80lacZ Δ M15 Δ lacZYA-argF U169 endA1 recA1 supE44 thi-1 gyrA96 relA1 tonA panD was used (kindly provided by the Dortmund Protein Facility at MPI Dortmund).

The cells were cultured in LB (Luria Bertani) medium or on LB -agar plates containing the appropriated antibiotics and grown at 37 °C. Ingredients are listed in table 5.8. The medium was kindly provided by the media kitchen facility at MPI Dortmund.

Table 5.8: Components of the used media.

Medium	Ingredients
Luria Bertani (LB)	10 g/L Bacto tryptone 5 g/L yeast extract 10 g/L NaCl
LB agarose plates	LB-medium 1.5 % agarose

5.1.9 Cell lines

The used cell lines are listed in table 5.9. PC12 cells were kindly provided by Philippe Bastiaens (Departement of Systemic Cell Biology, Max Planck Institute for Molecular Physiology, Dortmund, Germany) and HeLa Cells were kindly provided by Andrea Musacchio (Departement of Mechanistic Cell Biology, Max Planck Institute for Molecular Physiology, Dortmund, Germany).

Table 5.9: Cell lines.

Cell line	origin
HeLa	Cervix Adenocarcinoma, human
PC12	Rat

5.1.10 Software

The following softwares were used to analyze the data or preparing the figures (table 5.10).

Table 5.10: Software.

Software	Version	Supplier/Developers
Illustrator CS5.1	15.1.0	Adobe
Photoshop CS5.1	12.1	Adobe
ImageJ	1.46r	National Institute of Health
Excel	14.7.3	Microsoft
Prism	6.0h	Graphpad
Pymol	1.6.0.0	Schrödinger LLC
ChemBioDraw Ultra	6.5.00	PerkinElmer
TexStudios	2.12.6	by Benito van der Zander and others
Imaris	7.3.4	Bitplane
Origin	7.0	Origin Labs

5.1.11 Instruments

The used instruments and machines are listed up in table 5.11.

Table 5.11: Instruments.

Instruments	Manufacturer
Balances	Sartorius (Göttingen, Germany)
BioPhotometer	Eppendorf (Hamburg, Germany)
Centrifuges	Beckmann (Münster, Germany) Eppendorf (Hamburg, Germany)
ChemiDoc MP Imaging System	BioRad (Munich, Germany)
CLARIOstar microplate reader	BMG LABTECH (Ortenberg, Germany)
DNA electrophoresis chambers	BioRad (Munich, Germany)
FPLC (Gradifrac systems)	Pharmacia (Stockholm, Sweden)
Liquidator96	Steinbrenner (Wiesenbach)
Magnetic stirrer RCT basic	Eppendorf (Hamburg, Germany)
PAGE chambers	BioRad (Munich, Germany)
pH meter	Knick (Berlin, Germany)
Pipettes	Eppendorf (Hamburg, Germany)
Sonifier 450	Branson (Dietzenbach, Germany)
Countess automated cell counter	Invitrogen (California, USA)
3i Marianas	Intelligent Imaging Innovations (Denver, USA)
Axio Observer Z1 microscope	Carl Zeiss Microscopy GmbH (Cologne, Germany)
SX. 18MV Stopped-flow apparatus	Applied Photophysics (Leatherhead, UK)
LCQ Fleet	Thermo Fisher Scientific (Schwerte, Germany)
DeltaVision Microscope	GE Healthcare (Freiburg, Germany)
Microplate reader Infinite M200 PRO	Tecan (Männedorf, Switzerland)
NanoDrop2000 spectrophotometer	Thermo Fisher Scientific (Schwerte, Germany)

5.2 Methods

5.2.1 Cloning, Expression and Purification of Proteins

Thanks to Patricia Stege for cloning, expression and purification of the used proteins. Cloning, expression and purification of APT proteins is described in [52] and [46]. APT1 and APT2 cDNAs were obtained from ImaGenes GmbH (Berlin, Germany). The full length gene was gateway cloned into a pGEX 4T3 expression vector (GE Healthcare, Buckinghamshire, UK). Specific modified primers encode a PreScission protease cleavage site and immediately upstream the start codon of the APT gene. Single APT mutations were introduced by a site directed mutagenesis, using specific designed primers, which implements the mutation in a Polymerase Chain Reaction (PCR). To generate the His versions of APT, genes were cloned into a pProEX-HTB vector. Ras genes were cloned into a pTAC vector.

5.2.1.1 Polymerase Chain Reaction (PCR)

The Polymerase Chain Reaction (PCR) was used to amplify DNA e.g. for sequencing (see 5.2.1.6) or was used for site directed mutagenesis. The mutagenesis reaction contains: 30-60 ng DNA template, 0.4 mM primer (forward and reverse), 0.2 µg/µL dNTPs, 4 % DMSO, 1x Pfu reaction buffer (Promega) and 1x Polymerase. Either Pfu-Polymerase (Promega) or Phusion-polymerase (Finnzymes) was used as thermostable polymerase. The PCR programs for Pfu- and Phusion-polymerase are listed in the table 5.12. After PCR, methylated template DNA was digested with 1 unit of the endonuclease DpnI for 1 h at 37 °C.

Table 5.12: Standard PCR program for Pfu- or Phusion-polymerase.

Pfu-polymerase			Phusion-polymerase		
Number of repetitions	Temperature	Time	Number of repetitions	Temperature	Time
1 x	98 °C	3 min	1 x	98 °C	1 min
30 x	98 °C	20 s	30 x	98 °C	30 s
	55 °C	1 min		60 °C	50 s
	65 °C	12 min		72 °C	3 min
1 x	65 °C	10 min	1 x	72 °C	10 min
	8 °C	∞	1 x	8 °C	∞

5.2.1.2 Determination of DNA concentration

The DNA concentration was determined by measuring the absorbance at 260 nm with a NanoDrop spectrometer. If $A_{260}=1$ the dsDNA has a concentration of 50 µg/mL. Additionally, to investigate if the DNA sample is free of protein contaminations, the absorbance at 280 nm was measured. To exclude salt contaminations the absorbance at 230 nm was measured. The ratios of A_{260}/A_{280} and A_{260}/A_{230} were calculated. If both ratios have a higher value than 1.8, the DNA is pure without any protein or salt contamination. Only DNA that was determined to be pure was used for any experiments during this thesis' work.

5.2.1.3 Transformation of DNA into chemically competent bacteria cells

To transform plasmids into *E. coli* cells, a heat shock protocol was performed. Therefore chemically competent *E. coli* DH5 α or OmniMax cells were thawed on ice. 0.2-1 µg of plasmid DNA were added to 100 µL cells. The mixture was gently mixed and incubated on ice for 15-30 minutes. After incubation a heat shock followed at 42 °C for 90 s. To develop resistances against antibiotics, 800 µL LB medium were added to the cells and they were incubated at 37 °C for 1 h shaking at 300 rpm. Cells were spinned down and the supernatant was discarded apart 50-100 µL. The cells were resuspended in the remaining supernatant and plated on a LB-agar plate containing the appropriate antibiotic. Plates were incubated over night at 37 °C.

5.2.1.4 Plasmid isolation from bacteria cells

The protocol for alkaline lysis followed by a chromatographic purification was performed to isolate plasmid DNA out of bacteria cells. For small scale preparation 3 mL LB-medium containing the appropriate antibiotic were inoculated with a mono colony and incubated over night at 37 °C. For large scale plasmid isolation a 250 mL over night culture was used. To isolate DNA the Mini- or Maxiprep Kits (Macherey-Nagel, Qiagen) or the Roti-Prep Plasmid MINI Kit (Carl Roth) was utilized by the manufacturer's instructions.

5.2.1.5 Agarose gelelectrophoresis

To separate DNA fragments according to their electrophoretic mobility which corresponds to their molecular weight, agarose gelelectrophoresis was used. The elctrophoresis was performed in horizontal chambers with an agarose concentration of 0.9 % (w/v). The agarose was dissolved in 1x TAE buffer (10x: 48.4 g Tris, 11.4 ml glacial acetic acid, 3.7 g EDTA, fill up to 1 l with H₂O) and Midori green advanced DNA stain (1:25000) (Nippon Genetics) was added. The DNA samples were mixed with 6x DNA loading buffer (30 % (w/v) sucrose, 20 % (v/v) glycerol, 0.2 % (w/v) orange G) and transfered to the gel. The electrophoresis was performed at constant voltage of 100 V for 30 min. The DNA fragments were detected and visualized with UV light.

5.2.1.6 DNA sequencing

The Sanger method was used to analyze the DNA sequence. Sequencing was performed by the in-house sequencing facility. For that 500-800 ng DNA template, 4 µL sequencing buffer, 10 pmol sequencing primer and 2 µL terminator-mix was mixed and ddH₂O was added to reach a final volume of 20 µL. Then a PCR run was performed with the following protocol (table 5.13).

Table 5.13: Standard PCR program DNA sequencing.

Number of repetitions	Temperature	Time
1 x	96 °C	2 min
30 x	98 °C	30 s
	50 °C	15 s
	60 °C	4 min
1 x	60 °C	5 min
	8 °C	∞

After PCR, 80 µL ddH₂O, 10 µL 3 M sodium acetate and 250 µL Ethanol were added to the reaction mixture. Thereafter, a centrifugation (10 min, 13000 rpm) has been carried out and the supernatant was discarded. The pellet was washed with 500 µL 70 % Ethanol, followed by another

centrifugation step (10 min, 13000 rpm). The supernatant was discarded and the pellet was dried in the air.

5.2.1.7 Protein expression and purification

GST-fusion proteins:

The required plasmid was transformed into *E. coli* BL21 Codon + RIL cells. Cells were grown at 25~°C in LB medium containing the appropriated antibiotics in a LEX bioreactor (Harbinger Biotech, Toronto, Canada). At OD₆₀₀=1, 0.1 mM IPTG (Isopropyl β -D-1-thiogalactopyranoside) was added and the protein was expressed over night at 18 °C. The next day cells were harvested and lysed in presence of 0.1 mM PMSF and DNaseI by sonification. To remove cell debris a centrifugation step with 25000 g at 4 °C for 30 min was performed. APT proteins are N-terminally tagged with glutathione-S-transferase (GST). Therefore the GST-APT fusion proteins can bind specifically to a GSH column. The supernatant was loaded on a Glutathione Sepharose 4 fast flow column (GE Healthcare). After washing, the GST-Tag was removed by PreScission protease (GE Healthcare). The GSH affinity chromatography was performed in the following buffer: 50 mM Tris-HCl pH 8.0, 150 mM NaCl, 5 % Glycerol and 3 mM β -mercaptoethanol. The protein was eluted and concentrated with an Amicon Ultra Centrifugal Filter (Merck Millipore, Billerica, USA). A final size exclusion chromatography was performed with a Sephadex S200 column (GE Healthcare) with the following buffer: 20 mM Tris-HCl pH 8.0, 30 mM NaCl, 1 mM TCEP-HCl. The protein was concentrated, aliquoted, snap frozen and stored at -80 °C. All steps of the protein expression and purification were monitored by SDS gelelectrophoresis.

His-tag proteins:

The required plasmid was transformed into *E. coli* BL21 Codon + RIL cells. Cells were grown at 25 °C in LB medium containing the appropriated antibiotics in a LEX bioreactor (Harbinger Biotech, Toronto, Canada). At OD₆₀₀=1, 0.1 mM IPTG was added and the protein was expressed over night at 18 °C. The next day cells were harvested and lysed in presence of 0.1 mM PMSF and DNaseI by sonification. To remove cell debris a centrifugation step with 25000 g at 4 °C for 30 min was performed. His tagged fusion proteins were loaded to a pre-washed Talon column (in the following buffer: 50 mM Tris-HCl pH 8.0, 150 mM NaCl, 5 % Glycerol and 3 mM β -mercaptoethanol) and washed with this buffer. To elute the protein the Imidazol concentration was increased with a linear gradient from 0 mM up to 400 mM. Fractions containing the pure protein were collected and concentrated. A final size exclusion chromatography was performed with a Sephadex S200 column (GE Healthcare) with the following buffer: 20 mM Tris-HCl pH 8.0, 30 mM NaCl, 1 mM TCEP-HCl. The protein was concentrated, aliquoted, snap frozen and stored at -80 °C. All steps of the protein expression and purification were monitored by SDS gelelectrophoresis.

Ras Proteins:

The required plasmid was transformed into *E. coli* CK600K cells. Cells were grown at 30 °C in TB medium containing the appropriated antibiotics. At OD₆₀₀=1, 1 mM IPTG was added and the protein was expressed over night at 30 °C. The next day cells were harvested and lysed in presence of 0.1 mM PMSF and DNaseI by sonification in buffer A (50 mM Tris pH 7.9, 2 mM MgCl₂ and 5 mM DTE). To remove the cell debris a centrifugation step with 25000 g at 4 °C for 25 min was performed. The supernatant was loaded on a pre-washed Ni-column. The column was washed with 10 times column volume of buffer A including 450 mM NaCl followed by a washing step with buffer A. A second washing step was performed with 10 times column volume of buffer A including 1 mM ATP and 400 mM KCl, followed by a washing step with buffer A. The protein was eluted with buffer A containing 250 mM Imidazol. The protein was concentrated with an Amicon Ultra Centrifugal Filter (Merck Millipore, Billerica, USA). A final size exclusion chromatography was performed with a Sephadex S75 column (GE Healthcare) with the following buffer: 20 mM Tris-HCl pH 7.9, 2 mM MgCl₂ and 5 mM DTE. The protein was concentrated, aliquoted, snap frozen and stored at -80 °C. All steps of the protein expression and purification were monitored by SDS gelelectrophoresis.

5.2.1.8 SDS-PAGE and coomassie blue staining

To separate proteins according to their molecular weight Sodium dodecyl sulfate polyacrylamide gel electrophoresis (SDS-PAGE) was used. This analytical method supports the monitoring of the different steps during protein purification and the purity of proteins. The anionic detergent denaturates the protein structure and generates a negative charge proportional to its size. The protein movement in the gel is dependent on the size of the protein, because small proteins are able to pass the acrylamid network faster than larger proteins. The concentration of SDS can be variated to create bigger or smaller pores in the gel. The SDS gel is divided into two zones. The upper zone is the stacking gel, in which the proteins are collected in one single band. This part consists of 5% (w/v) acrylamide/bisacrylamide in 125 mM Tris/HCl pH 6.8 buffer. Followed by the resolving zone (second zone) where the proteins are separated. This zone consist out of 8-18% (w/v) acrylamide/bisacrylamide and 125 mM Tris/HCl pH 8.8. Both zone solutions were polymerized by adding 0.1% (w/v) APS and 0.04% (w/v) TEMED. Before the proteins were transferred to the gel, the samples were mixed with a 5x SDS loading buffer (0.25 M Tris-HCl pH 6.8, 15% (w/v) SDS, 50% (v/v) glycerol, 25% (v/v) b-mercaptoethanol, 0.01% (w/v) bromophenol blue) and denaturated for 5 min at 95 °C. SDS-Page was performed at 180 V for 40-60 min with an anode (20 mM Tris pH 8.8, 1.2% (v/v) HCl) and a cathode buffer (1M Tris pH 8.3, 1 M tricine, 30 mM SDS). To visualize separated protein bands the gel was visualized by coomassie staining (0.2% (w/v) using coomassie brilliant blue G250, 7.5% (v/v) acetic acid, 50% (v/v) ethanol) and destained, in 10% (v/v) acetic acid in ddH₂O, for several hours on a shaker

5.2.1.9 Determination of protein concentration

To determine the protein concentration, the absorbance at 280 nm was measured, using a Nanodrop 1000 Photometer (PeqLab). Moreover the concentration was calculated according to the Labert-Beer law.

5.2.2 Cell biological methods

5.2.2.1 Cell culture and transfections

HeLa cells were grown in 6 cm dishes (Sarstedt) in DMEM medium (PAN Biotech) supplemented with 10% FBS (Clontech), penicillin and streptomycin (GIBCO) and 2 mM L-glutamine (PAN Biotech).

PC12 cells were grown in 6 cm poly-l-lysine coated dishes in DMEM medium (PAN Biotech) supplemented with 5% FBS (Clontech), 10% horse serum (Clontech), penicillin and streptomycin (GIBCO), 2 mM L-glutamine (PAN Biotech) and 1% non essential amino acids. Cells were grown in a humidified atmosphere of 37 °C and 5% CO₂. Transient transfections were performed with LTX200 reagent and carried out according to manufacturer's instructions. All working steps were performed under laminar flow, to avoid contaminations.

5.2.2.2 Thawing cells

Cells stored at -150 °C were thawed at 37 °C. After thawing, the cells were resuspended in the corresponding medium and centrifugated for 5 min at 1200 rpm. Thereafter the pellet was resuspended in fresh medium and cells were transferred to the culture dish.

5.2.2.3 Freezing cells

To store cells at -150 °C, cells were frozen in a medium containing 10% DMSO as cryoprotective agent. To allow a slow and continuous freezing, cells were placed in special containers containing isopropanol and stored over night at -80 °C. On the next day, frozen cells were transferred from -80 °C to -150 °C.

5.2.2.4 PC12 cell differentiation assay

To test if APT inhibition, with different inhibitors, has an effect on neuronal outgrowth of PC12 cells, a differentiation assay was performed. Cells from a 10 cm dish were counted and diluted with medium to the desired cell number. After the dilution approximately 10000 cells were seeded,

in growth medium, on a poly-l-lysine coated 24 well plate. To start the differentiation, 2 hours after plating, the medium was changed to a medium containing 100 ng/mL NGF (Neuronal Growth Factor, Merck) and the corresponding APT inhibitor. Cells were differentiated for 10 days (change medium (containing NGF and inhibitor) every 2 days). To visualize the neuronal outgrowth of PC12 cells, cells were stained with coelestin blue. Therefore cells were washed with 200 μ L PBS and fixed with 4% PFA for 10 minutes. Cells were two times washed with dest. H₂O. Afterwards cells were stained with 200 μ L coelestin blue (for 100 mL solution: add 5% Ammonium iron(III) sulfate and 0.5 g coelestin blue to 100 mL H₂O, boil for 3 minutes, cool down to room temperature, filter the solution and add 14 mL glycerol) for 30 seconds. After staining, 100 cells were counted on an Evos FL Microscope. A cell, with a neuron two times longer than the cell body, was classified as a differentiated cell. The HRasG12VmCitrine construct was transiently transfected by the use of LTX2000 by Thermo Fisher (transfection was performed accordingly to the manufacturer's protocol). After 4 hours the medium was replaced by a medium containing the inhibitors. The cells were fixed after 48 h and 100 cells were counted with help of a fluorescence microscope.

5.2.2.5 Determination of the mitotic index and preparation of mitotic gallery

Cells from a 10 cm dish were counted and diluted with medium to the desired cell number, so that on the first day approximately 15000 cells (per well) were seeded on a poly-D-Lysine coverslip in a 24 well plate. Cells were transfected the next morning with the respective vector using LTX2000 (transfection was performed accordingly to the manufacturer's protocol). In the evening of the second day cells were treated with the CDK inhibitor 9 μ M RO3306. A wash out followed after 18 hours. Afterwards fresh medium with or without 25 μ M of the respective inhibitor was added. For the mitotic index cells were fixed at various time points with 4% PFA (remove old medium and add 180 μ L PFA, incubate for 10 minutes and wash 3 times with PBS) and cells were immunofluorescently stained as described in subsection 5.2.2.6. For the mitotic index, 500 cells were counted and classified according to their mitotic state (interphase, prophase, metaphase or anaphase).

For the mitotic galleries, cells from a 10 cm dish were counted and diluted with medium to the desired cell number and approximately 15000 HeLa H2BmCherry cells were seeded on a poly-D-Lysine coverslip in a 24 well plate. Cells were transfected the next morning with the respective vector using LTX2000 (transfection was performed accordingly to the manufacturer's protocol). After 5 hours the medium was replaced by fresh medium. In the next morning cells were fixed with 4% PFA (remove old medium and add 180 μ L PFA, incubate for 10 minutes and wash 3 times with PBS). Microscope pictures were taken on a 3i Marianas™ system (Intelligent Imaging Innovations Inc.) equipped with Axio Observer Z1 microscope (Zeiss), Plan-Apochromat 63x/1.4NA Oil Objective, M27 with DIC III Prism (Zeiss), Orca Flash 4.0 sCMOS Camera (Hamamatsu). Images were acquired as z-sections at 0.27 μ m. Images were converted into maximal intensity projections, exported and formatted into 8-bit.

5.2.2.6 Immunofluorescence staining

Fixed cells on coverslips (fixation protocol see subsection 5.2.2.5) were permeabilized with 0.3% Triton X-100 in PBS for 10 minutes. The blocking step was performed afterwards with 3% BSA in PBST for 45 minutes. The first antibodies were diluted (dilution factors are listed in table 5.6) in 1% BSA-PBST and incubated for 2 hours. Then coverslips were washed three times with PBST. The second antibodies, coupled with a fluorophor, were diluted (dilution factors are listed in table 5.7) in 1% BSA-PBST and were added to the coverslips for one hour. Afterwards the coverslips were washed three times with PBST. DNA was stained with 0.5 $\mu\text{g}/\text{mL}$ DAPI for 1 minute. The final washing steps were performed with PBST and H_2O . Coverslips were dried in the air and mounted with Mowiol mounting media (Calbiochem).

5.2.2.7 Electroporation

Cells were seeded on a 10 cm dish with a confluency of approximately 50%. The next morning cells were transfected with the respective vector using LTX2000 (transfection was performed accordingly to the manufacturer's protocol). After 5 hours, cells were trypsinized and added to 50 mL PBS. Afterwards the cells were centrifuged for 5 min at 1200 rpm and the supernatant was discarded. Resuspend the cells in 2 mL PBS and count them. Transfer 2×10^6 cells to an eppendorf reaction vessel, spin cells down and discard the supernatant. Resuspend cells in 110 μL of buffer R (Thermo Fisher). Dilute the APTmCherry protein in buffer R to a final concentration of 60 μM , centrifuge the protein solution to remove protein aggregates. Add 10 μL of the protein solution to the cell suspension. Afterwards electroporation was performed using NEON (Thermo Fisher) with two pulses at a voltage of 1005 V for 35 ms. Wash cells with 15 mL PBS, centrifuge at 1200 rpm for 5 minutes and discard the supernatant. Resuspend the cells in 2-4 mL trypsin (according to pellet size) and incubate for 5 minutes at 37 $^\circ\text{C}$. Wash cells with 15 mL PBS, centrifuge for 5 minutes at 1200 rpm and discard the supernatant. Resuspend cells in 1 mL imaging medium (CO_2 Independent Medium (Gibco®), 10% FBS and 2 mM l-glutamine) and transfer 200-300 μL cell solution to a 24 well Ibidi coated plate and adjust to a final volume to 500 μL . Add 0.5 μL SiR-DNA (Spirochrome) to stain the the nuclei. Cells were imaged 24 hours after electroporation with a 3i Marianas™ system (Intelligent Imaging Innovations Inc.) equipped with Axio Observer Z1 microscope (Zeiss), Plan-Apochromat 63x/1.4NA Oil Objective, M27 with DIC III Prism (Zeiss), Orca Flash 4.0 sCMOS Camera (Hamamatsu). Images were acquired as z-sections at 0.27 μm . Images were converted into maximal intensity projections, exported and formatted into 8-bit.

5.2.3 Vesicle assays

5.2.3.1 Preparation of Large Unilamellar Vesicles (LUVs)

Stock solution of DOPC (1,2-dioleoyl-sn-glycero-3-phosphocholine) in chloroform (10 mg/mL) was diluted to the desired concentration and if stained vesicles are required 0.1 mol % N-Rh-PE (N-(Lissamine™ Rhodamine B sulfonyl)-1,2-dihexadecanoyl-sn-glycero-3-phosphoethanolamin, Molecular Probes®, Life Technologies Inc., Stocksolution $c = 1$ mM in Methanol) was added to label the vesicles. A large part of the chloroform was evaporated with a nitrogen stream. The remaining chloroform was removed by drying under vacuum over night. The dried lipids were hydrated in 5 mM ammonium carbonate buffer to a final concentration of 10 mM. The mixture was sonicated for 15 minutes. Afterwards five freeze–thaw–vortex cycles and brief sonication were conducted to generate large multilamellar vesicles (LMV). These LMV were transformed to LUVs, of a homogeneous size, by use of a mini-extruder (Avanti Polar Lipids) with polycarbonate membranes of 100 nm pore size. The generated LUVs were stored at 4 °C for a maximum period of 7 days. LUVs were used in Stopped-Flow experiments (see section 5.2.3.4) and for FRET measurements (see section 5.2.3.3) to investigate the activity of APT to a membrane bound peptide.

5.2.3.2 Preparation and imaging of Giant Unilamellar Vesicles (GUVs)

Giant unilamellar vesicles were created by the method of electroformation. Therefore stock solution of lipids in chloroform (10 mg/mL) was diluted to 1 mg/mL. To label the vesicles 0.1 mol% of N-Rh-PE or 0.2 mol% of Bodipy FL C₁₂ were added and mixed. A 15 μ L aliquot of the lipid solution was spread on an indium tin oxide (ITO)-coated coverslip (SPI Supplies/Structure Probe Inc.). The remaining chloroform was removed by drying under vacuum over night. The lipid coated and an untreated ITO-coverslip were embedded in a Large Closed Bath Imaging Chamber RC-21B (cell volume 358 μ L, Warner Instruments Inc.) and fixed to the corresponding Platform P-2 (Warner Instruments Inc.). The assembled unit was filled with the respective buffer. A scheme of the electroformation chamber is depicted in figure 5.1. Electroformation was performed for 2 hours at room temperature with a sinusoidal alternating low-frequency voltage (10 Hz, 1.7 V).



Figure 5.1: Assembled electroformation chamber.

After 2 hours the vesicles were imaged with a 3i Marianas™ system (Intelligent Imaging Innovations Inc.) equipped with Axio Observer Z1 microscope (Zeiss), Plan-Apochromat 100x/1.4NA Oil Objective, M27 with DIC III Prism (Zeiss), Orca Flash 4.0 sCMOS Camera (Hamamatsu). Images were acquired as 3 z-sections at 0.4 μm . Images were converted into maximal intensity projections, exported and formatted into 8-bit.

To investigate the membrane affinity of APTs to vesicles, 2 μM hAPT-mCherry was added to Bodipy FL C₁₂ labeled vesicles. Pictures were taken before and 20 minutes after the APT injection.

To analyze APT's activity on a membrane bound peptide, 10 μM FITC labeled palmitoylated N-terminal APT1 peptide was injected to N-Rh-PE labeled vesicles. A picture at $t=0$ min was taken. Afterwards 2 μM APT was injected and pictures were taken every minute for 90 minutes. The FITC intensity was determined with the program Fiji. With the versatile wand tool the shape of the vesicle was defined. A band was created to rim the vesicle. Then the vesicle intensity was measured. Background intensity was determined and subtracted from the vesicle intensity to receive the final total intensity.

5.2.3.3 FRET measurements

To investigate APT activity on a membrane bound substrate, FRET measurements were performed with CLARIOstar microplate reader (BMG LABTECH, Ortenberg). For FRET measurements the excitation wavelength λ_{ex} was set to 450 nm, while the emission was recorded at wavelength λ_{em} that is 590 nm. To measure just the Donor (FITC) intensity the excitation wavelength λ_{ex} was always set to 475 nm, while the emission was recorded at wavelength λ_{em} that is 517 nm. The signal gain and the focal height were automatically optimized once and kept constant for all following experiments. A simultaneous measurement of FRET- and Donor- intensity was performed to analyze APT activity on membrane bound substrate. Therefore 90 μL of 200 nM FITC labeled palmitoylated APT Peptide (sequence: $(\text{NH}_2)\text{MC}(\text{palm})\text{GNNMSTK}(\text{FITC})-(\text{COOH})$, StorkBio, Estonia) used as the donor, were incubated in a 96-well microplate (Greiner Bio-One, Kremsmünster, Austria). When a stable baseline was reached, 5 μL of the acceptor 0.1 mol% N-Rh-PE labeled DOPC vesicles (final DOPC concentration: 500 μM) were added and rapidly mixed. The increase in FRET- and the decrease in Donor- intensity was measured. If the intensity values stayed constant 5 nM APT protein was added. All measurements were performed at room temperature in 5 mM Ammoniumcarbonate buffer, pH: 7.4.

5.2.3.4 Ambient Stopped-Flow Fluorescence Spectroscopy

To determine the association- and dissociation- rate of the FITC labeled palmitoylated APT Peptide (sequence: $(\text{NH}_2)\text{MC}(\text{palm})\text{GNNMSTK}(\text{FITC})-(\text{COOH})$, StorkBio, Estonia) to DOPC vesicles Stopped-Flow experiments were performed using the SX-18MV stopped-flow apparatus. For the FRET signal FITC labeled palmitoylated APT Peptide was excited at 435 nm and fluorescence emission of N-Rh-PE occurring from FRET was recorded through a 570 nm cutoff filter. 8 to 10

single injections were accumulated for each experiment. Determination of the dissociation- and association- rate was performed as previously described in [53]. The dissociation experiments were performed with a tenfold excess of unlabeled liposomes over labeled liposomes that were pre-equilibrated with the 400 nM APT peptide (final concentration in the observation cell: 200nM peptide). For the association experiment the peptide concentration in the observation cell was kept constant at 200 nM and the N-Rh-PE labeled DOPC vesicles were used in different concentrations. For APT activity measurements, labeled DOPC vesicles were pre-equilibrated with 400 nM APT peptide (final concentration in the observation cell: 200nM peptide) and transferred to one stopped flow syringe. In the other syringe, 200 nM APT protein (final concentration in the observation cell: 100nM protein) was added. For the measurement, solutions from both syringes were rapidly mixed and the decrease of the FRET signal was measured. All measurements were performed at room temperature in 5 mM Ammoniumcarbonate buffer, pH: 7.4.

5.2.4 Electron spray ionization - mass spectrometry (ESI-MS)

5.2.4.1 Protein ESI

To identify the precise mass of a protein Electron-Spray Ionization mass spectrometry coupled to liquid chromatography (LC-MS) was used. The protein solution to be analyzed was diluted with ddH₂O to a final concentration of 100 µM. 10 µL of the diluted protein solution was combined with 10 µL acetonitrile. 2.5 µL 1 % TFA (0.1 % stock solution) was added, gently mixed and centrifugated at 16000 rpm for 10 minutes. The supernatant was transferred to a HPLC vial. LC-MS using a LCQ (ThermoFisher) was performed as follows: 10 µL of the protein solution (containing ~400 pmol protein) were injected to a C4 column that was run with a linear gradient from 0% to 80% within 5 min, coupled to ESI-MS. MS spectra were analyzed with Xcalibur software (ThermoFisher, Waltham, USA) and MagTran.

5.2.4.2 Detection of APT activity on palmitoylated substrates

To investigate the activity of APT on different palmitoylated substrates Electron spray ionization - Mass spectrometry (ESI-MS) was used. The amount of the required substrates was aliquoted to a reaction vessel. A nitrogen flow was used to evaporate a large part of the solvent. The remaining solvent was removed by drying under vacuum over night. Afterwards the substrate was dissolved in 5 mM (NH₄)₂CO₃ buffer, pH 7.4. For the enzymatic reaction APT protein and the prepared substrate was mixed at the desired concentrations in a glass vial. To prepare ESI-samples and simultaneously stop the reaction at various time points, 50 µL of the reaction mixture were mixed with 50 µL MeOH. The prepared ESI sample was transferred to a HPLC vial. 10 µL of the sample were directly injected into the ESI-MS system. ESI-spectra were analyzed by Xcalibur software (ThermoFisher, Waltham, USA). The peak intensity of the appropriated peak was measured. Due to the lack of establishing a standard, for each point in time two to three samples of 50 µL were

taken out and each sample was measured three times, resulting in a 9 times measurement for each time point. The average values were plotted against time.

5.2.5 Sortase ligation

Sortase ligation of a palmitoylated peptide to a H-Ras protein was used to generate a full length palmitoylated H-Ras protein. For the ligation 400 μM palmitoylated peptide, containing a sortase recognition sequence ((NH₂)GGGGHKLRKLNPPDESGPGSMSC(palm)KSVLS(COOH), StorkBio, Estonia), was dissolved in buffer (20 mM Tris-HCl pH 7.9, 2 mM MgCl₂ and 5 mM DTE) with 5 % n-Dodecyl- β -D-maltoside. H-Ras Q179LPETG-(His)₆ was added to the solution to a final concentration of 200 μM . To start the reaction, sortase (final concentration: 100 μM) was added. The reaction mixture was gently mixed and incubated at 4 °C for 3 hours. To remove the sortase and the unligated Ras protein, the mixture was loaded on a 0.5 mL Ni-NTA column and was washed with 2.5 mL buffer (20 mM Tris-HCl pH 7.9, 2 mM MgCl₂ and 5 mM DTE). The flow through was loaded on a 1 mL DEAE column. To remove the unligated peptide, the column was washed with 10 times column volume. Elution of the full length Ras peptide was performed with buffer containing 250 mM KCl. The product was concentrated in an Amicon Ultra Centrifugal Filter (Merck Millipore, Billerica, USA). Labeling of the product was performed with FITC maleimid. For this, the used buffer was changed to 20 mM Tris-HCl pH 7.9, 2 mM MgCl₂ and 5 mM TCEP, with a NAP 5 column. Then 1.5x fluorescence dye was added and the reaction was kept in the dark for 1.5 hours. The reaction was purified with a nap 5 column and the product was concentrated in an Amicon Ultra Centrifugal Filter. At all steps of the ligation and the labeling SDS samples were taken and verified by a SDS-Gel.

5.2.6 DTNB assay

APT activity on Acetyl-CoA was detected with DTNB (5,5-dithiobis(2-nitrobenzoic acid)) [54]. For this DTNB (final concentration in the assay: 1 mM) dissolved in gelfiltration buffer without TCEP (50 mM Tris-HCl pH 8.0, 30 mM NaCl) was incubated in a 96-well microplate (Greiner Bio-One, Kremsmünster, Austria) for 5 minutes. Afterwards APT protein (final concentration: 100 nM) was added and incubated for 10 minutes. The reaction was started by adding AcCoA (final concentration: 1 mM) to the solution. Changes in the absorbance were detected at $\lambda_{abs}=410$ nm for 1 hour (every 45 sec) at 27 °C with the Microplate reader Infinite M200 PRO (Tecan, Switzerland).

5.2.7 OPTS assay

APT inhibition was ascertained by the OPTS (8-octanoyloxypyrene-1,3,6-trisulfonic acid trisodium salt, Sigma-Aldrich) assay. In this assay the hydrolysis of OPTS to the fluorescent HPTS (8-hydroxypyrene-1,3,6-trisulfonic acid) was detected in a Tecan Infinite M200 microplate reader

using 96-well microplates (GreinerBio-One, Kremsmünster, Austria) with $\lambda_{ex}=415$ nm and $\lambda_{em}=520$ nm.

To investigate the inhibition of APT by DTNB, 500 μ M APT was incubated with 0.25, 0.5 or 1 mM DTNB for 1 hour in a reaction vessel at room temperature. Afterwards 1 μ L of the APT-DTNB mixture was added to 99 μ L OPTS (final concentration: 100 μ M) in a 96-well microplates (GreinerBio-One, Kremsmünster, Austria). After adding the enzyme, the formation of fluorescent HPTS was recorded ($\lambda_{ex} = 415$ nm, $\lambda_{em} = 520$ nm) at 27 °C subsequently The reaction mixture was shaken prior to every new time point.

5.2.8 Crystallization

Highly pure hAPT1 Δ M60 S114C C186S C206S was used for the crystallization. DTNB was added to the protein, resulting in the following final concentrations: 875 μ M hAPT1 Δ M60 S114C C186S C206S and 0.75 mM DTNB. The crystallization screening was performed at 20 °C in TTP IQintelli 96-well sitting drop plates (TTP Labtech, Melbourn, UK) using different pre-composed crystallization screens from Qiagen. Therefore, 100 nL protein-DTNB solution were mixed on the plates with 100 nL of mother liquor by a TTP labtech Mosquito pipetting robot and 70 μ L of mother liquor were used as reservoir. Crystallization plates were tightly sealed to allow vapor diffusion between the protein drop and the reservoir solution. The crystallization growth was tracked by the Formulatrix Rock Imager. A final crystal was fished and stored in liquid nitrogen.

Data collection:

First the crystal diffraction was tested in-house at 100 K using either a Bruker Microstar or a Rigaku Micromax HF-007 rotating anode and mar345 CCD detectors. Well diffracting crystals were sent to the Swiss Light Source (SLS) at the Paul Scherrer Institute (Villigen, Switzerland) where a complete data set of crystal diffraction on beamline PXII was recorded.

Data processing:

The datasets were indexed, integrated and scaled using XDS and XSCALE and converted to .mtz file format by XDSCONV, all part of the XDS program package. All phases for the structure could be obtained by maximum likelihood molecular replacement using PhaserMR from the CCP4i program package. The structure was iteratively refined using Refmac5 and Coot, also from CCP4 program package.

Structure validation and illustration:

The structure model was validated using implemented plugins of coot. Additionally, the structure was uploaded to the validation service of the protein data bank (PDB). The shown structures are generated with the program PyMOL version v1.7.2.3.

6 Results

6.1 Development of an assay for physiological APT substrates

6.1.1 DTNB assay for colorimetric detection of free thiol groups

Several types of assays can be employed to investigate the thioesterase activity of APT proteins *in vitro*. An assay previously described in [30] is a colorimetric approach, where modified para- nitro- phenol (pNP) esters are hydrolyzed by APT, resulting in an increase of the yellow pNP product (Figure 6.1 a)). Another assay that was also established in our group is the fluorescence based OPTS assay (1-octanoyloxy pyrene-3,6,8-trisulfonic acid) (Figure 6.1 b)). Here, the reaction can be followed by the increase of fluorescent HPTS (1-hydroxy pyrene-3,6,8-trisulfonic acid) which arises from the APT cleavage reaction.

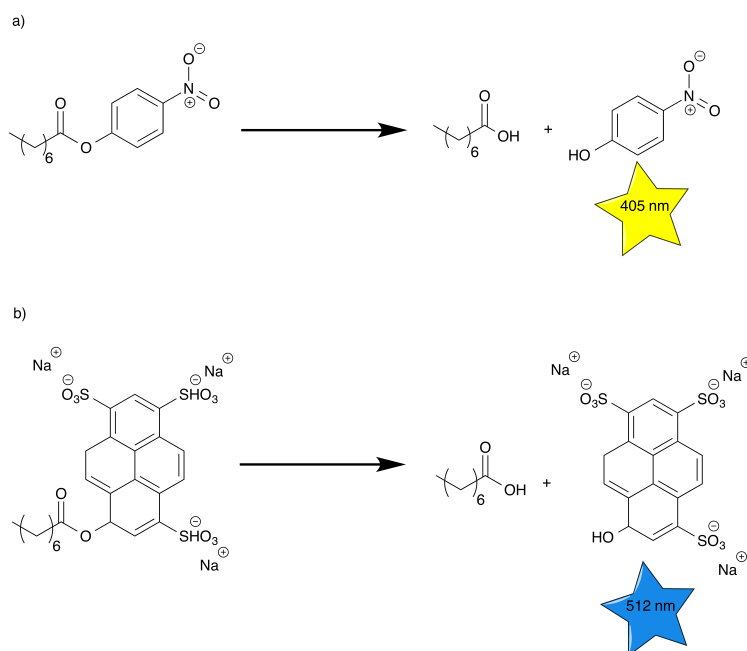


Figure 6.1: Two different artificial substrates to measure the thioesterase activity of APT.

Figure a) shows the para- nitro- phenyl octanoate. The fatty acid hydrolysis of this substrate by APT leads to the yellow pNP product that can be detected by its absorbance at 405 nm. Figure b) shows the hydrolysis reaction of the non-fluorescent OPTS (1-octanoyloxy pyrene-3,6,8-trisulfonic acid trisodium salt) to the fluorescent HPTS (1-hydroxy pyrene-3,6,8-trisulfonic acid trisodium salt) with an excitation of 320 nm and an emission of 396 nm.

Another fluorescence based approach to monitor APT's activity is the DiFMUO assay (6,8-difluoro-4-methylumbelliferyl octanoate) based on a coumarin substrate [46]. An issue for the pNP and DiFMUO assays is that the substrates are often difficult to solubilize so that detergents like CHAPS or Triton are required. Furthermore, the used substrates are artificial substrates and until now no assay for natural substrates is available.

To overcome the problem that these assays are only for artificial substrates, a DTNB (5,5-dithiobis (2-nitrobenzoic acid)) assay (previously described in [54]) was considered to investigate the APT activity on natural substrates (Figure 6.2). For this assay every natural substrate with a thio ester bond can be chosen. The resulting product from the APT cleavage then contains a free thiol group, to which one TNB (5-thio-2-nitrobenzoic acid) molecule can bind (Figure 6.2). The other free TNB molecule shows an absorption signal at 410 nm. Accordingly, if APT hydrolyzes the natural substrates there should be an increase in the amount of the yellow TNB product. A scheme of this mechanism is shown in Figure 6.2.

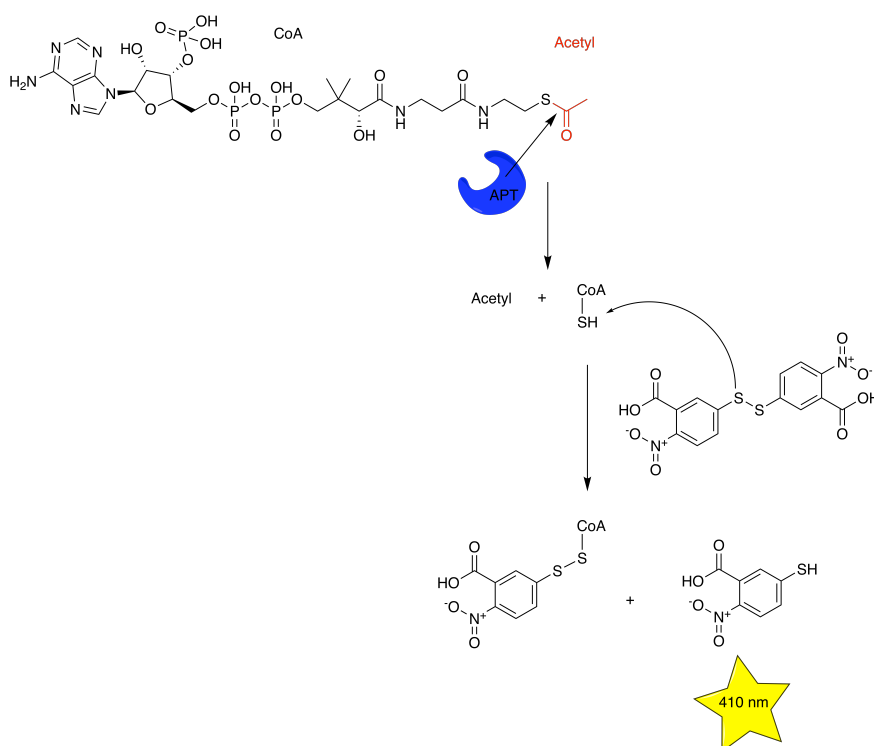


Figure 6.2: Mechanism of the DTNB assay. In the first step APT (blue) hydrolyzes the substrate (in this example: Acetyl-CoA (acetyl coenzyme A)). After the hydrolysis, the product contains a free thiol group, to which one TNB molecule can bind. The other free TNB molecule gives an absorbance signal at 410 nm [54].

A potential problem of the DTNB assay is that APT contains cysteine residues with a free thiol group, to which TNB can bind. But investigation of APT's crystal structure (displayed in Figure 6.3) shows that three out of five hAPT1's cysteine residues (purple) are buried, whereas modification

of the other two cysteine residues should not affect the substrate binding, since they are away from the active site.

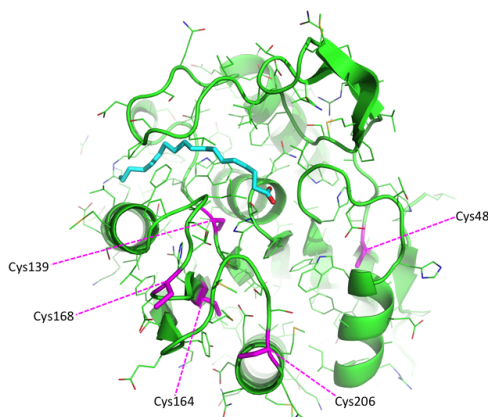


Figure 6.3: Crystal structure of hAPT (green). A fatty acid (blue) from xenopus APT1 is superimposed to indicate the active site and adjacent binding tunnel. Five cysteine residues that can be potentially modified with TNB are shown in purple.

The substrate Acetyl-CoA (acetyl coenzyme A) was used to test the DTNB assay. It was reported that hAPT1 shows an hydrolase activity on acyl-CoA substrates [55]. 100 nM hAPT1 and 1 mM DTNB were preincubated to saturate any potentially modifiable cysteine residues, then the reaction was started by addition of Acetyl-CoA. Unexpectedly, no changes in the absorption signal was observable, shown in Figure 6.4.

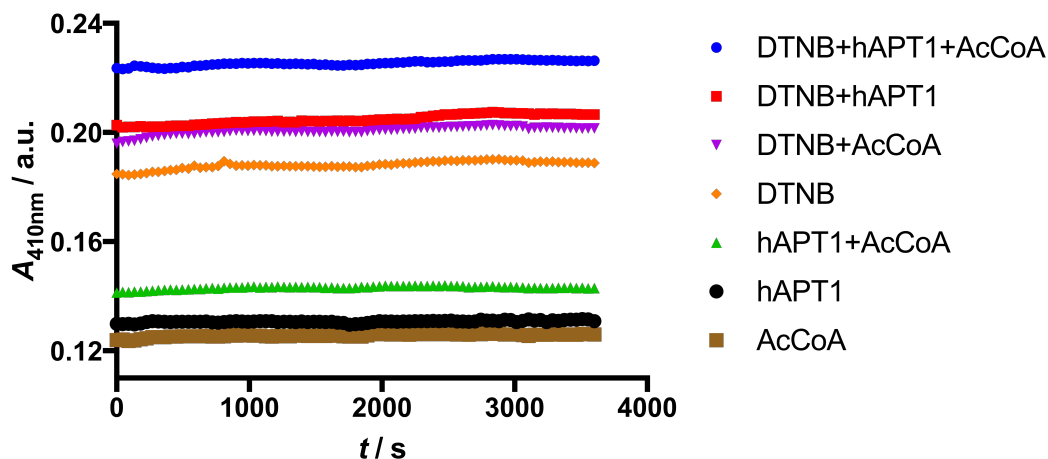


Figure 6.4: DTNB assay to investigate the activity of hAPT1 on Acetyl-CoA. After 10 minutes incubation of 1 mM DTNB with 100 nM hAPT1, 1 mM Acetyl-CoA was added and the changes in absorption were measured for 1 hour every 45 seconds at 410 nm. The reaction with all components is shown as the blue dots. Control experiments with two components DTNB+hAPT1, hAPT1+Acetyl-CoA and DTNB+Acetyl-CoA are shown in red, green and purple, respectively. In addition, single component control measurements were shown in orange (DTNB), black (hAPT1) and brown (Acetyl-CoA).

It was expected that hAPT1 mediated deacetylation of Acetyl-CoA would induce an increase in free TNB molecules and consequently lead to an increase in the absorption intensity. But there was no deacetylation of acetyl-CoA detectable in the assay, resulting in the assumption that hAPT1 was unable to deacetylate acetyl-CoA in presence of DTNB.

Due to the fact that TNB binds to free thiol groups, it was examined if TNB can bind to hAPT1's cysteines (shown in Figure 6.5) and thus possibly lead to the inactivity of hAPT1.

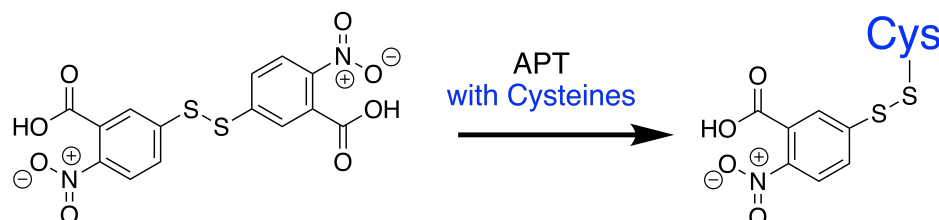
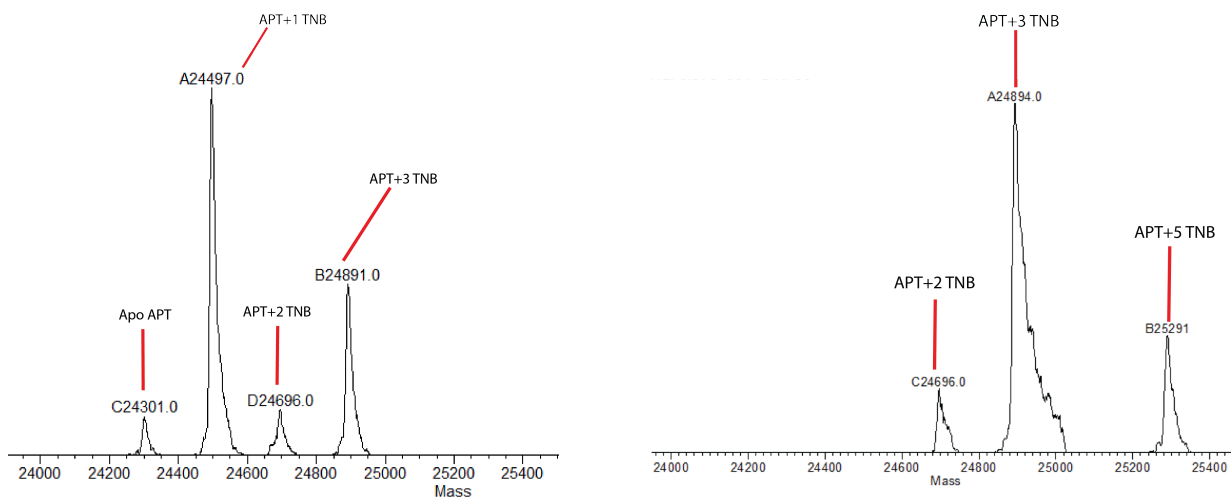


Figure 6.5: Scheme of how DTNB can bind to the cysteine residues of APT. One TNB molecule can bind to the cysteine residues (blue) of hAPT1 via a disulfide bond.

Therefore, the covalent binding of TNB molecules to hAPT1 was investigated by ESI-Mass spectrometry (detailed information about the method in section 5.2.4) to detect if there is a gain in APT's molecular weight. Figure 6.6 displays the protein masses of hAPT1 after incubation with different concentrations of DTNB.



(a) 20 μ M hAPT1 were incubated with 250 μ M DTNB for 15 minutes at room temperature. The reaction was stopped by adding the components which are required for the ESI-Measurement (Acetonitrile and formic acid). The resulting ESI-spectrum was transformed with the program MacTran to calculate the protein masses. Besides the mass of the apo hAPT1 protein (24301 Da), there were also masses corresponding to the binding of one (24497 Da), two (24696 Da) or three (24891 Da) TNB molecules per hAPT1.

(b) 20 μ M hAPT1 were incubated with 4 mM DTNB for 15 minutes at room temperature. The reaction was stopped by adding the components which are required for the ESI-Measurement (Acetonitrile and formic acid). The resulting ESI-spectrum was transformed with the program MacTran to obtain the protein masses. No apo hAPT1 protein (24301 Da) is detectable anymore, but there are masses corresponding to the binding of two (24696 Da), three (24891 Da) or five (25291 Da) TNB molecules per hAPT1.

Figure 6.6: Masses of hAPT1 after incubation with DTNB.

After incubation with 250 μM DTNB for 15 minutes (Figure 6.6 a), four masses were detectable. The lightest mass of 24301 Da belongs to the apo-APT protein. The second mass (24497 Da) shows a mass shift of 196 Da, corresponding to the binding of one TNB (MW: 199 Da, expected mass shift: 198 Da, difference of -1: loss of one H) to a cysteine residue of APT. The error of 2 Da is within the expected accuracy (± 3 Da) of the instrument LCQ (ThermoFisher). The third traceable mass has a molecular weight of 24696 Da, in comparison to the apo-APT protein a mass shift of 395 Da occurs due to the binding of two TNB molecules to two cysteine residues. Finally the fourth detectable mass has a molecular weight of 24891 Da. The increase of 590 Da compared to the apo Protein is caused by the binding of three TNB molecules to three cysteines. Thus the ESI-MS measurement reveals that TNB can bind to one, two or three cysteine residues. The DTNB binding test was repeated with higher DTNB concentrations (Figure 6.6 b). Here, all 5 cysteine residues (25291 Da) were covalently modified with TNB, even the cysteines buried in the core of the protein, which is not possible without serious destabilization of the protein fold due to the steric clashes of the DTNB moieties.

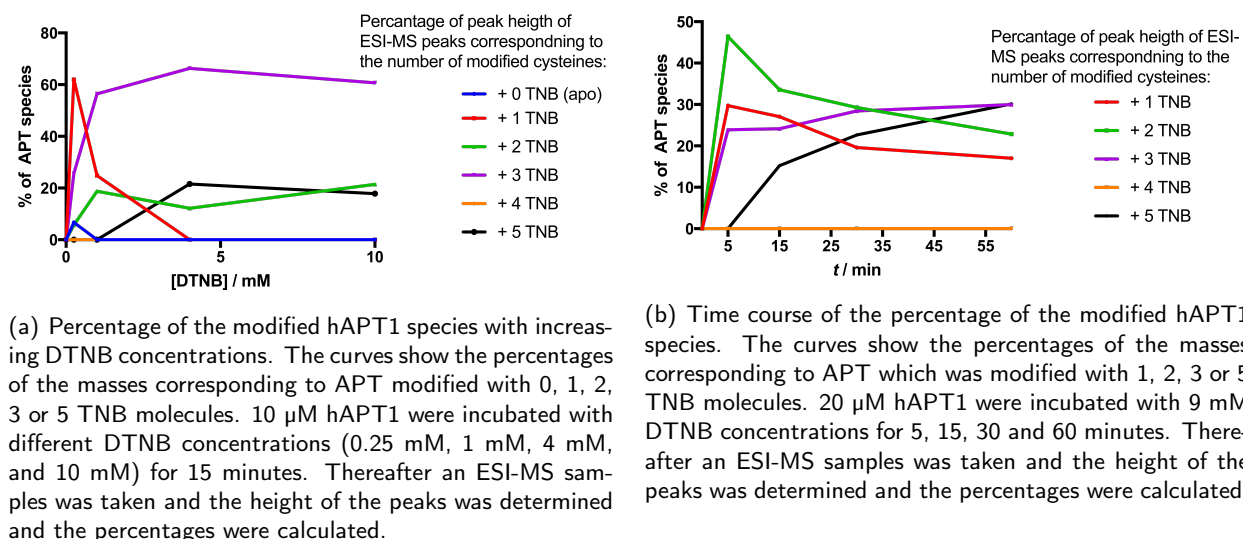


Figure 6.7: DTNB concentration and time depended cysteine modification of hAPT1.

To investigate the time and concentration dependence of the cysteine modification by TNB, an additional ESI-MS experiment was performed. The curves in Figure 6.7 a) show how many cysteines are modified after 15 min at different DNTB concentrations, and Figure 6.7 b) shows the time dependent modification of the cysteines by TNB at 9 mM DTNB. At a DTNB concentration up to 0.25 mM DTNB concentrations mostly 1 or 2 cysteines can be modified with TNB. However, with increasing DTNB concentrations the amount of 3 and 5 modified cysteines increases. In presence of 9 mM DTNB the time dependent experiment shows that hAPT1s with 1 and 2 modified cysteines decreases over the time. In parallel to that the amount of 3 and 5 modified cysteines increases over time. Apparently the modification of 4 and 5 cysteines is always parallel since no species with 4 modified cysteines is detectable.

The fact that all five APT cysteines can be modified, was quite unexpected and indicates a rather low stability of the APT protein. The instability seems to be an APT specific issue, because for other proteins, e.g. in [56] it was shown that DTNB was used to facilitate protein crystallization. It is still unknown in which order the cysteines were modified. According to the solvent accessibility the most likely order is Cys168 (61.6 % is H₂O accessible), Cys206 (40.2 %), Cys48 (10.7 %), Cys139 (0 %, completely buried) and Cys164 (0 %, completely buried).

However, this does not explain the failure of the assay in Figure 6.4: At 1 mM DTNB incubated for 10 minutes, only one or two cysteines should be modified, so that some APT activity should have remained. Thus, APT activity was tested with a fluorescence-based assay as described in the following.

To ascertain if the binding of TNB to APT has indeed an effect on APT's activity, an OPTS (8-octanoyloxypyrene-1,3,6-trisulfonic acid trisodium salt, Sigma-Aldrich) assay was performed after incubating hAPT1 with different concentrations of DTNB (Figure 6.8, for buffer and assay conditions see section 5.2.7).

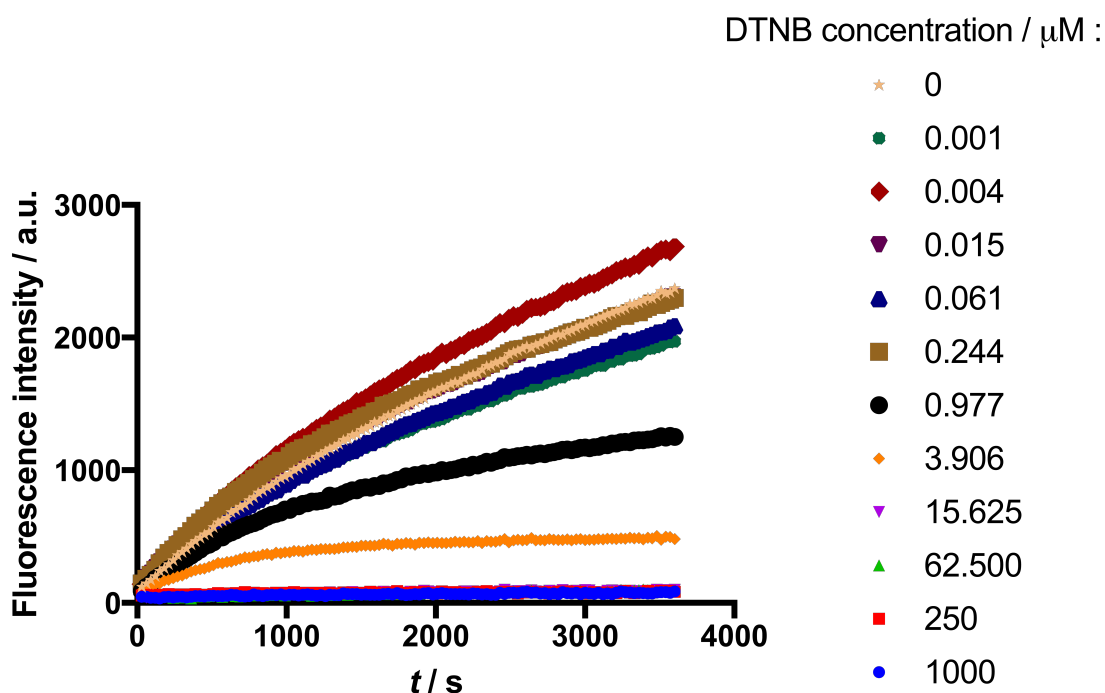


Figure 6.8: OPTS activity assay of hAPT1 after 15 min incubation with DTNB at concentration of 0-1 mM. 5 nM hAPT1 were pre-incubated with different DTNB concentrations for 15 minutes at room temperature, then 100 μM OPTS was added to the APT DTNB solution. The curves show the increase of HPTS fluorescence after OPTS cleavage by hAPT1. The curves indicate that the reaction velocity decreases with increasing DTNB concentration.

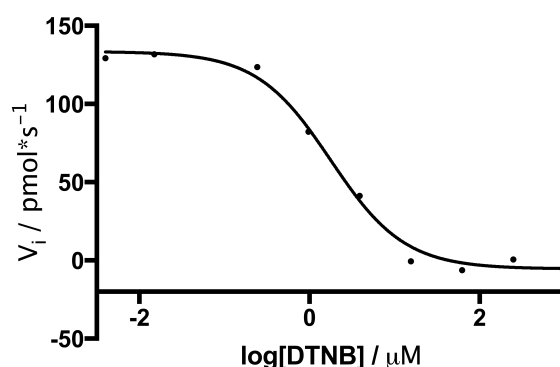


Figure 6.9: Reaction velocities of 5 nM hAPT1 hydrolysis on 100 μM OPTS with different DTNB concentrations. The K_i value is 350 nM according to the Cheng-Prusoff equation.

The curves of the OPTS assay (Figure 6.8) show that the reaction velocity decreases with increasing DTNB concentration. Thus DTNB is able to inhibit the APT activity. The question is if this inhibition is due to the unfolding of the enzyme or if there is another mode of inhibition. The reaction velocities were plotted against the DTNB concentrations (Figure 6.9) and the K_i was calculated (with the program Graphpad by Prism) as 350 nM. Since this K_i is much lower than expected from the DTNB-concentration dependent cysteine modifications, it was further investigated if the APT inactivation is caused by the unfolding after cysteine modification with TNB or if DTNB is a (competitive) inhibitor and can bind to the active site. Thus an OPTS assay with a parallel ESI-MS measurement was performed.

The hAPT1 hydrolysis of OPTS in absence of DTNB is displayed in orange (Figure 6.10). An increase of the fluorescence intensity over the time is detectable, caused by the formation of the fluorescent product HPTS. If hAPT1 is incubated in a ratio of 1:0.5 with DTNB, the hydrolyzation of OPTS (blue curve) is almost as fast as without DTNB (orange curve). However, with increasing DTNB concentrations (1:1 (red curve), 1:2 (green curve) or 1:10 (purple curve) APT:DTNB ratio) the hydrolysis of OPTS by hAPT1 is almost completely abolished.

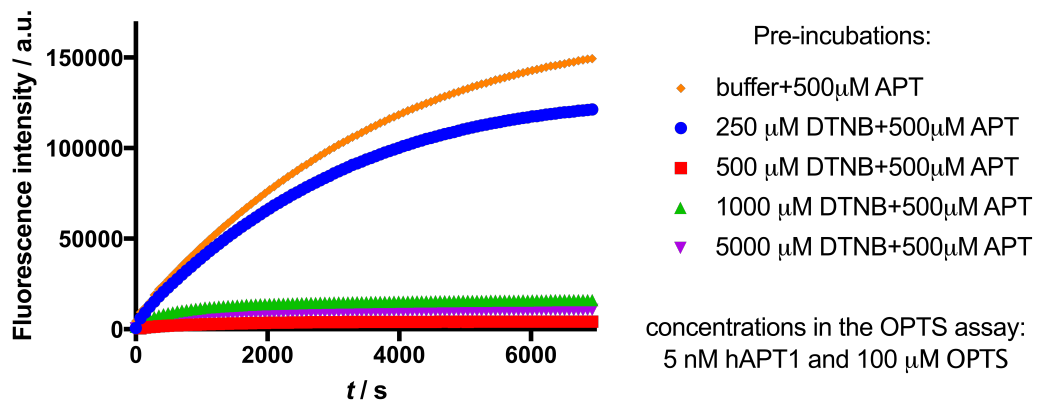


Figure 6.10: OPTS activity assay of hAPT1 after 1 h incubation with different concentrations of DTNB. A stock solution of 500 µM hAPT1 was pre-incubated with different concentrations (250, 500, 1000 or 5000 µM) of DTNB for 1 hour at room temperature. After incubation, the solution was diluted with gelfiltration buffer (see section 5.2.6) without TCEP in a ratio of 1:1000. For the OPTS assay, 1 µL of the diluted protein solution was added to 99 µL 101 µM OPTS solution (final concentrations: OPTS: 100 µM, hAPT1: 5 nM, DTNB: 2.5, 5, 10, and 50 nM) and the fluorescence of the reaction was measured in a plate reader for 2 hours. The curves show the increase of HPTS fluorescence after OPTS cleavage by hAPT1. The orange curve displays the hydrolysis of apo APT protein in absence of DTNB. If hAPT1 is incubated with DTNB in a ratio of 1:0.5 (blue curve) the reaction almost as fast as with the apo protein. However, if the DTNB concentration is increased to a 1:1 (red curve) or 1:2 (green curve), or 1:10 (purple curve) hAPT1:DTNB ratio the hAPT1 hydrolysis of OPTS is almost completely inhibited.

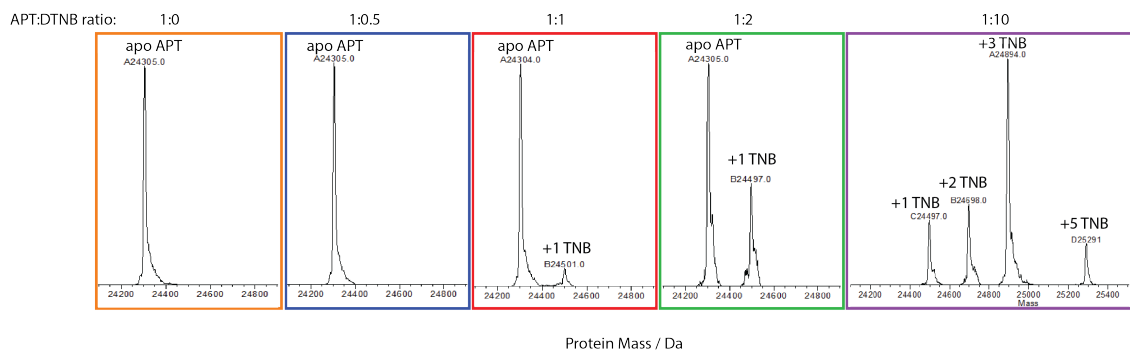


Figure 6.11: Results of the ESI-MS measurements after hAPT1 incubation with DTNB in different concentrations. The orange, the blue, the red, the green and the purple squared figures belong to the 1:0, 1:0.5, 1:1, 1:2 and 1:10 hAPT1 to DTNB ratio, respectively. In the first four ESI-MS measurements the mass of the apo hAPT1 protein (24307 Da) is detectable. With increasing DTNB concentrations (1:1 and 1:2), a mass of the modified hAPT1 protein with one TNB molecule (24503 Da) appears. In the 1:10 hAPT1 to DTNB ratio, no apo hAPT1 protein is detectable anymore, but masses of hAPT1 modified with 1, 2, 3 and 5 TNB molecules are present.

Directly before the OPTS assay (after incubation of hAPT1 with DTNB for 2 h), a sample for an ESI-MS measurement was prepared by adding acetonitrile and TFA. The results are displayed in Figure 6.11. hAPT1's mass without any DTNB incubation is 24307 Da. When 500 μ M hAPT1 is incubated with 250 μ M DTNB for 1 h at room temperature (in a ratio of 1:0.5) only the apo protein mass of 24307 Da is detectable. Upon incubation in a 1:1 hAPT1 DTNB (500 μ M+500 μ M) ratio mainly the mass of the apo Protein is detectable, but there is a small peak (~5 % of the height of the apo peak) at 24503 Da visible, which corresponds to the mass of hAPT1 modified with one TNB molecule. Furthermore, when 500 μ M hAPT1 is incubated with twice the concentration of DTNB, the peak of the protein modified with one TNB (24503 Da) increases to approximately 30 % of the apo peak. In the 1:10 hAPT1 to DTNB ratio, no apo hAPT1 protein is detectable anymore, but masses of hAPT1 modified with 1, 2, 3 and 5 TNB molecules are present.

The combination of the results of the OPTS activity assay with the ESI measurements (Figure 6.10 and 6.11) shows that in a 1:0 and 1:0.5 hAPT1 to DTNB ratio there is no protein modified by TNB and the OPTS hydrolyzation rate is fast in both cases. In the 1:1 hAPT1 to DTNB ratio there is just 5 % of the hAPT1's modified with one TNB molecule but there is no turnover of the OPTS detectable, thus the protein is completely inactive, but 95 % of the protein is not modified at all, leading to the conclusion that DTNB is also a non-covalent APT inhibitor. In the 1:2 and 1:10 hAPT1 to DTNB ratio the modifications of hAPT1 increase, but the protein is still inactive as expected. Unfortunately the crystallization with DTNB was unsuccessful, probably due to the mixture of modified and unmodified hAPT1 species. The crystallization experiment was set up with high DTNB concentrations (1:2 DTNB to hAPT ratio). Due to the low calculated K_i of 350 nM, a crystallization set up was performed with lower DTNB concentration (875 μ M hAPT1 Δ M60 S114C C186S C206S with 0.75 mM DTNB), where no cysteine is modified but APT is inhibited by DTNB, but the electron density for DTNB was only weak 7.1.

In summary, the DTNB assay turned out to be unsuitable for monitoring APT activity on physiological substrates. The fundamental reason why the assay shows no activity was the non-covalent binding of DTNB/TNB to hAPT1, leading to a catalytically dead hAPT1. A $K_i=350$ nM indicates a very tight binding, most likely in the substrate binding tunnel. At higher DTNB concentrations, DTNB apparently destabilizes and/ or unfolds the hAPT1 structure. To prevent this, the five cysteine residues could be mutated to e.g. serine, so that TNB is unable to bind to hAPT1. But even in that case the problem of the non-covalent inhibition would make this assay unsuitable.

6.1.2 ESI-MS measurements for physiological APT substrates

As described in section 6.1.1 several assays can be used to monitor APT's activity on artificial substrates. Until now, no assay shows how APT could depalmitoylate any biological substrates. Since the DTNB assay turned out to be unsuitable for measuring the APT activity on biological substrates, an electrospray ionization-mass spectrometry (ESI-MS) approach was established

together with Stefan Baumeister to determine the kinetics of catalysis of hAPT1 and hAPT2 on different biological substrates. Three different kinds of substrates were used for this assay as shown in Figure 6.12. The first one is lyso-palmitoylphosphocholine (lyso-PPC, Avanti Polar Lipids, US) to investigate the lyso-phospholipase activity of hAPT, as described in [20]. The second substrate is di-palmitoylphosphocholine (DPPC, Avanti Polar Lipids, US), to analyze if hAPTs have no detrimental effect on these lipids that are used as model membranes as described in section 6.2.2.1. It was reported that both human APT isoforms are N-terminally palmitoylated on their Cys2, and that both show autodepalmitoylation [33]. Furthermore, it was proposed that hAPT1 is able to depalmitoylate isoform 2 *in vivo* but not vice versa [33], [34]. Thus, an N-terminal hAPT1-peptide was used to investigate hAPT1 and hAPT2 activity on the palmitoylated hAPT1 N-terminus *in vitro*, so the third substrate is a palmitoylated peptide, corresponding to the N-terminus of hAPT1 (sequence: (NH₂)MC(palm)GNNMSTK(FITC)-(COOH), StorkBio, Estonia).

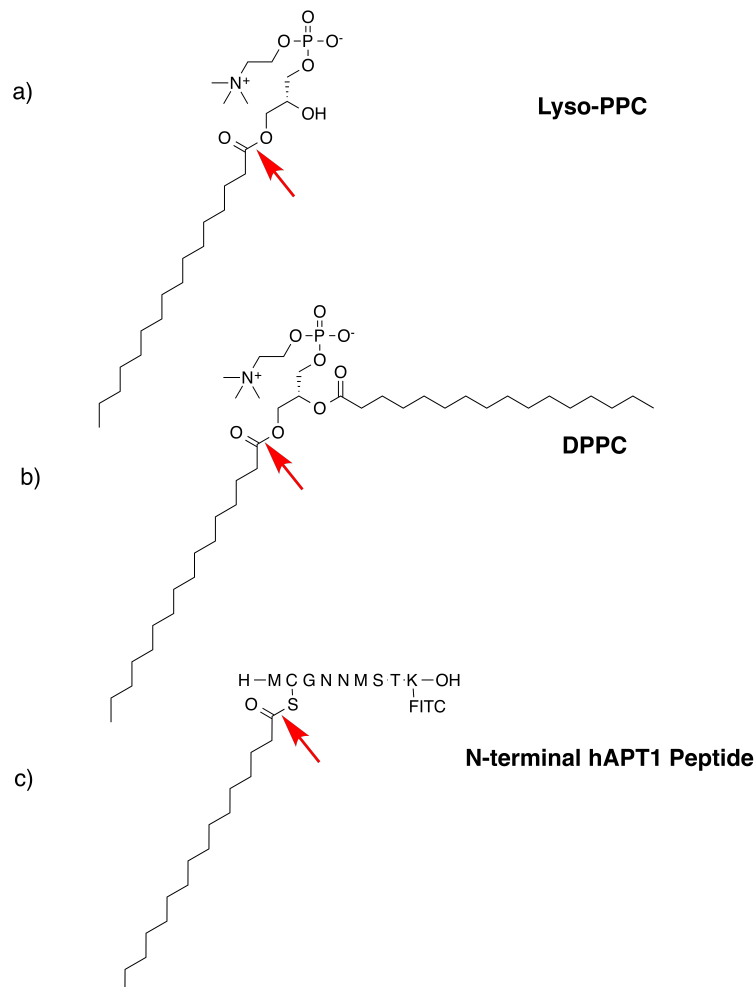
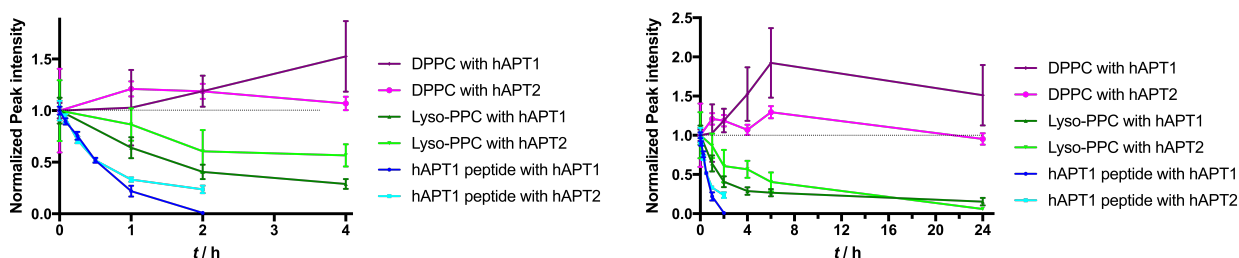


Figure 6.12: Chemical structures of three different physiological substrates of hAPT. a) Lyso-palmitoylphosphocholine (lyso-PPC), b) di-palmitoylphosphocholine (DPPC) and c) a palmitoylated peptide corresponding to the hAPT1 N-terminus. The red arrows show the ester bond which can be hydrolyzed by hAPTs.

For the assay, substrates and hAPT1 or hAPT2 were incubated in 5 mM (NH)₄CO₃ buffer and the reaction was stopped with MeOH at different time points (up to 24 hours). The maximum soluble concentrations for lyso-PPC was 0.2 μM and for DPPC 0.1 μM, whereas the peptide is well soluble in (NH)₄CO₃ buffer and could be used at 100 μM. For each time point a positive ESI-spectrum was measured (see section 5.2.4). The peak intensities of the substrates were assigned, integrated and plotted against the time (Figure 6.13). Regrettably, the use of a fatty acid standard, like palmitic acid, was impossible because of a very weak ionization efficiency of the fatty acid. Nevertheless the decrease of the substrate peak intensity could be monitored and for every time point six to nine samples were measured. The relatively good reproducibility is indicated by the error bars (in Figure 6.13).



(a) Relative peak intensities of different APT substrates in the first 4 hours.

(b) Relative peak intensities of different APT substrates monitored for 24 hours.

Figure 6.13: ESI-MS measurements to investigate the activity of human APT isoforms on different substrates. Substrates (100 μM hAPT1 peptide, 0.2 μM lyso-PPC and 0.1 μM DPPC) and hAPT1 or hAPT2 (for peptide measurement: 1 nM hAPT1/hAPT2 and for the phospholipids: 100 nM hAPT1/hAPT2) were incubated in 5 mM (NH)₄CO₃ at room temperature and samples were taken at different time points for an ESI-measurement. For each time point at least 6 replications were measured. The relative peak intensities were plotted against the time and the error bars indicate the standard error.

Figure 6.13 shows the time dependence of ESI-MS peak intensities for three different physiological APT substrates after incubation with hAPT1 or hAPT2. In the first 4 hours (Figure 6.13 a) a decrease in the amount of the hAPT1 peptide and lyso-PPC, but not DPPC is detectable for both hAPT1 and hAPT2. This trend is confirmed after 24 hours, where the DPPC peak intensity is still not decreasing significantly (as far as one can tell with the large errors), but significant cleavage activity can be clearly seen for lyso-PPC and the hAPT1 peptide. To estimate the turnover rate of the substrates the initial slope was calculated and apparent k_{cat} values were determined according to the following formula:

$$k_{cat} = \frac{\left(-\frac{d[S]}{dt}\right)_{max}}{[E]_0}$$

k_{cat} calculation with [S] = substrate concentration, t=time and [E] = Enzyme concentration,
 $(d[S]/dt)_{max}=V_{max}$ (assuming saturation of the enzyme)

These calculations take the hydrolyzed amount of substrate (100 μM hAPT1 peptide, 0.2 μM lyso-PPC and 0.1 μM DPPC) and protein concentrations (for peptide measurement: 1 nM hAPT1/hAPT2 and for the phospholipids: 100 nM hAPT1/hAPT2) into consideration. The determined k_{cat} values are summarized in table 6.1.

Table 6.1: Calculated (apparent) k_{cat} values for hAPT1 and hAPT2 hydrolyzing the APT1-peptide and lyso-PPC. The values reveal that hAPT1 and hAPT2 possess almost identical activity on the three substrates. No activity was observed for DPPC.

Apparent k_{cat}	hAPT1-peptide	Lyso-PPC
k_{cat} (hAPT1) / s^{-1}	26.2	$1.7 \cdot 10^{-4}$
k_{cat} (hAPT2) / s^{-1}	27.2	$1.2 \cdot 10^{-4}$

The k_{cat} value describes the enzyme turnover rate of a substrate per second. In this case, hAPT1 can convert $1.7 \cdot 10^{-4}$ molecules of lyso-PPC per second and both hAPT1 and hAPT2 are not active on DOPC in aqueous solution. This turnover rate is drastically slower compared to the artificial PPTS substrates (e.g. OPTS $k_{\text{cat}} = 4.5 \text{ s}^{-1}$) determined by Stefan Baumeister [30]. hAPT2 exhibits similar hydrolysis rate of $1.2 \cdot 10^{-4}$ molecules of lyso-PPC per second in aqueous solution. This might coincide with the poor solubility of lyso-PPC and especially DPPC, both are probably present in the form of micelles, but it shows that APT is clearly not a lipase (lipases are often activated by micelles and show k_{cat} values of $1 \cdot 10^4 \text{ s}^{-1}$ [57]). The amount of "soluble" phospholipids accessible to hAPTs is very likely much lower than the total substrate concentration, since they probably form aggregates, micelles or can stick to surfaces (for a better solubilization the phospholipids were sonicated before the measurements). Thus the calculated k_{cat} values for the phospholipids can be regarded as an upper limit of the turnover rate of hAPT1 and hAPT2. To improve the poor solubility, detergents can be used. A test ESI-MS measurement with DPPC and detergents was performed, but since the detergent had to be used in high concentration (above the critical micelle concentration (CMC)), it leads to a strong signal in the ESI-MS spectrum and also reduces the ionization efficiency of the phospholipid substrate.

A more physiological substrate in the ESI-MS measurement was the palmitoylated N-terminal hAPT1 peptide. It was tested if both human isoforms are able to depalmitoylate the hAPT1 peptide *in vitro*, because it was proposed that *in vivo* only isoform 1 is able to depalmitoylate hAPT1 and not isoform 2 [33]. Figure 6.13 shows the fast decrease of palmitoylated peptide and accordingly the hydrolyzation rate of both human isoforms. Compared to the phospholipids the peptide solubility is much higher and therefore the measured values are more reliable, which is also supported by the smaller error bars. As a result hAPT1 can convert 26.2 molecules of hAPT1-peptide and hAPT2 can convert 27.2 hAPT1-peptides per second in aqueous solution (see table 6.1). This is a lower limit, since it is not clear that both enzymes are saturated with the substrate, also depending on the accessibility of the palmitoylated peptide. At least the substrate is in 200 fold excess (200 nM peptide vs 1 nM enzyme). In contrast to the claimed fact in the literature that hAPT2 is unable to depalmitoylate hAPT1 *in vivo*, in the ESI-MS measurement both human isoforms are able to depalmitoylate the N-terminal APT1-peptide with similar efficiency.

Therefore hAPT2's inability of depalmitoylating hAPT1 *in vivo* must have another reason, perhaps due to a different localization in the cell, or due to a different regulation.

In summary, the ESI-MS measurements indicate that both human APT isoforms are able to (slowly) hydrolyze (lyso-)phospholipids, but to efficiently depalmitoylate an N-terminal hAPT1-peptide respectively. For phospholipids the determined kinetic parameters are a rough estimate because of the poor solubility and micelle formation. For the better soluble N-Terminal APT1-peptide the values are more reliable. The fact that hAPT1 and hAPT2 hydrolyze DPPC not at all makes it possible to use phospholipids as model membranes in further experiments. Furthermore, the ESI-MS data shows that both human isoforms are able to depalmitoylate the N-terminal APT1-peptide *in vitro* so that hAPT2's inability to depalmitoylate hAPT1 *in vivo* must be caused by another reason than an intrinsic difference between hAPT1 and hAPT2.

6.2 A FRET-based system to study the activity of human APTs on a membrane bound substrate

APT gained prestige when its ability to depalmitoylate proteins like $G\alpha$ and Ras in yeast [23] and later also the oncogenic Ras protein of higher organisms was described [15]. Studying the depalmitoylation of the protein substrates is of importance since most of them can be linked to diseases or malfunctions in biological systems. Accordingly, these depalmitoylation reactions are highly relevant, because interfering with these processes can be a starting point to develop potential drugs e.g. against cancer [32]. Several studies focused on the depalmitoylation of protein substrates *in vivo*, but the mechanism how APT gains access to the palmitoylated proteins is still unknown. It remains unclear if APT can actively extract and depalmitoylate the proteins, if APT's palmitoylation at Cys2 has an effect on the substrate extraction/depalmitoylation, or if some helper proteins (for instance FKBP12, which was described as a cofactor in Ras depalmitoylation [58]) are required to extract the membrane bound substrates and to present it to APT.

Furthermore, all known *in vitro* assays to date are focusing on (more or less soluble) artificial substrates (described in section 6.1.1) and APTs activity in solution. To analyze APT's activity in a more natural environment, model membranes made of DOPC are used in the following studies. To investigate the interaction of APT with a membrane bound substrate and simultaneously test the ability of human APT isoforms to depalmitoylate the Cys2 of hAPT1, *in vitro* assays with model membranes were performed. Therefore a palmitoylated and fluorescein (FITC)-labeled nonapeptide (Figure 6.14) with the N-terminal sequence of APT1 (that was also used for the ESI-measurements described above) was bound to vesicles and then treated with APT.

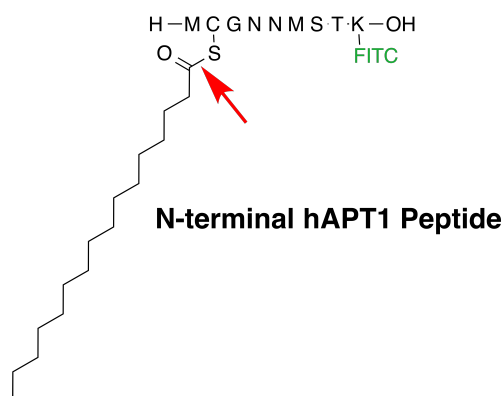


Figure 6.14: Chemical structure of the palmitoylated peptide corresponding to the hAPT1 N-terminus. The red arrow shows the ester bond that can be hydrolyzed by APTs.

Binding of the FITC labeled peptide to the vesicles labeled with 0.1 mol% 1,2-dioleoyl-sn-glycero-3-phosphoethanolamine-N-(lissamine rhodamine B sulfonyl) (N-Rh-PE) was detected by FRET. Figure 6.15 displays the fluorescence spectra of the two dyes, where FITC is used as donor (ϵ_{max} : 501 nm, ϵ_{max} : 515 nm) and rhodamine is used as acceptor (ϵ_{max} : 568 nm, ϵ_{max} : 591 nm). The overlap of the FITC (donor) emission and the rhodamine (acceptor) excitation that is necessary for the FRET effect, is discernible in Figure 6.15. The experiments were performed with a stopped-flow machine and the FRET from the FITC labeled peptide to the rhodamine labeled vesicles was measured at $\lambda_{em} = 435$ nm and recorded through a 570 nm cutoff filter (see section 5.2.3.4).

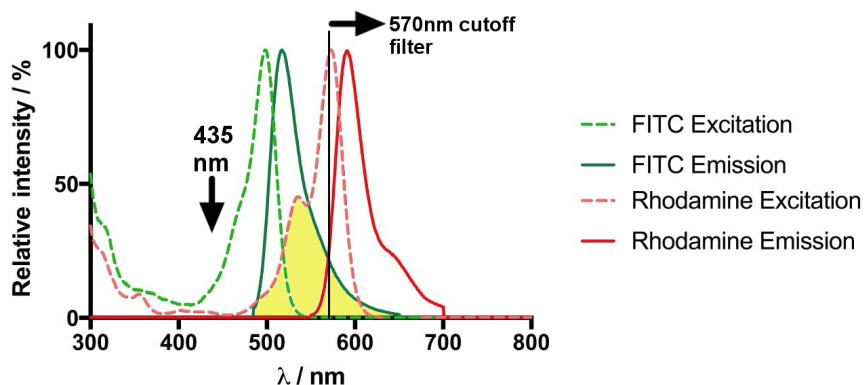


Figure 6.15: Fluorescence spectra of fluorescein (FITC) and rhodamine. The graphic displays the emission and excitation spectra of fluorescein and rhodamine in green and red, respectively. The yellow area highlights the overlap of the FITC excitation and rhodamine emission that is important for the FRET mechanism. The figure was designed with the ThermoFischer Fluorescence SpectraViewer and then modified. A suitable excitation wavelength is 435 nm, and FRET to the rhodamine can be seen with a 570 nm cutoff filter.

6.2.1 Determination of the association and dissociation rate of the palmitoylated N-terminal hAPT1 peptide to model membranes

To get insights if APT is able to actively extract a membrane bound substrate from the membrane, several kinetic parameters need to be determined. First of all the association and the dissociation rate of the palmitoylated peptide to or from the membrane has to be measured. These values are of importance for the comparison of the dissociation rate to the hydrolyzation rate of the peptide (k_{cat} values from section 6.2.2.1) potentially provides information if APT can access the peptide in membrane. If the hydrolysis rate for the membrane bound substrate (k_{cat}) is considerably higher than the dissociation rate (k_{diss}), APT must be able to either accelerate the dissociation or to depalmitoylate the peptide in the membrane. Vice versa, if the hydrolyzation rate of the membrane bound peptide is less than or equal to the dissociation rate, APT has to wait in solution for the peptide to leave the membrane to be able to depalmitoylate it. An example protein which can actively extract proteins from the membrane is the GDI (GDP dissociation inhibitor). This protein is able to accelerate the membrane dissociation of Rab GTPases from membranes [59].

Determination of the association and dissociation rates of the FITC-labeled palmitoylated N-terminal APT1 peptide to rhodamine labeled DOPC vesicles was implemented as previously described in [53]. DOPC lipids were chosen because they can form uncharged vesicles which are quite stable and, as shown above, APTs showed no activity on DOPC phospholipids. The vesicles were easily prepared by the freeze-thaw method (see section 5.2.3.1). The experiments were performed with a stopped-flow machine (SX. 18MV Stopped-flow apparatus, Applied Photophysics (Leatherhead,UK)) and the FRET from the FITC labeled peptide to the rhodamine labeled vesicles was measured at $\lambda_{\text{ex}} = 435 \text{ nm}$ and recorded through a 570 nm cutoff filter 6.15.

To measure the association rate, the FITC labeled peptide and the rhodamine labeled vesicles were mixed in a stopped-flow machine. The binding of the peptide to the vesicles leads to an increase in the FRET signal which can be measured over time. The dissociation rate can be determined by a decreasing FRET signal, which occurs, when the peptide dissociates from the rhodamine labeled vesicles to unlabeled vesicles that are added after equilibration, as shown in Figure 6.16.

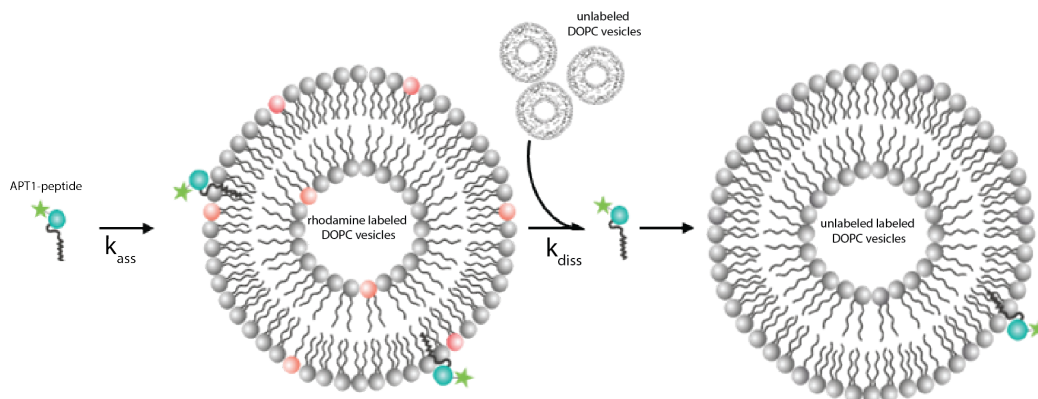
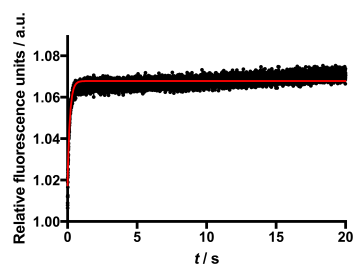


Figure 6.16: Scheme of the FRET-based assay to determine the association and dissociation rate of the APT1 peptide to DOPC vesicles. The association rate is monitored by the increased FRET signal which occurs upon the binding of the FITC labeled peptide to the rhodamine labeled vesicles (k_{ass}). The dissociation rate can be determined from the decreasing FRET signal which occurs when the peptide dissociates from the rhodamine labeled vesicles to the unlabeled vesicles added in excess (k_{diss}).

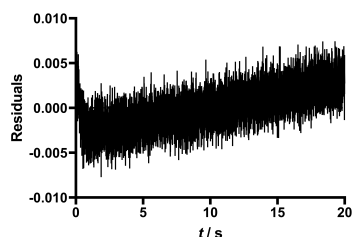
As shown in Figure 6.17, the association reaction of the palmitoylated APT1 peptide to the rhodamine labeled DOPC vesicles was accompanied by an increase in the FRET intensity as expected. The peptide-membrane association was found to be a single step process, as the time evolution of the association process could be described by a single exponential function with a k_{obs} of 5.91 s^{-1} (Figure 6.17).

The next step is determination of an apparent K_{d} value for binding of the FITC-labeled palmitoylated hAPT1 peptide to the DOPC vesicles by varying the vesicle concentration.

Figure 6.18 shows that by increasing the lipid concentration (and therefore also the vesicle concentration) stepwise from $0.39 \mu\text{M}$ to $100 \mu\text{M}$ while holding the APT1-peptide concentration constant, the observed association rates first decrease from ~ 4 to 1 s^{-1} , then increase to 10 s^{-1} (table 6.2). The calculated number of DOPC lipids in the bilayer of one DOPC vesicle with a diameter of 100 nm is approximately 93000 , assuming a surface area of 67.4 \AA^2 per DOPC lipid [60]. $0.39 \mu\text{M}$ DOPC can form 4.2 pM vesicles, so that an average of ~ 48000 peptides are bound per vesicle at 200 nM peptide concentration. On average 9300 N-Rhodamine-PE lipids are present per vesicle, covering 10% of the vesicle surface (corresponding to $0.1 \text{ mol}\%$ N-Rh-PE). At $100 \mu\text{M}$ DOPC, there are on average 186 peptides per vesicle. Thus at the highest ratios of peptide to lipids, each peptide has an area of $\sim 66 \text{ \AA}^2$ available (counting only the outer monolayer) or even 132 \AA^2 (if the peptide can flip in and out).



(a) Representative association curve.



(b) Residuals of the measured data.

Figure 6.17: a) Representative association curve of $0.2 \mu\text{M}$ hAAPT1-peptide to $75 \mu\text{M}$ rhodamine labeled DOPC vesicles. Due to the binding of the FITC-labeled peptide to the rhodamine labeled vesicles, the FRET signal increases over the time. The single exponential fit with a k_{obs} of 5.91 s^{-1} is shown in red. The slight increase of FRET in the plateau phase is probably due to dissolving micelles formed by peptide, leading to a second, slower phase of attachment to the vesicles. b) Residuals of the measured data to a single exponential fit. The fit was performed with the program Prism (by Graphpad).

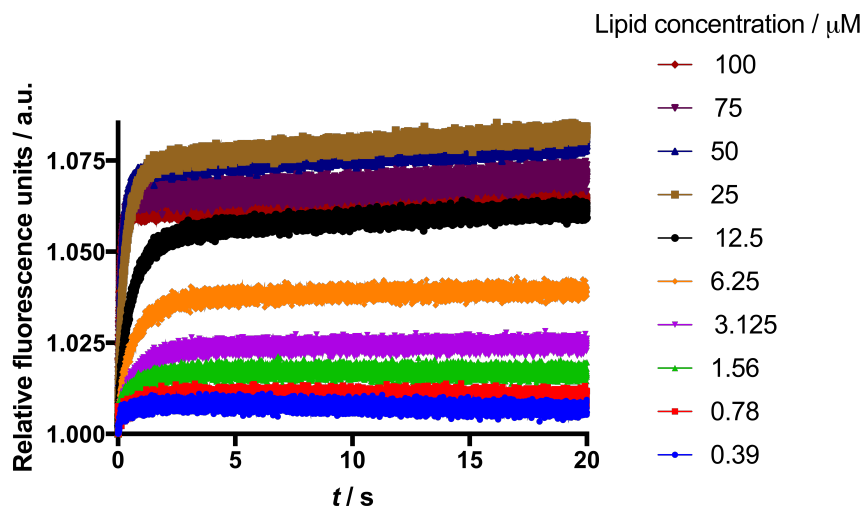


Figure 6.18: Association curves of $0.2 \mu\text{M}$ FITC-labeled, palmitoylated hAAPT1-peptide to rhodamine-labeled DOPC vesicles. The lipid concentration was increased from $0.39 \mu\text{M}$ to $100 \mu\text{M}$. As expected, an increased DOPC concentration gives rise to higher association rates. The experiments were performed with a stopped-flow machine and the FRET from the FITC labeled peptide to the rhodamine labeled vesicles was measured at $\lambda_{\text{ex}} = 435 \text{ nm}$ and recorded through a 570 nm cutoff filter.

This means that the peptides are extremely tightly packed. So the initial decreasing association rates can be explained like this: at the lower DOPC concentrations the vesicles are saturated with peptide, so that on average every third "lipid" in the vesicle would be a peptide molecule. This probably leads to formation of aggregates or mixed micelles that do not show a real association rate to an intact DOPC membrane, but artificially increase the values. The minimum k_{obs} is observed at 3.125 μM DOPC lipid concentration (table 6.2) which corresponds to $\sim 6\%$ peptides, making the presence of intact vesicles likely.

Table 6.2: Total amplitudes and observed rate constants for the different DOPC concentrations of the association curves. Additionally the number of peptide molecules per single DOPC vesicle are listed.

DOPC concentration / μM	0.39	0.78	1.56	3.125	6.25	12.5	25	50	75	100
Amplitudes/ a.u.	0.007	0.01	0.017	0.024	0.039	0.059	0.079	0.076	0.068	0.062
$k_{\text{obs}}/ \text{s}^{-1}$	3.99	1.50	1.38	1.06	1.12	1.12	1.86	3.96	5.91	10.45
Peptide molecules per vesicle	47805	23903	11951	5966	2983	1492	746	372	248	186

As expected, the overall amplitudes of the FRET signals displayed in the association experiments are also increasing with the lipid concentration. Since the binding reaction is $P + V \rightleftharpoons PV$ (with P=peptide, V=vesicle and PV=peptide-vesicle complex), the equilibrium is shifted towards the complex PV (the peptide-vesicle complex) with increasing V. This concentration dependency can therefore be used to estimate a K_d value for the interaction between the APT1-peptide and DOPC vesicles (previously described in [53]). Also, number of lipid molecules needed to constitute a binding site for one APT1-peptide can be determined. The amplitudes (listed in Table 6.2) were plotted against the lipid concentration. This is shown in Figure 6.19.

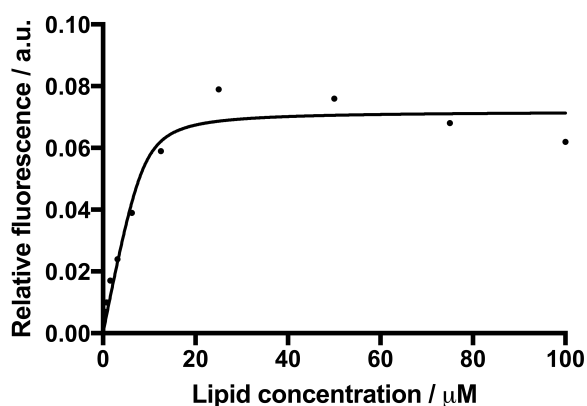


Figure 6.19: Amplitudes of the association curves. The amplitudes of Figure 6.18, corresponding to the end are plotted against the DOPC concentration.

The following equation was used to determine the K_d and the number of DOCP molecules that form one peptide binding site as previously described in [53]:

$$F = F_0 + \left(([P_0] + [L_0]n + K_d - \left(([P_0] + [L_0]n + K_d)^2 - 4[P_0][L_0]n \right)^{1/2}) \times (F_\infty - F_0) / (2[P_0]) \right)$$

With $[P_0]$: initial peptide concentration (0.2 nM), $[L_0]$: initial DOPC concentration, $[F_0]$: initial fluorescence signal, F_∞ : asymptotic limit, K_d : dissociation constant and n : fraction of DOCP molecules that form one peptide binding site. K_d , n and F_∞ are the only parameters that have to be fitted.

From the fit the constant n was found to be 0.023, meaning that one DOPC molecule represents 2.3 % of the membrane surface needed to bind one APT1-peptide, leading to the conclusion that 43 DOPC molecules are necessary to form an APT1-peptide binding site. The estimation for the K_d for binding of the palmitoylated hAPT1 peptide to the DOPC vesicles is 18.3 nM.

With these values for K_d and n , the association and dissociation rates for the APT1-peptide to the DOPC vesicles can be estimated. The observed rate constants from the association processes (Table 6.2) were plotted against the lipid concentrations (Figure 6.20). The slope of the line corresponds to k_{ass} and the y-axis intercept gives the k_{diss} value.

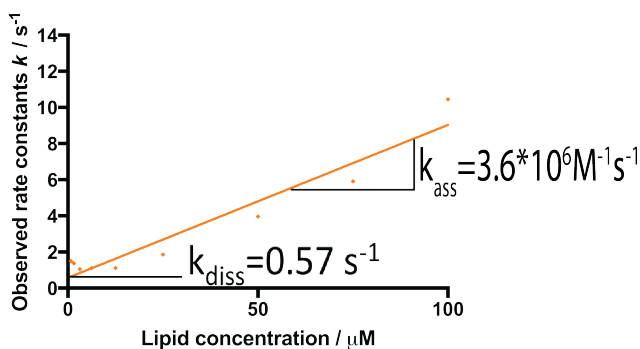
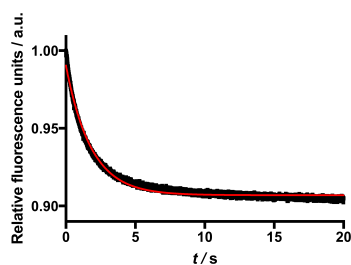


Figure 6.20: Observed rate constants of the association curves shown in Figure 6.18. The observed rate constants were plotted against the DOPC concentration. The slope of the line corresponds to k_{ass} and the y-axis intercept gives the k_{diss} value.

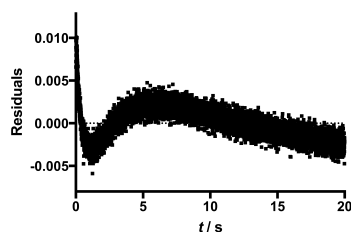
The number of DOPC lipid molecules per APT1-peptide binding site allows to normalize the concentration of the lipid and thus a determination of the apparent association rate constant for the first order process can be given. The slope from Figure 6.20 must therefore be multiplied by 43 (equivalent to dividing the DOPC concentration on the x-axis by 43), resulting in an association rate of $k_{\text{ass}} = 3.6 \times 10^6 \text{ M}^{-1} \text{ s}^{-1}$. The dissociation rate is given in this plot from the intercept on the y-axis and was found to be $k_{\text{diss}} = 0.57 \text{ s}^{-1}$. To investigate if these results are consistent with each other, the individual rate constants can be used to determine the K_d value, given by $K_d = k_{\text{diss}} / k_{\text{ass}}$. This value is $K_d = 158.3 \text{ nM}$, which is with consideration of measurement inaccuracy, especially with the y-axis intercept and therefore k_{diss} (Figure 6.20), being extremely sensitive to errors, in a

similar range to the estimated K_d value of 18 nM which was obtained from the amplitude titration 6.19.

Fortunately, another way to determine the dissociation rate of the APT1-peptide from DOPC vesicles is a direct measurement of the dissociation rate. For this, the APT1-peptide was bound to labeled rhodamine vesicles, and a ten fold excess of unlabeled ("dark") DOPC vesicles was added. Due to the exchange of the peptide from labeled to unlabeled vesicles the FRET intensity decreases. This dissociation measurement is displayed in Figure 6.21.



(a) Dissociation curve of 0.2 μM FITC labeled hAPT1-peptide bound to 25 μM rhodamine labeled DOPC vesicles after adding 250 μM unlabeled DOPC vesicles. The single exponential fit is shown in red.



(b) Residuals of the measured data to a single exponential fit. The fit was performed with the program prism by Graphpad. It's a quiet stable fit, with very small errors.

Figure 6.21: Dissociation curve of 0.2 μM FITC labeled hAPT1-peptide localized on 25 μM rhodamine labeled DOPC vesicles to 250 μM unlabeled DOPC vesicles.

The estimated dissociation rate from the single exponential fit (Figure 6.21) is $k_{\text{diss}}=0.55\text{s}^{-1}$. This is in very good agreement with the value of 0.57s^{-1} calculated for k_{diss} from the association measurements.

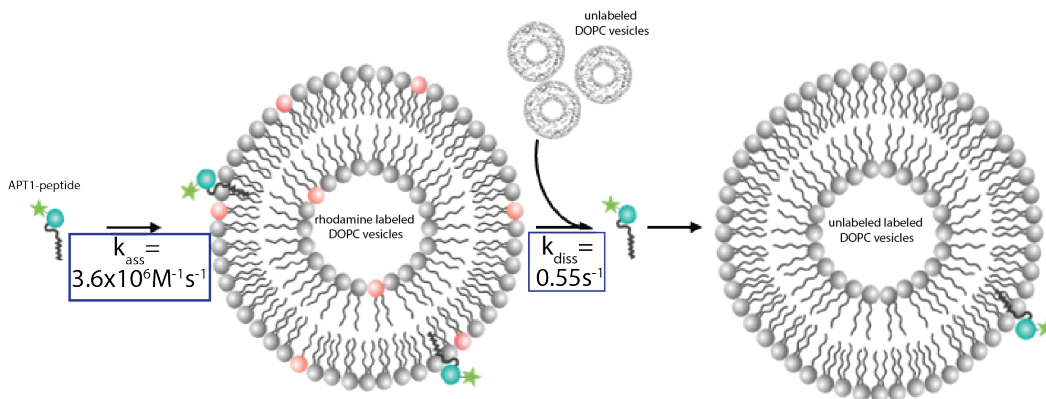


Figure 6.22: Association and dissociation process of the APT1-peptide to DOPC vesicles. The association rate was estimated as $k_{\text{ass}}=3.6 \times 10^6 \text{M}^{-1} \text{s}^{-1}$ and the dissociation rate as $k_{\text{diss}}=0.55 \text{s}^{-1}$, giving a K_d of 158 nM or 18 nM from the amplitude fit.

In summary, both the association and dissociation of the APT1-peptide to and from DOPC vesicles are single step processes. The complete association and dissociation reaction is shown in Figure 6.22. The association rate of the peptide to the rhodamine labeled vesicles was found to be $k_{\text{ass}}=3.6 \times 10^6 \text{M}^{-1} \text{s}^{-1}$, the dissociation rate was estimated as $k_{\text{diss}}=0.55 \text{s}^{-1}$. In addition, the estimated dissociation constant K_d was 158 nM according to the rate constant determination, or 18 nM from the amplitude fit. In the literature it can be found that typical dissociation rates for palmitoylated peptides are in the range of 0.69-6.9 molecules per second [61]. This is in a good agreement with the experimentally determined $k_{\text{diss}}=0.55 \text{s}^{-1}$. The estimated K_d for palmitoylated peptides in literature is around 60-196 nM [61], thus also the K_d values of 18 nM or 158 nM, also fits in the range of the literature value.

6.2.2 Steady state FRET assay for APT catalytic activity on palmitoylated peptides in DOPC vesicles

6.2.2.1 APT activity on the palmitoylated N-terminal APT1-peptide in DOPC vesicles

Following the determination of the fast association and slow dissociation rates of the APT peptide using stopped-flow kinetics, steady state kinetic measurements of the FITC labeled peptide associated to rhodamine labeled DOPC vesicles were performed using a Clariostar plate reader (BMG LABTECH). An advantage of the plate reader is that it can measure the changes in donor and acceptor fluorescence simultaneously. Vesicles were prepared by the freeze-thaw method and labeled with 0.1 mol% of the acceptor fluorophore N-Rh-PE. The wavelength for the donor signal measurements was set to $\lambda_{em} = 475 \text{ nm}$ and $\lambda_{ex} = 517 \text{ nm}$ and for the acceptor fluorescence to $\lambda_{em} = 450 \text{ nm}$ and $\lambda_{ex} = 590 \text{ nm}$. Figure 6.23 shows the fluorescence measurements, where first the peptide with the donor FITC label was bound to the vesicles and subsequently depalmitoylated after addition of hAPT1/2. In the first approximately 30 minutes, the fluorescence

signal of the peptide alone was measured until a reasonably stable baseline was reached. Thereafter, 500 μM rhodamine labeled DOPC vesicles were added. Due to binding of the FITC-labeled peptide to the vesicles the FRET efficiency increases, as expected. That means the acceptor (rhodamine) emission signal rises due to the electron transfer from donor (FITC) to acceptor, and the donor signal intensity decreases, due to the absorption of the emitted photons by the acceptor. After a constant baseline was reached, the addition of the enzymes followed. In presence of either the human APT isoform 1 or 2 the FRET signal decreases and the donor signal increases as expected, owing to the depalmitoylation of the peptide and therefore the loss of the binding to the vesicles. In presence of the catalytically inactive hAPT1S119A mutant the donor and acceptor signal stays practically unchanged, thus proving that the observed effects are really due to cleavage of the thioester bond of the peptide, leaving the palmitoyl moiety bound to the vesicles.

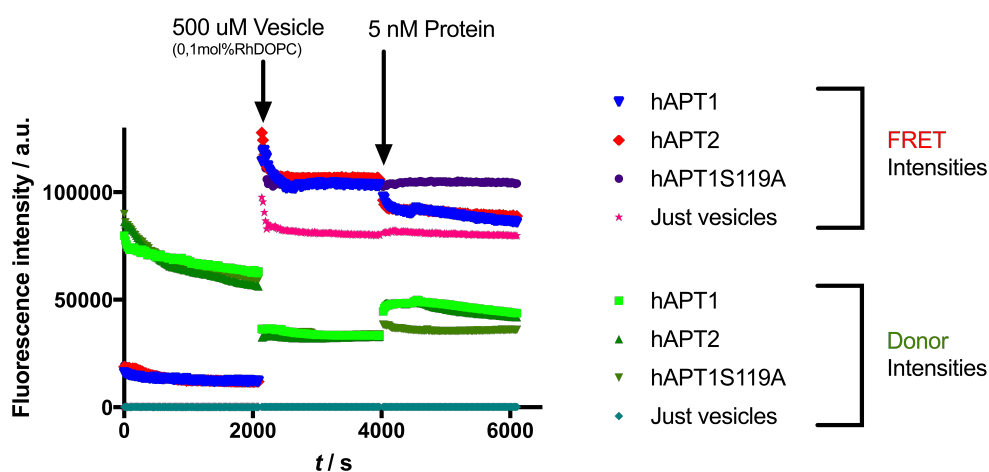


Figure 6.23: Measuring the APT activity on vesicle bound palmitoylated peptide. The donor and the acceptor intensities were measured simultaneously with donor fluorescence at $\lambda_{em} = 475 \text{ nm}$ / $\lambda_{ex} = 517 \text{ nm}$ and FRET fluorescence: $\lambda_{em} = 450 \text{ nm}$ / $\lambda_{ex} = 590 \text{ nm}$. In the beginning 200 nM hAPT1 peptide was measured until a baseline was reached. Upon addition of 500 μM rhodamine labeled DOPC vesicles the FRET intensity increases whereas the donor intensity decreases. After a stable plateau was reached, 5 nM of either active hAPT1, hAPT2, the catalytically inactive hAPT1S119A, or buffer were added. The depalmitoylation of the peptide by hAPT1 or hAPT2 results in the loss of the membrane anchor and loss of affinity of the peptide to the membrane. This is clearly shown by the decrease of the FRET signal and the simultaneous increase of the donor signal.

As Figure 6.23 shows, both hAPT1 and hAPT2 are able to depalmitoylate the palmitoylated hAPT1 peptide which was pre-bound to vesicles. It is clearly visible that both APTs can quantitatively depalmitoylate the vesicle-bound peptide since the intensities of the FRET signals will decrease over time to the ground state fluorescence FRET signal of vesicles alone (pink curve).

The apparent reaction velocity was estimated from the linear slope directly after APT addition and the k_{cat} values (assuming saturation of the enzyme) were calculated. They are for hAPT1: $k_{cat}=0.11 \text{ s}^{-1}$ and for APT2: $k_{cat}=0.12 \text{ s}^{-1}$, i.e. both human isoforms show similar activity on the hAPT1 peptide.

As described earlier in section 6.1.2, the estimated hydrolysis rate of the hAPT1 peptide in solution by hAPT1 and hAPT2 was ~ 27 molecules per second. Thus, the hydrolysis rate of the vesicle-bound peptide is reduced by a factor of 250. Compared to the dissociation constant of the APT1-peptide from the DOPC vesicles ($k_{\text{diss}}=0.55\text{s}^{-1}$, section 6.2.1), the estimated k_{cat} values are in a similar range, in contrast to the k_{cat} in solution (~ 27). These comparisons show that the rate limiting step in this process is most likely the dissociation of the peptide from the membrane. This suggests that APTs have no direct access to the membrane-bound peptides and are unable to actively extract the peptides from the membrane. The peptide has a high membrane affinity (K_{d} was determined in section 6.2.1 to be between 18 nM and 158 nM). Thus, only a tiny fraction of the peptide is readily accessible for APT, as most of the peptide (97-99%) is bound to vesicles and is not "free" in solution. Furthermore, under the conditions used in Figure 6.23 only approximately 40 peptides (calculation with DOPC surface area of 67.4 \AA^2 [60]) are bound to one DOPC vesicle with a diameter of $0.1 \mu\text{m}$, so that the enzyme is not working at maximum speed.

To investigate if the dissociation of the peptide from the membrane really is the rate limiting step of the reaction, the enzyme concentration has to be saturating. If the catalytic rate at saturating APT concentrations is still slower than k_{diss} of the peptide, the peptide dissociation is the rate limiting step.

Since in the FRET assay described in Figure 6.23 just 5 nM of the enzymes was used, the enzyme kinetic was measured at higher APT concentration (100 nM) with a stopped-flow machine. The association of the FITC labeled peptide to rhodamine labeled vesicles was again measured by FRET, with $\lambda_{\text{em}} = 435 \text{ nm}$ and recorded through a 570 nm cutoff filter. Results of the stopped flow experiment are displayed in Figure 6.24.

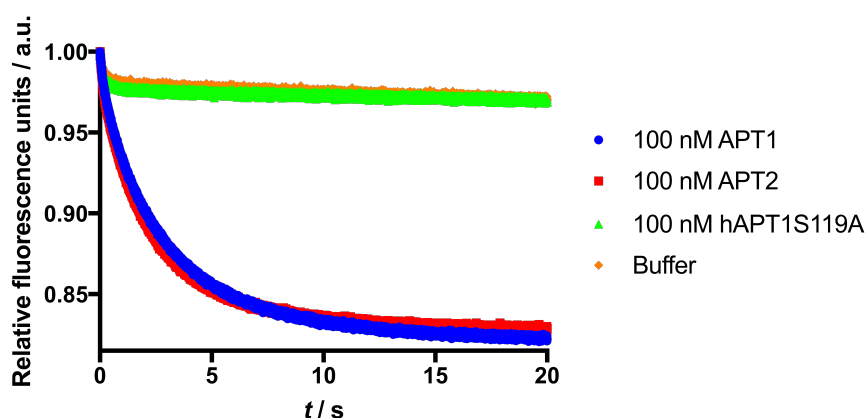


Figure 6.24: Stopped-flow measurement indicating the catalytic activity of hAPTs on the vesicle bound APT1-peptide. $0.2 \mu\text{M}$ APT1-peptide was bound to $25 \mu\text{M}$ $0.1 \text{ mol}\%$ rhodamine labeled DOPC vesicles. The graph shows the FRET signal decrease after mixing with $0.1 \mu\text{M}$ hAPT1 or hAPT2. A decrease of the FRET signal is detectable for both human isoforms hAPT1 and hAPT2 displayed in blue and red respectively. A single exponential fit yielded the k_{obs} values shown in table 6.3. Both controls, buffer (orange) and the dead hAPT1 mutant S119A (green) show no significant changes in the FRET intensity.

In presence of either of the human isoforms, hAPT1 (blue) and hAPT2 (red), a decrease in the FRET intensity is detectable. Both proteins were able to depalmitoylate the peptide which was localized to the DOPC vesicles, confirming the ESI-MS measurements (section 6.1.2) and the FRET measurements on the plate reader (section 6.2.2.1). Both control experiments, with buffer (orange) or the "dead" hAPT1 mutant S119A, show no changes in the FRET intensity. The k_{obs} values were determined by a single exponential fit with the software Prism7 (Graphpad). With these values, the estimated k_{cat} for both hAPT proteins was determined. All values are shown in table 6.3.

Table 6.3: Measured k_{obs} values and calculated (apparent) k_{cat} values for 100 nM hAPT1 or hAPT2 hydrolyzing 200 nM APT1-peptide bound to DOPC vesicles. hAPT1 and hAPT2 possess almost identical apparent catalytic activity on the substrate. The values for 5 nM APT are derived from the experiment described in Figure 6.23.

	$k_{\text{obs}} / \text{s}^{-1}$	k_{cat} with 100 nM APT / s^{-1}	k_{cat} with 5 nM APT / s^{-1}
hAPT1	0.33	0.47	0.11
hAPT2	0.39	0.57	0.12

The values in table 6.3 indicate again that both human isoforms show almost identical activity on the substrate peptide. Compared to the turnover rate with lower (5 nM) hAPT concentration ($k_{\text{cat}}=0.11 \text{ s}^{-1}$ and for APT2: $k_{\text{cat}}=0.12 \text{ s}^{-1}$), there is a significant increase of the k_{cat} values detectable in presence of higher APT concentrations (100 nM). Compared to the determined dissociation values ($k_{\text{diss}}=0.55 \text{ s}^{-1}$, section 6.2.1) of the APT1-peptide from the DOPC vesicles, the estimated k_{cat} values are now in a similar range. Assuming that the APT concentration is saturating in the stopped-flow experiment, i.e. each dissociating peptide is immediately hydrolyzed by APT, (Figure 6.24), the rate limiting step in this process is indeed the dissociation of the peptide from membranes, indicating that APT is unable to "actively" extract the peptide from the membrane. To determine a "real" k_{cat} value, the substrate should be in saturation, which is probably not the case here.

In summary, the FRET measurements show that hAPT1 as well as hAPT2 are able to depalmitoylate a peptide which was bound to DOPC vesicles. Calculation of the k_{cat} values reveals that both hAPT1 ($k_{\text{cat}} = 0.47 \text{ s}^{-1}$) and hAPT2 ($k_{\text{cat}} = 0.57 \text{ s}^{-1}$) show almost identical depalmitoylation activity on the peptide. The estimated k_{cat} values are in the same range as the dissociation value ($k_{\text{diss}}=0.55 \text{ s}^{-1}$, section 6.2.1) of the peptide from the DOPC membranes. Therefore it is likely that the dissociation is the rate limiting step, corroborating the assumption that APT is unable to extract the peptide from the membrane, but is "waiting" for the peptide outside of the membrane.

To further investigate these hypothesis, other techniques can be used to follow the depalmitoylation of the membrane bound substrate, e.g. fluorescence polarization. Stefan Baumeister showed with his method that both APT's are able to depalmitoylate the membrane bound peptide. APT1 in this assay shows a k_{cat} (0.38 s^{-1}) in the range of the dissociation rate. His assay showed that

hAPT2 is slightly faster (0.62 s^{-1}) than hAPT1 [30], but the values are still quite similar and corroborate the values found in this work. A microscopy assay to directly follow the depalmitoylation of the APT peptide in giant unilamellar vesicles is described in section 6.4.

6.2.2.2 APT activity on a palmitoylated H-Ras peptide in DOPC vesicles

APT was found to have many different biological substrates. For example various heterotrimeric G protein α subunits [23], [27], eNOS [28], RGS4 [23] and SNAP-23 [29] and Ras proteins [23]. To investigate APT's activity on other biological substrates, a longer (24 amino acid) mono-palmitoylated, FITC labeled C-terminal H-Ras peptide (Storkbio, Estonia) was used in the FRET assay (Figure 6.25). Compared to the short hAPT1 peptide this longer H-Ras peptide predicted to be able to interact with APT regions outside the binding tunnel.

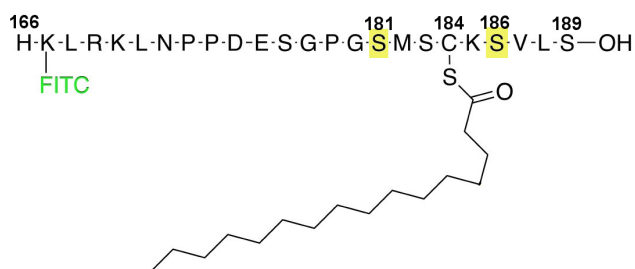


Figure 6.25: Chemical structure of the palmitoylated peptide corresponding to the C-terminus of H-Ras. Two cysteines (Cys186 from the CAAX box that is normally palmitoylated and Cys181 that can also be palmitoylated) were mutated to serine (highlighted in yellow) to prevent unwanted site reactions, the palmitoyl chain is attached to Cys184.

The same FRET experiment using rhodamine labeled vesicles that was performed for the palmitoylated hAPT1 peptide (in section 6.2.2.1) was repeated for the palmitoylated H-Ras peptide. The result is shown in Figure 6.26.

At time point zero, the H-Ras peptide is incubated for 30 minutes in the plate (Figure 6.26). In this pre-incubation time the fluorescence intensity of the FITC decreases. The loss of intensity could arise due to the formation of peptide aggregates or micelles: When the FITC molecules are very close to each other, the fluorophores can quench themselves [62], leading to a decreased signal intensity. In contrast to the hAPT1 peptide, the H-Ras peptide signal does not stabilize, which is shown in the noisy decrease of the donor intensities, indicating an inhomogeneous distribution of the peptide.

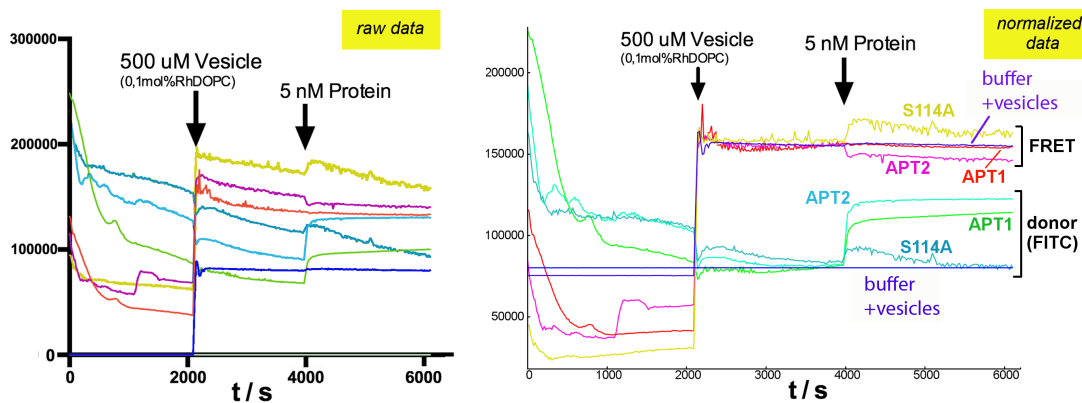


Figure 6.26: Measuring the APT activity on vesicle bound palmitoylated H-Ras peptide. The donor and the acceptor intensities were measured simultaneously with donor fluorescence at $\lambda_{em} = 475$ nm and $\lambda_{ex} = 517$ nm and acceptor fluorescence: $\lambda_{em} = 450$ nm and $\lambda_{ex} = 590$ nm. In the beginning 200 nM H-Ras peptide was measured for 30 minutes. Upon addition of 500 μ M rhodamine labeled DOPC vesicles the FRET intensity (acceptor intensity) increases, but this effect was not accompanied by a significant decrease in donor intensity. After a plateau was reached, 5 nM of either active hAPT1, hAPT2, the catalytically inactive hAPT1S119A or buffer were added, and now a clear increase in donor fluorescence is evident. The left graph presents the raw data whereas the right graph showed normalized to a base line after vesicle addition.

After approximately 30 minutes rhodamine labeled vesicles were added, and the FRET intensity ("Acceptor" in Figure 6.26) increases, but almost as much in the buffer control as in the peptide containing samples, however, the donor intensity does not decrease significantly. In comparison to the changes caused by the addition of hAPT1 peptide the changes for the H-Ras peptide are much smaller. A possible reason for the missing FRET signal could be a close contact quenching of the FITC label of the peptide with the rhodamine labeled lipids [63]. Another possible reason for the lower FRET efficiency could be a "propeller" effect of the (longer) peptide. That means that the fluorophor is rotating so fast that the electron transfer is quite inefficient. This assumption is supported by the fluorescence polarization experiments performed by Stefan Baumeister. In his polarization assay, there was no increased peptide polarization after addition to DOPC vesicles, as well [30]. Also the greater length of the H-Ras peptide by itself and thus the larger distance (56 Å in the "stretched" peptide between the FITC label and the palmitoyl chain) between the donor and acceptor could reduce the FRET efficiency, but it was shown by Masuko *et al.* that the fluorescein-rhodamine pair has a large Förster distance (~ 50 Å) [64]. Thus the length is not the major effect which leads to the

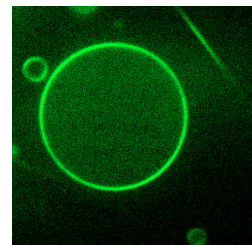


Figure 6.27: Rhodamine labeled DOPC vesicle with 10 μ M palmitoylated H-Ras peptide. The H-Ras peptide is enriched at the DOPC vesicle, indicating that the peptide in general can bind to DOPC vesicles.

reduced FRET efficiency, although the Förster radius of the FITC-rhodamine pair is ~ 50 Å, and the FRET usually allows measurement of distances of ± 50 % within the Förster distance, so that a FITC-rhodamine pair should be measured from 25 Å to 75 Å [64]. An other explanation would be if the peptide affinity to the peptide aggregates would be higher than to the DOPC vesicles. But at least a significant fraction does bind to vesicles, which is shown in a microscope experiment, where the palmitoylated, FITC-labeled H-Ras peptide is successfully bound to the DOPC vesicles (Figure 6.27), so the other explanations are more likely.

To investigate APT's activity on the membrane bound H-Ras peptide 5 nM, either active hAPT1, hAPT2, the catalytically inactive hAPT1S119A or buffer were added after approximately one hour (Figure 6.26). It is expected that the depalmitoylation of the peptide by hAPT1 or hAPT2 results in the loss of the membrane anchor and therefore the loss of its membrane affinity. This should be seen by a decrease of the FRET signal and the simultaneous increase of the donor signal. In presence of hAPT1 as well as hAPT2 the donor intensities increases indeed, whereas in presence of hAPT1S119A the signal stays practically unchanged and continues the slow decrease. From this intensity changes an estimated k_{cat} was calculated. For hAPT1 the k_{cat} is 0.37 s^{-1} and for hAPT2 the k_{cat} is 0.6 s^{-1} . Thus under the same conditions (200 nM peptide, 5 nM APT and 500 μM DOPC vesicles), as also used in the FRET experiment with the APT-peptide APTs can depalmitoylate the Ras peptide 5 fold faster than the APT-peptide ($\sim 0.1 \text{ s}^{-1}$).

For the FRET signals, just the signal in presence of hAPT2 slightly decreases, whereas the signal for hAPT1S119A shows a slight increase, and the signal for hAPT1 shows no change. Since there was no significant and clear FRET effect after the addition of the vesicles, this result is not surprising. Fortunately, the donor intensity clearly shows a very significant effect of the active APTs, in contrast to the hAPT1S119A and buffer controls. The hypothesis would be that the release of the peptide from the vesicles due to cleavage of the palmitoyl moiety also release the self- or close contact quenching of the FITC. Again, hAPT2 seems to be slightly faster than hAPT1, corroborating the results of Stefan Baumeister [30]. It is also evident that the palmitoyl moiety is the reason for the steady decline of all fluorescence intensities in Figure 6.26 since after cleavage by APT the intensities are perfectly stable. This also argues for a quantitative cleavage of the H-Ras peptide.

In summary, the FRET system for the H-Ras peptide has (in contrast to the hAPT1 peptide) some problems, probably because the palmitoylated H-Ras peptide is more prone to aggregate or micelle formation, resulting in a quenching of the FITC molecules. Nevertheless it was shown via microscopy (Figure 6.27) that at least a fraction of the peptide can bind to the vesicles and that both hAPT1 and hAPT2 are able to depalmitoylate the membrane bound peptide efficiently.

6.3 Investigation of hAPT's membrane affinity *in vitro*

Post-translational modifications of proteins play a major role in the way proteins interact with each other, bind nucleotides, and are located to cellular compartments. The (reversible) S-palmitoylation of cysteine residues leads to an increase in the hydrophobicity and hence the membrane affinity of many peripheral membrane proteins. Recently, it was reported that APT1 and APT2 are palmitoylated at Cys-2, and that APT1 is capable of depalmitoylating itself as well as APT2, but that APT2 can just depalmitoylate APT2 but not APT1 [34], [33]. The dynamic palmitoylation of APT1/2 may be needed for a steady state membrane localization and/or for efficient depalmitoylation activity on their membrane anchored substrates. Since all APT orthologs have extended hydrophobic areas, the first question is whether APT itself can bind to the membrane (Figure 6.28) or if an affinity tag like palmitoylation is necessary for APT's membrane localization, and/or if the function of the physiological palmitoyl moiety can be replaced by localising His-tagged APT to the membrane with artificial Ni-(NTA) bearing lipids (Figure 6.29b). For this task, the establishment of an artificial membrane system was required.

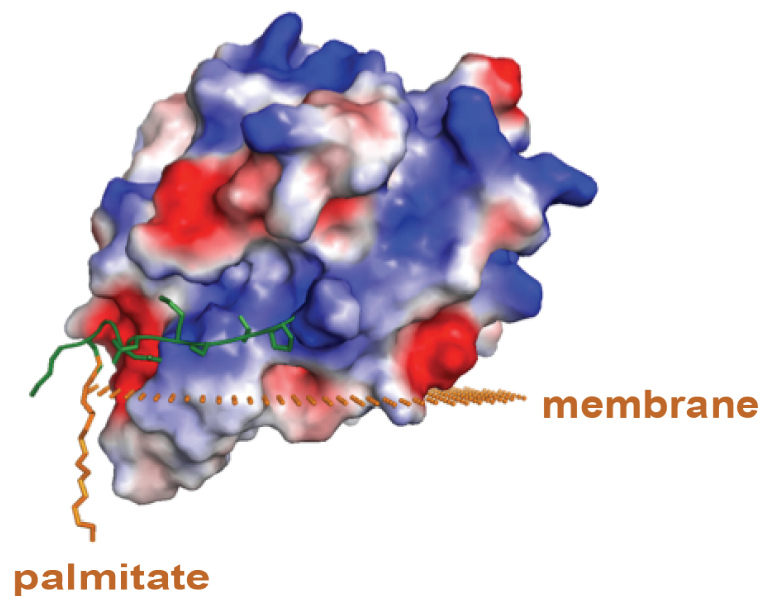


Figure 6.28: Prediction of how APT1 could be localized within the cell membrane (orange) by insertion of its hydrophobic patches. The APT model is palmitoylated (orange) at the N-terminal (green) Cys-2. The server <http://opm.phar.umich.edu/server.php> was used to predict the mode of insertion into the membrane.

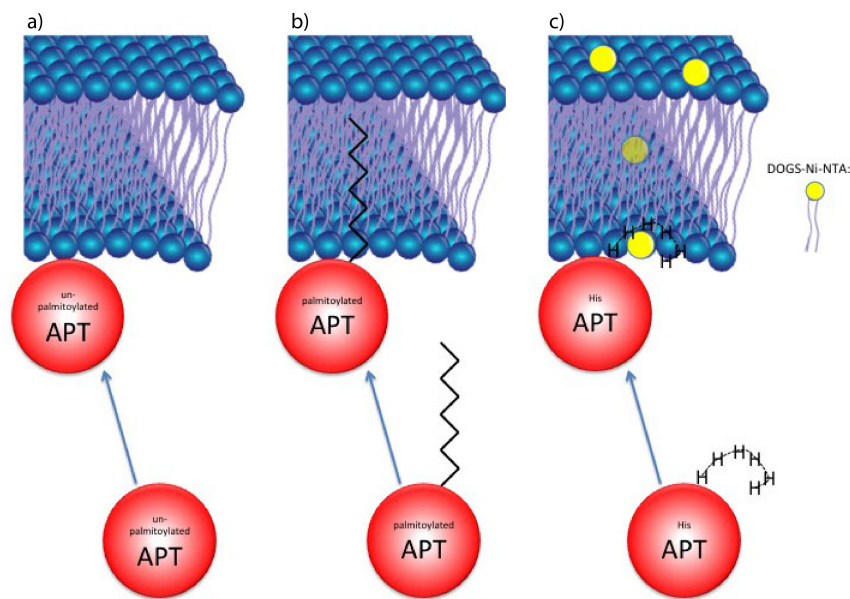


Figure 6.29: Scheme of APT (red) binding to the membrane (blue, purple). Two possibilities are depicted. a) APT can bind to the membrane by itself due to its hydrophobic patches. Or b) APT needs a membrane affinity tag like the palmitoyl chain for membrane localization. c) To force APT to the membrane, the palmitate can be replaced by a N-terminal His-Tag (black), which can bind to DOGS-Ni-NTA lipids (yellow lipids), see also Figure 6.30.

All organisms are surrounded by a plasma membrane, consisting of lipids that form a semipermeable bilayer with a thickness of 4-5 nm, in which integral or peripheral proteins are integrated. Lipid membranes build a protecting wall around the cells and enable a controlled exchange of materials. Furthermore, plasma membranes play an important role in cell-cell communication and in signal transduction pathways, to translate extracellular signals into inner cellular responses. Lipids forming the plasma membrane are glycerophospholipids, phosphosphingolipids and sterols, which all own a polar headgroup and a hydrophobic tail. The glycerophospholipids or phosphoglycerides are glycerol-based phospholipids that represent the main components of the eukaryotic plasma membrane. The phosphoglycerides' headgroup can be classified in an unmodified phosphoric acid (PA), the anionic phosphatidylserine (PS), phosphatidylglycerol (PG), phosphatidylinositol (PI), and the zwitterionic phosphatidylcholines (PC). Besides the different lipid constructs and headgroups, the plasma membrane lipids vary in their fatty acid modifications. The carbon chain in phosphoglycerides is between 12 and 24 carbon atoms long and can be saturated or unsaturated. The combinations of all these different lipid components allow a high lipid diversity in the plasma membrane [65], [66].

For *in vitro* studies lipid vesicles are used to simulate the plasma membrane. It was shown that simple lipid compositions in vesicles are sufficient to analyze the behavior of plasma membrane associated proteins *in vitro* [65]. The most commonly used lipids are DOPC (as a neutral model membrane) alone or in combination with DOPG (anionic lipids, to mimic the negatively charged plasma membrane). The lipids are shown in Figure 6.30.

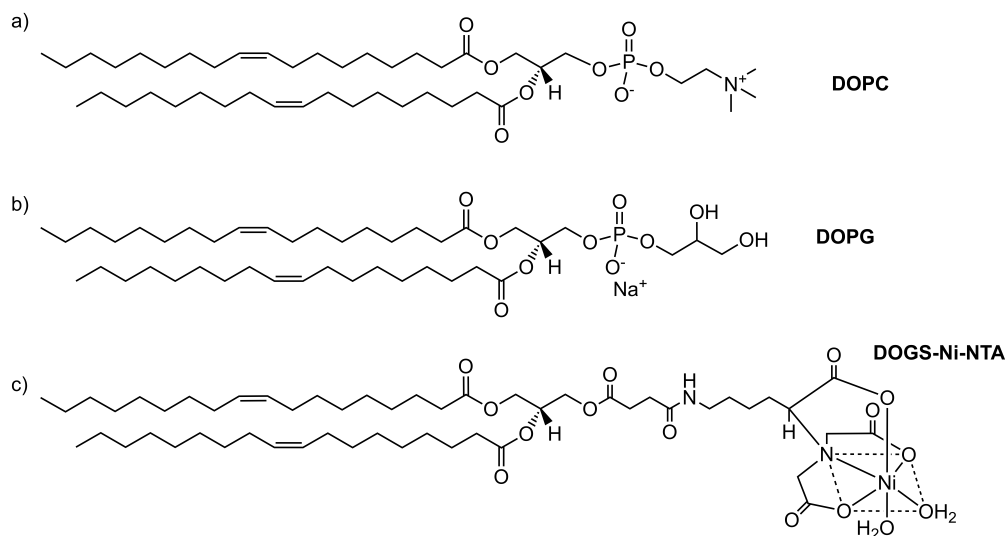


Figure 6.30: Chemical structures of a) DOPC (1,2-dioleoyl-sn-glycero-3-phosphocholine), b) DOPG (1,2-dioleoyl-sn-glycero-3-phospho-(1-*rac*-glycerol) (sodium salt)) and c) DOGS-Ni-NTA (1,2-dioleoyl-sn-glycero-3-((N-(5-amino-1-carboxypentyl)iminodiacetic acid)succinyl) (nickel salt))

For fluorescence microscopy analysis, giant unilamellar vesicles (GUV) with a diameter of usually 5-60 μm were prepared by the method of electroformation (see section 5.2.3.2) [67]. Here, a thin lipid layer is spread on an indium tin oxide (ITO)-coated cover slip. After mounting of the cover slips into the microscopy cell holder the lipids were hydrated with buffer and electroformation was performed with a sinusoidal alternating low-frequency voltage (for more information see section 5.2.3.2) [66]. The electric field decreases the attraction between lipid layers and destabilizes the bilayers, which facilitates the bending of the budding vesicles. A scheme of the GUV preparation with electroformation is shown in Figure 6.31. The used temperature, voltage and frequency depend on the particular used lipid mixture.

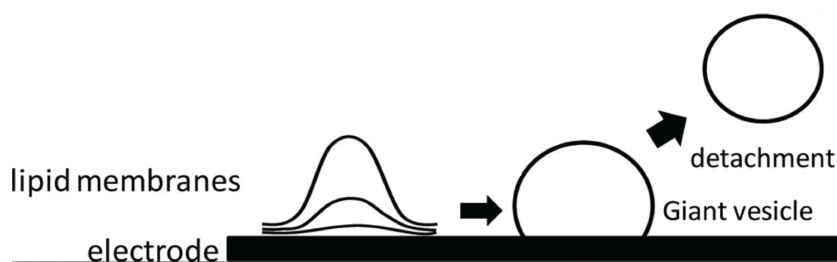


Figure 6.31: Scheme of GUV electroformation modified from [68]. Thin lipid layers are spread on an ITO coated cover slip. After voltage application the vesicles starts to bend. A detachment of a vesicle from the cover slip follows after a vesicles is completely formed.

Before testing APT's activity on a membrane anchored peptide in GUV's it was tested if APT itself can bind to GUV's as predicted (Figure 6.28).

Thus, the association of mCherry labeled hAPT1 or hAPT2 with BODIPY-FL_{C12} labeled DOPC vesicles was investigated. As control, a His-tagged APT1-mCherry was used in conjunction with DOPC vesicles containing 20 mol% DOGS-Ni-NTA lipids (chemical structure is shown in Figure 6.30).

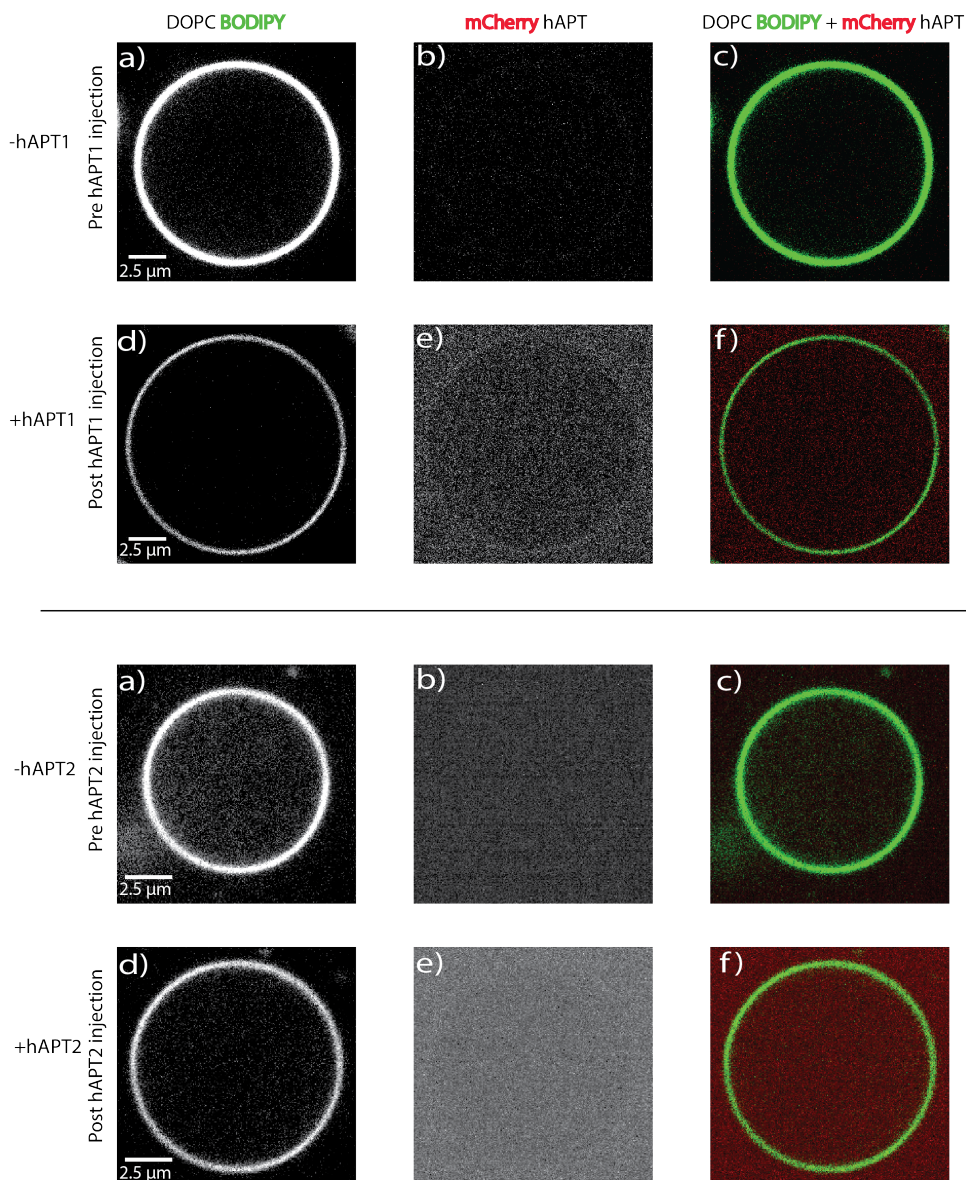


Figure 6.32: Experiment to investigate if hAPT1/hAPT2 can bind to model membranes.

a) DOPC vesicles containing 0.2 mol% BODIPY-FL-C12 (green) were produced using the method of electroformation. b) Before the addition of hAPT1-mCherry or hAPT2-mCherry there is no signal detected in the red channel. c) Merge of the green and red channel, before the addition of hAPT1/2-mCherry. d) After the addition of 2 μM hAPT1/2-mCherry the green channel stays unchanged. e) A random distribution of hAPT1 exists around the vesicles. f) There is no enrichment of hAPT1/2 on the membrane detectable when images are merged.

As shown in Figure 6.32, neither hAPT1-mCherry nor hAPT2-mCherry show any significant enrichment at the DOPC model membrane, in contrast to the control experiment shown in Figure 6.33.

As a positive control and to investigate if the membrane-anchored APT is detectable at all, N-terminally His-tagged hAPT1 was used in combination with DOGS-Ni-NTA lipids to mimic the palmitoyl moiety (Figure 6.29 c). In presence of this affinity tag, it is possible to attach APT to the membrane and visualize it, as shown in Figure 6.33. Around $8 \cdot 10^7$ (or $4 \cdot 10^7$ on the outside) binding sites (i.e. Ni-NTA-lipids) for His-hAPT1 molecules are present at the vesicle with a diameter of approximately $9.2 \mu\text{m}$, shown in Figure 6.33 e) (calculation is based on the DOPC surface area of 67.4 \AA^2 [60]), corresponding to a saturation concentration of one APT molecule per 333 \AA^2 of the vesicle surface, or twice this area if assuming that 50 % of the Ni-NTA lipids are in the inner leaflet of the vesicle. Since the diameter of an APT molecule is approximately $30\text{-}40 \text{ \AA}$, this should be sterically possible. In a Z-section of $1 \mu\text{m}$ thickness, approximately 10^7 APT molecules should be available for visualization.

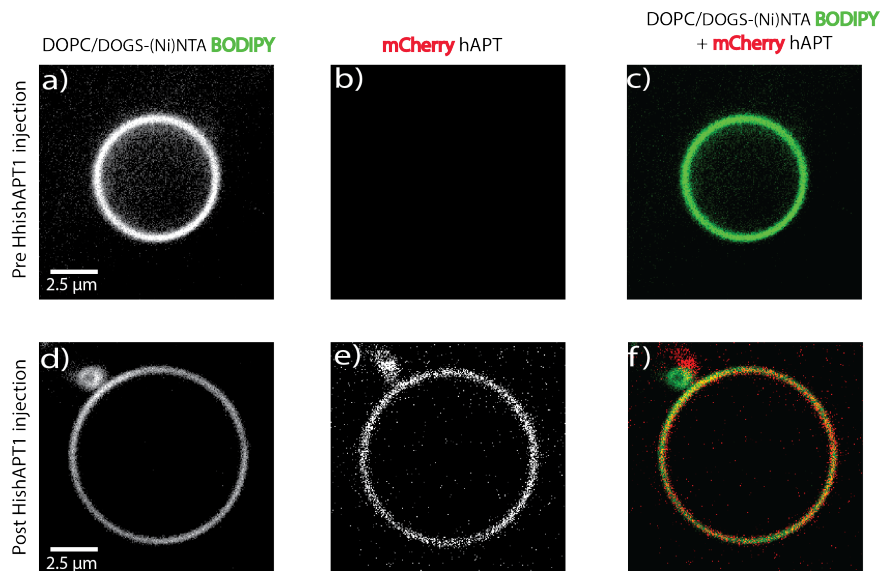


Figure 6.33: Control experiment to test if APT1 can be detected when anchored to vesicles in the microscope. a) 80 mol% DOPC/20 mol% DOGS-(Ni)NTA vesicles containing 0.2 mol% BODIPY FL C12 (green) were produced using the method of electroformation. b) Before the addition of HishAPT1-mCherry there is no detectable signal in the red channel. c) The merge of the green and red channel, before the addition of HishAPT1-mCherry. d) After addition of $2 \mu\text{M}$ His-hAPT1-mCherry the green fluorescence of the vesicle stays unchanged from controls. e) The red channel shows accumulation of HishAPT1-mCherry in shape of the vesicle. f) Merge of d) and e) to show enrichment of HishAPT1 on the DOPC vesicle that contains additional DOGS-Ni-NTA lipids to capture the His-tag of APT1.

It is well known that the charge of the membrane can influence the membrane binding of proteins. DOPC is zwitterionic and therefore is a neutral lipid. To investigate if a negatively charged membrane can induce hAPT1 localization to the membranes, an assay with DOPC-GUV containing 30% negatively charged DOPG lipids was performed (Figure 6.34).

As a result, the assay indicated that hAPT1 does not bind to negatively charged vesicles either.

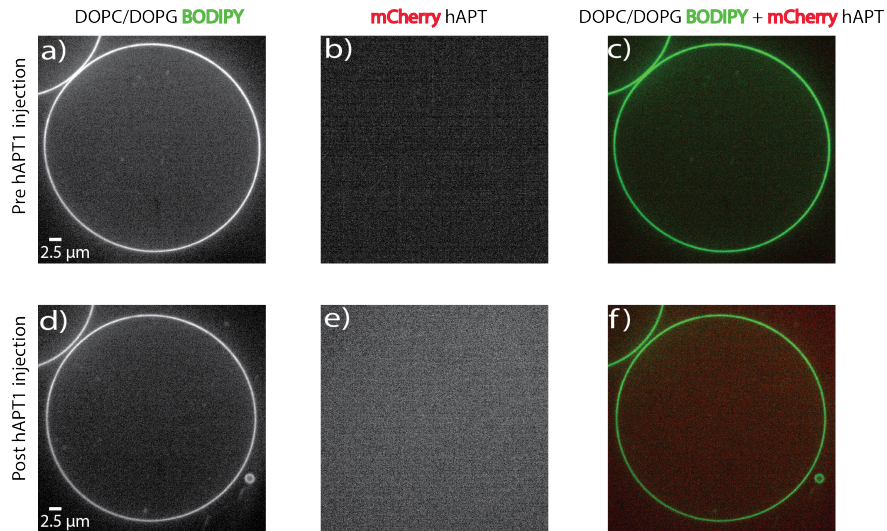


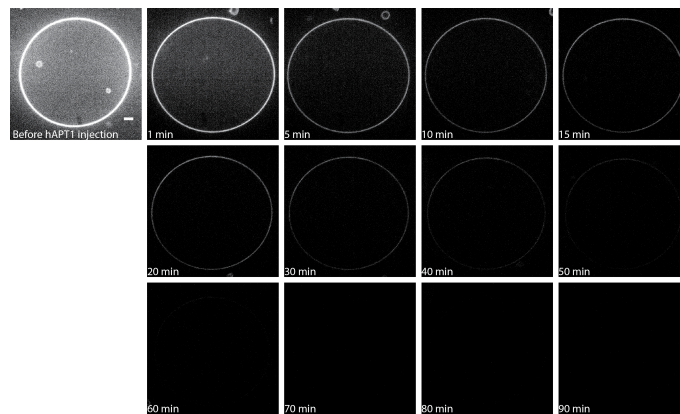
Figure 6.34: Experiment to investigate if hAPT1 can bind to negatively charged model membranes. a) 70 mol% DOPC/ 30 mol% DOPG vesicles containing 0.2 mol% BODIPY FL C12 (green) were produced using the method of electroformation. b) Before the addition of hAPT1-mCherry there is no signal detected in the red channel. c) Merge of the green and red channel, before the addition of hAPT1-mCherry. d) After the addition of 2 μ M hAPT1-mCherry the green vesicle stays unchanged. e) A random distribution of hAPT1 exists around the vesicles. f) There is no enrichment of hAPT1 on the negatively charged membrane detectable when images are merged.

In summary, APT does not appear to be significantly enriched at artificial, neutral or negatively charged membranes without a membrane affinity tag, i.e. APT is unable to bind to membranes with just its hydrophobic patches. It apparently needs a membrane anchor for the binding to membranes. Thus it seems likely that the Cys2 is responsible for the observed localization of hAPTs to membranes in the cell. *In vivo* studies are described later in section 6.7.1 to test this hypothesis, but at first, the ability of APT to cleave GUV-membrane-bound peptides is investigated as described in the following.

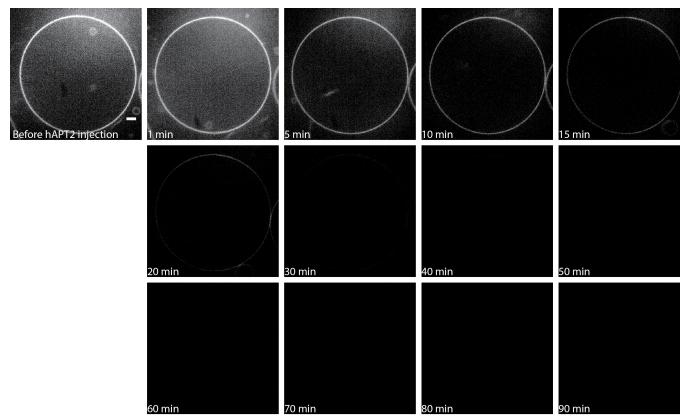
6.4 Microscope assay to investigate the APT activity on a palmitoylated N-terminal APT1 peptide associated to giant unilamellar vesicles (GUV)

Another approach besides fluorescence polarization or FRET to investigate APT's depalmitoylation activity on a membrane bound APT1-peptide is fluorescence microscopy. This method allows to get closer to *in vivo* conditions and to explore potential effects of the vesicle size. Giant unilamellar vesicles (GUV), prepared by electroformation (described in section 5.2.3.2), were used as a model membrane. 10 μM FITC labeled and palmitoylated APT1-peptide was injected into the microscopy chamber with the pre-formed vesicles and incubated for 20 minutes to allow the peptide binding to the vesicles, as evidenced by the green membrane stain. Afterwards, 2 μM human APT1 or APT2 was injected and the reaction was observed for 90 minutes. Due to the depalmitoylation of the FITC labeled peptide caused by APT, the peptide loses its membrane affinity and therefore the green fluorescence intensity around the vesicle decreases. As control, the same experiment was conducted with buffer without APT. The FITC intensities were determined with help of the program Fiji (described in section 5.2.3.2), and the vesicles were labeled with 0.01 mol% N-Rh-PE. Representative examples of the microscope pictures highlighting the decreasing FITC intensities over time are displayed in the following Figures (6.35 and 6.36).

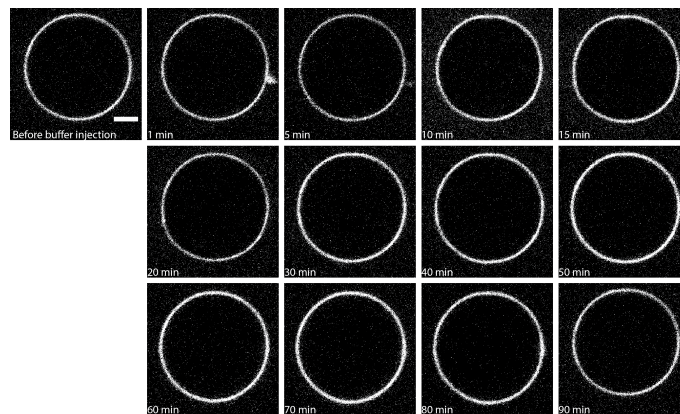
Figure 6.35 shows the FITC intensities of the membrane bound APT1-peptide. In presence of 10 μM hAPT1 or hAPT2 the FITC fluorescence intensity around the vesicles decreases over time. To quantify the intensities, a mask was applied in Fiji that encompasses the vesicle in form of a ring. The integrated intensities are shown in Figure 6.36. As expected, the intensities decrease, because depalmitoylation of the peptide by hAPT1 or hAPT2 drastically reduces the membrane affinity and therefore the FITC intensity around the vesicles is lost. As a control experiment, a bleaching experiment with just buffer injection was performed. Here, the FITC intensity around the vesicle stays relatively constant over the time, the observed decrease of approximately 30 % is rather probably due to deformation/ shrinking of the observed vesicle than to bleaching as the comparison with the rhodamine control shows. The DOPC vesicles are stained with 0.01 mol% rhodamine red, and the rhodamine control shows no significant bleaching effect over the observation period. The vesicle pictures of the rhodamine channel as well as the rhodamine intensities are shown in the appendix (Figure A.1 and A.2). Quantification of the experiments is challenging as the vesicles tend to change their shape, and the integration of the vesicle fluorescence intensities with Fiji is quite subjective. Thus this assay serves more as a qualitative assay, than a quantitative one, but at least it shows direct evidence for the depalmitoylation activity of APT.



(a) FITC intensities around a giant unilamellar DOPC vesicle after hAPT1 injection. The intensity reduces over the time.



(b) FITC intensities around a giant unilamellar DOPC vesicles after hAPT2 injection. The intensity reduces over the time.



(c) FITC intensities around a giant unilamellar DOPC vesicles after buffer injection. The intensity stays constant over the time, no bleaching is observed.

Figure 6.35: Time series of FITC intensities around the vesicles after addition of hAPT1, hAPT2, and buffer, respectively. $10 \mu\text{M}$ FITC-APT1-peptide was injected into the microscope chamber with the DOPC vesicles and incubated for 20 minutes. After the first picture was taken, $2 \mu\text{M}$ hAPT1, hAPT2 or buffer were injected. In presence of the enzymes, the FITC intensity decreases over time since the depalmitoylation of the peptide by APT reduces its binding affinity to the membrane, whereas the intensity in the control experiment stays constant over the measurement time, apart from the bleaching effects. The amount of bleaching observed in the control experiment c) was less than 33 % of the starting intensity (Figure 6.36). The scale bars indicate a size of $2.5 \mu\text{m}$ and the measurements were performed in 5 mM Ammoniumcarbonate buffer, pH: 7.4 at room temperature.

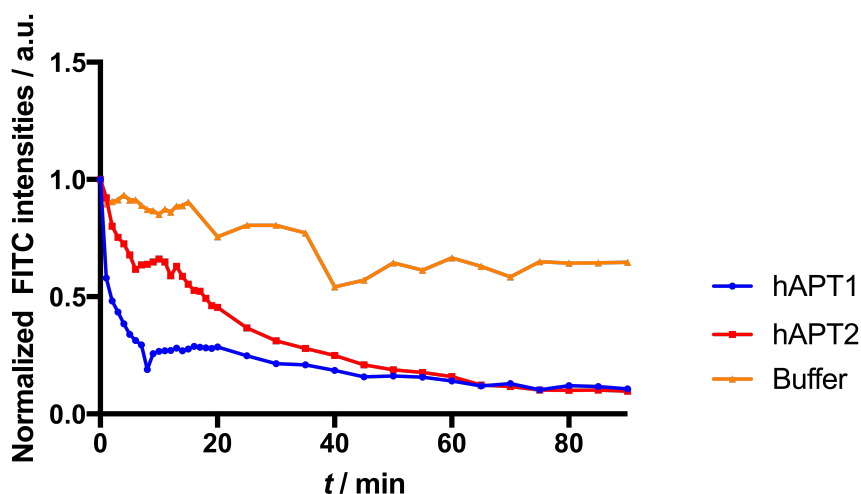


Figure 6.36: Integrated and normalized (to the first image and with also the highest intensity) FITC intensities around the DOPC vesicles shown in Figure 6.35. The calculation is described in section 5.2.3.2. In presence of the enzymes, the FITC intensity reduces over the time (the depalmitoylation of the peptide by APT reduces the binding affinity of the peptide to the membrane), whereas the intensity in the bleaching experiment stays relatively constant over the measurement time.

In summary, both hAPT1 and hAPT2 are able to depalmitoylate a FITC-labeled, palmitoylated hAPT1 peptide bound to GUV vesicles. With this technique the process of the depalmitoylation can be visualized directly, but it is a qualitative technique and not a quantitative one. The lack of information, e.g. the exact concentration of peptide on a DOPC vesicle, makes it difficult to determine reaction velocities. With a k_{cat} of 0.5 s^{-1} for membrane-bound peptides, $2 \text{ }\mu\text{M}$ APT should be able to cleave $\sim 1 \text{ }\mu\text{M}$ peptide per second. However, the peptide is partially still in the form of micelles (as seen in the microscope images as bright green blobs) and thus probably not immediately accessible for APT, due to the excess peptide and "overloading" of the GUVs. This probably explains why the reaction is much slower than expected from the FRET-measurements. But still it is an useful method to monitor the binding of the peptide to vesicles and the peptide's depalmitoylation by APT, since it provides direct evidence for the high membrane affinity of the peptide as well as for the catalytic activity of APTs on the peptide.

6.5 *In vitro* reconstitution of a mono-palmitoylated H-Ras by a sortase mediated ligation

Lipidated proteins play an important role in many biological processes, for example in signal transduction, membrane trafficking, immune response and pathology. Investigation of their function *in vitro* requires a preparation and purification of lipid-modified protein in larger quantities. Several chemical approaches where a chemically synthesized peptide is coupled to a purified protein can be used to synthesize a lipid modified protein, e.g. expressed protein ligation (successfully implemented for: Rab7 or N-Ras), maleimide ligation (successfully implemented for: H-Ras and N-Ras) or the click-ligation (successfully implemented for: Rab7 and Rab1) [69]. The disadvantage of these methods is that all lipidated proteins are synthesized in non-physiological conditions, and contain a specific non-natural, chemical linker.

A relatively new biological approach to modify proteins is the sortase mediated ligation of a (modified) peptide to a protein. For this, a protein containing the C-terminal sortase recognition sequence LPETG can be linked to a synthesized peptide with a N-terminal poly-glycin sequence. The mechanism how sortase can link the protein with the peptide is shown in Figure 6.37. The target protein and the sortase have a His-tag, so that the reaction can be easily purified via a Ni-NTA column, since the His-tag of the target protein will be removed after successful ligation.

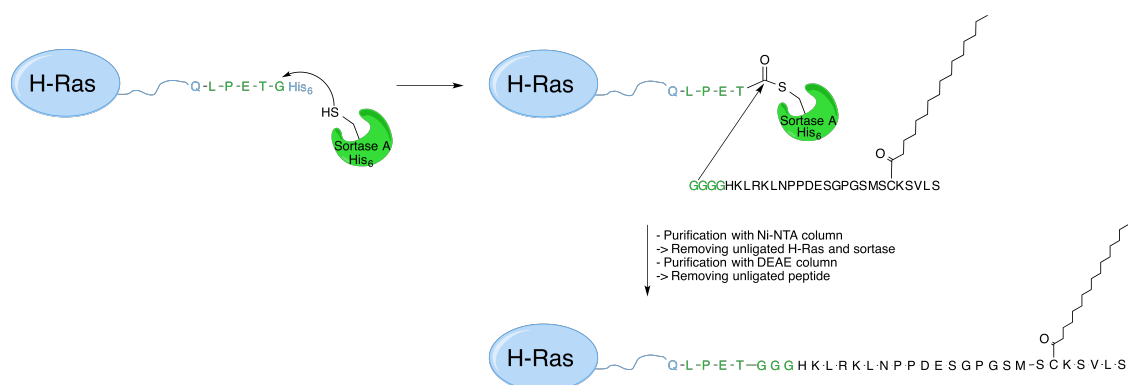


Figure 6.37: Mechanism of the *in vitro* reconstitution of H-Ras by a sortase mediated ligation. H-Ras-Q165-LPETG-His₆ was coupled by a His-tagged sortase to a palmitoylated GGGG peptide with the C-terminal sequence of H-Ras. The reaction was purified by a Ni-NTA and a subsequent DEAE column. Mechanism was drawn on basis of [69].

Investigation of APT activity on a full length palmitoylated H-Ras requires a lipidated H-Ras protein, which was generated by the sortase mediated ligation described in Figure 6.37. For this, H-RasQ165-LPETG-His₆ was expressed and purified. Furthermore, a peptide containing the C-terminal sequence of H-Ras (with the cysteines (181 and 186) in the sequence are mutated to serines to avoid the formation of disulfide bonds) with a palmitoyl moiety (at Cys184) and the sortase recognition sequence GGGG was ordered from the company Storkbio (Estonia). The ligation was performed as shown in Figure 6.37. After the ligation and purification the full length

palmitoylated H-Ras was labeled with FITC maleimide at cysteine 118. All steps of the ligation, purification and labeling were monitored on a SDS-gel as displayed in Figure 6.38.

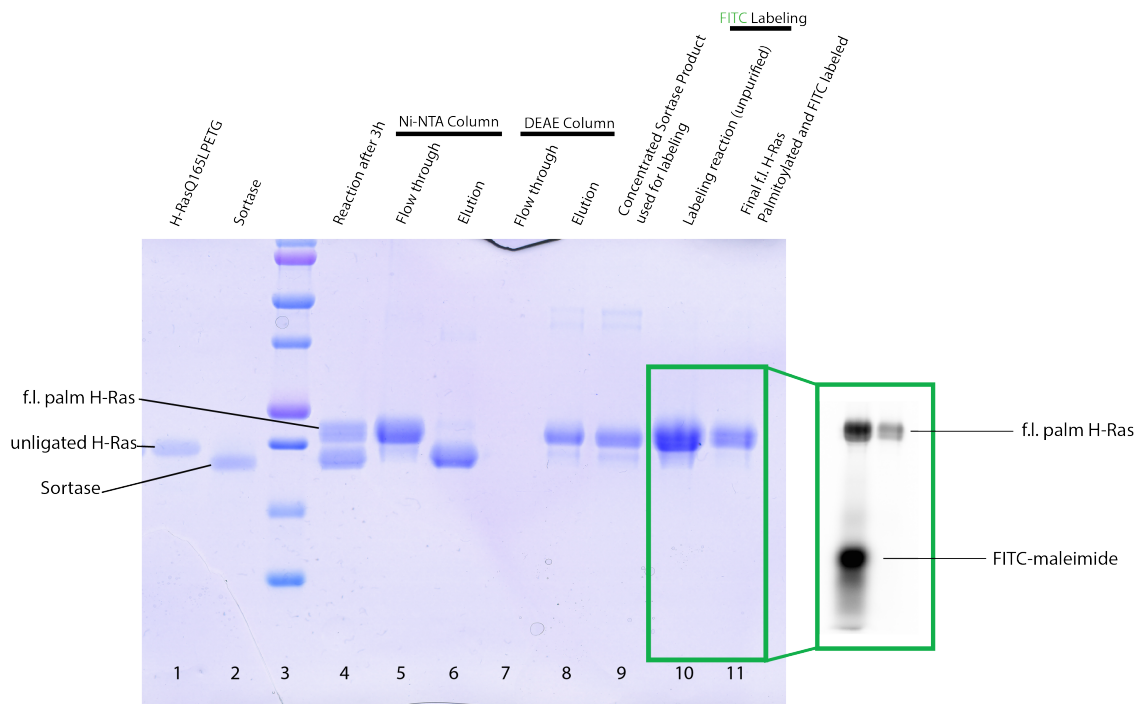


Figure 6.38: SDS-gel of the *in vitro* synthesis of palmitoylated H-Ras by a sortase mediated ligation. For the ligation, 400 μM palmitoylated peptide was dissolved in buffer (detailed information see section 5.2.5) with 5 % n-Dodecyl- β -D-maltoside. H-Ras Q179LPETG-His₆ (lane: 1) was added to the solution to a final concentration of 200 μM . To start the reaction, sortase (final concentration: 100 μM , lane: 2) was added. Lane 3 shows a prestained marker. The reaction was incubated at 4 °C for 3 hours (lane: 4). To remove the sortase and the unligated Ras protein, the mixture was loaded on a Ni-NTA column. In the elution volume (500 mM imidazol) the unligated protein and sortase were found and discarded (lane: 6). The flow through, containing the product and the unligated peptide (lane: 5), was loaded on a Ras-binding DEAE column. To remove the unligated peptide, the DEAE column was washed (lane: 7). Elution of the full length modified Ras protein was performed with buffer containing 250 mM KCl (lane: 8). The product was concentrated to 2.7 mg/mL (lane: 9). Labeling of the product was performed with FITC maleimide (ThermoFisher Scientific). For this, 1.5x fluorescence dye-maleimide was added to the solution and the reaction was kept in the dark for 1.5 hours (lane: 10). The reaction was purified with a nap 5 column (GE healthcare) to remove the unreacted dye and the modified H-Ras was then concentrated to 6.35 mg/mL. The inset gel next to the comassie stained gel shows the fluorescence scan of the gel and thus the FITC containing bands. The final full length palmitoylated and FITC labeled H-Ras is shown in lane 11.

Figure 6.38 shows the successful sortase ligation, purification and labeling steps to produce full length palmitoylated and FITC labeled H-Ras (lane: 11). After the ligation (lane: 4) a shift of the H-Ras (lane: 1) band is visible, indicating that the sortase was able to ligate the peptide to the H-Ras. Purification via the Ni-NTA column shows a successful removal of the sortase as well as

the unligated H-Ras which is present only in a very small amount, indicating a very good reaction efficiency (lane: 6). In the flow through the product is nicely detectable (lane: 5). Further purification with a DEAE column allows the removal of the unligated peptide. The eluted (lane: 8) and concentrated full length palmitoylated H-Ras (lane: 9) was labeled with FITC maleimide at Cys118 (lane: 10). The fluorescence labeling and the purification was successful, as supported by the fluorescence scan of the SDS gel. After purification and concentration, the fluorescent full length palmitoylated H-Ras was obtained (lane: 11) in a concentration of 6.35 mg/mL.

In summary, the synthesis of a full length palmitoylated H-Ras protein by sortase ligation was successful. The FITC labeled protein can be used for further *in vitro* experiments, e.g. microscope experiments with giant unilamellar vesicles, FRET or FP experiments, to investigate the hAPT1 activity on H-Ras. Those experiments are not part of this thesis but proposed for future research in this field.

6.6 PC12 cell neuronal differentiation assay to investigate the *in vivo* activity of new APT inhibitors

Several APT1 and APT2 inhibitors have been described in the literature, like e.g. the covalently binding inhibitor palmostatin M [15] or the more specific non-covalent inhibitors for APT1 and APT2, ML348 and ML349, respectively, with K_i values in the nanomolar range (table 6.4) [70]. Since inhibitors with even lower affinities were desirable, especially for the less well characterized APT2, a screen of 500000 compounds was conducted by the European Lead Factory (ELF), using the DiFMUO (6,8-difluoro-4-methylumbelliferyl octanoate) assay [46]. The ELF is a collaborative public-private partnership between the European Screening Centre (ESC), the European Federation of Pharmaceutical Industries and Associations (EFPIA), small and medium-sized enterprises (SMEs), as well as public institutions. In this screen, the compound ESC1000595 was identified as the most promising candidate, with a K_i of 20 nM in the DiFMUO assay that is 11.5-fold better than the K_i of the APT2 inhibitor ML349, although a different substrate (Resorufin acetate) was used (table 6.4). The structure of a complex of this inhibitor with APT2 was solved by Stefan Baumeister [30] and revealed that this particular inhibitor was especially interesting, since it can serve as a modifiable precursor where functional groups could be attached to the nitrogen of the benzoxazole group in a position next to a water-filled pocket in APT2, to improve the affinity and specificity of the compound [30].

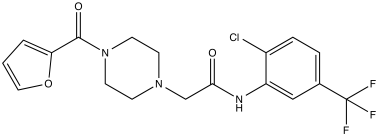
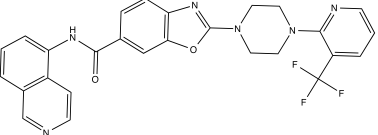
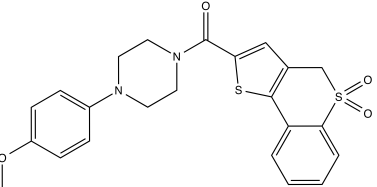
In contrast to the 20 nM K_i in the DiFMUO assay, ESC1000595 shows a lower affinity of 170 nM to APT2 in the OPTS assay (performed by Stefan Baumeister) [30]. Conversely, the APT2 inhibitor ML349 has a slightly higher K_i of 230 nM in a Resorufin assay as described in the literature [71], compared to a K_i of 50 nM in the OPTS assay (table 6.4).

The reason for this discrepancy between the OPTS- and the DiFMUO assays could be attributed to the fact that the K_m value for DiFMUO was determined under conditions different from the

ESC1000595 DiFMUO assay (in detergent-free buffer, [30], [46]). Another possible explanation could be the (relatively) better solubility of ESC1000595 in the DiFMUO assay where 0.01% Triton-X100 was used to improve the substrate solubility, whereas no detergent is needed in the OPTS assay. Indeed, calculation of the octanol/water partition coefficient logP shows that ESC1000595 has a relatively high logP value of 5.50 and a low aqueous solubility (logS) of -8.26 compared to ML348 and ML349 (table 6.4), indicating a higher lipophilicity. Consistently, prediction of the membrane permeabilities finds higher values for ESC1000595 (table 6.4). Typical drugs have logP values between -2.0 and 6.5, and logS values between -6.5 and 0.5.

For ML348 and ML349, an assay using Resorufin acetate was used as described in the literature [71], again in presence of a detergent (pluronic F127) [71], which could explain the different K_i values in the OPTS assay. In addition to the effect of the different solubilities, this might also be one of the cases where the detergents may not help to solubilize the inhibitor, but instead affect the assay due to sequestration of the inhibitor and/ or substrate as has been shown e.g. for CHAPS that quite specifically sequesters the inhibitor 2-Bromopalmitate [30].

Table 6.4: Structures and inhibition constants for non-covalent APT1 and APT2 inhibitors: Left: specific APT1 inhibitor, middle and right: specific APT2 inhibitors. For ML348 and ML349, an assay using Resorufin acetate was used (K_m for APT1 28.3 μM , for APT2 24.4 μM [71]) in PBS buffer adjusted to pH 6.5 with sodium acetate plus 0.2% pluronic F127 [71]. K_i values were calculated with the Cheng-Prusoff equation [71]. The OPTS assay was performed by Stefan Baumeister [30]. logP, logS (aqueous solubility) and membrane permeability values are calculated with the Schrodinger "QikProp v5.4" software, and the second set of logP values (*) with XLogP [72]. Cell permeabilities are in nm/sec, values < 25 indicate poor permeability, values > 500 very good permeability.

ML348 MW: 415.9 g/mol APT1 inhibitor	ESC1000595 MW: 518.5 g/mol new potential APT2 inhibitor	ML349 MW: 454.6 g/mol APT2 inhibitor
		
304 nM K_i Resorufin assay [71]	20 nM K_i DiFMUO assay [30]	230 nM K_i Resorufin assay [71]
70 nM K_i OPTS assay [30]	170 nM K_i OPTS assay [30]	50 nM K_i OPTS assay [30]
logP: 2.94/3.01*	logP: 5.50/4.98*	logP: 3.25/3.43*
logS: -4.01	logS: -8.26	logS: -5.35
Caco-2 permeability: 350	Caco-2 permeability: 1312	Caco-2 permeability: 664
MDCK permeability: 1319	MDCK permeability: 2172	MDCK permeability: 471

In the literature ML348 and ML349 were used in a competitive ABPP (activity-based protein profiling) assay, where an APT binding in HEK293T cell extracts was demonstrated [73]. An ABPP assay can be used for enzymes that lack known biomarkers (e.g. endogenous substrates or products) to report their *in situ* inhibition. For example, an activity-based probe, such as

Fluorophosphonate-polyethylen glycol-rhodamin (FP-peg-Rh) that covalently reacts unspecifically with a number of serine hydrolases (including APTs) [73], was used to block the active site of enzymes, so that competition for target engagement with protein specific inhibitors could be measured [73]. Specifically, the soluble proteome of HEK293T cells was incubated with the inhibitors ML348 or ML349 for 30 minutes at 37 °C, then 5 μM FP-peg-Rh was added and incubated for 30 minutes at room temperature. The labeled lysate was loaded on a SDS-PAGE gel and fluorescent bands were analyzed according to molecular weight. Control experiments showed that the bands for APT1 and APT2 are labeled. The APT2 labeling was abolished at a concentration of approximately 1 μM ML349 in the medium, which prevented the binding of the fluorescent probe to APT2 completely, whereas approximately 3 μM ML348 are needed to prevent binding of the covalent ABPP probe to APT1 [73]. Thus, an intracellular effect of ML348 or ML349 on APTs was expected at low micromolar concentrations of the inhibitors.

To investigate if the inhibitors reveal *in vivo* activity on the Ras signaling pathway, a PC12 neuronal differentiation assay was performed. This assay is a well established method to test effects on the Ras signaling pathway as described by Bar-Sagi *et al.* [74]. PC12 cells are rat pheochromocytoma cells that can be stimulated with Epidermal Growth Factor (EGF) or Neuronal Growth Factor (NGF), triggering differentiation into neuronal cells via either the MAP (mitogen-activated protein) kinase pathway or the PI3K/Akt pathway and leading to the growth of long neurites (an example picture of differentiated PC12 cells is shown in 6.39). In detail, NGF can activate the tyrosine kinase receptor type 1 (TrkA) which in turn activates the Ras downstream pathway, leading to the activation of a MAP kinase, e.g. ERK, and thus to the neuronal differentiation of the cells [75] (Figure 6.39). In contrast, the PI3K/Akt pathway bypasses Ras. Blocking of either pathway, e.g. with the specific MEK inhibitors U0126 and PD98059, or the PI3K inhibitor LY294002, decreases the percentage of neurite-bearing cells significantly [76]. MEK is the second kinase in the Ras or MAP kinase pathway (Ras → Raf → MEK → MAP kinase). PC12 cells express (at least) endogenous H-Ras [77], and Ras proteins are recruited to the plasma membrane upon NGF or EGF addition [78]. Overexpression of each of the Ras isoforms (when constitutively active) also leads to PC12 cell differentiation [79]. In addition, it has been shown that palmitoylation of N- or H-Ras is essential for their ability to induce neurite outgrowth [80]. Thus, inhibition of APT and subsequent mislocalization of Ras proteins away from the plasma membrane should potentially also be able to inhibit NGF- or EGF-stimulated differentiation via the Ras/ERK pathway.

If APT is active, palmitoylated H- and N-Ras proteins are assumed to be localized to the plasma membrane from where they can mediate the downstream pathway. In contrast, when APT is inhibited, H- and N-Ras are mislocalized to inner cellular membranes and the downstream signal from the plasma membrane should be disturbed, leading to a reduced neuronal differentiation.

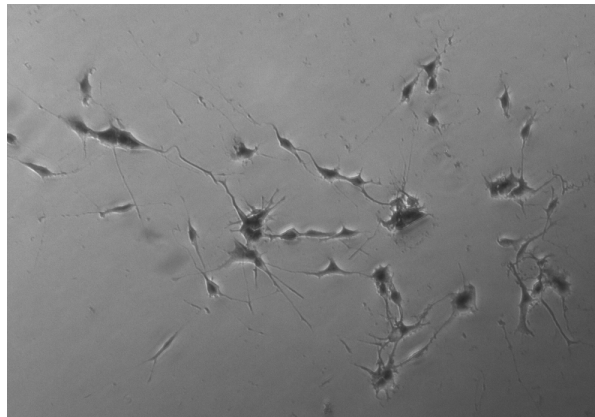


Figure 6.39: PC12 cells neuronal differentiation after stimulation with 100 ng/mL NGF for 10 days.

Deck *et al.* previously showed that APT inhibition with “Raspalin 3”, a benzodiazepinedione with an attached palmitoyl chain, indeed leads to a reduced PC12 neuronal differentiation, and also to a removal of fluorescently labeled, microinjected Ras from the plasma membrane of MDCK cells [81].

To test the effect of the known inhibitors ML348 and ML349 and especially of the new APT2 inhibitor ESC1000595, PC12 cells were stimulated with 100 ng/mL NGF. The APT inhibitors ML348, ML349, ESC1000585, and as a control the MEK1/2 inhibitor U0126 (New England Biolabs), were applied directly at a concentration of 25 μ M and incubated for 10 days. The medium with NGF and the inhibitors was replaced every second day, thus keeping the NGF concentration at 100 ng/ml. After this incubation, the cells were fixed, stained with coelestin blue and counted (see methods section 5.2.2.4). Cells with at least one neuron two times longer than the cell body were classified as a differentiated cell. The percentage of cells that were differentiated in presence and absence of the APT inhibitors are shown in Figure 6.40.

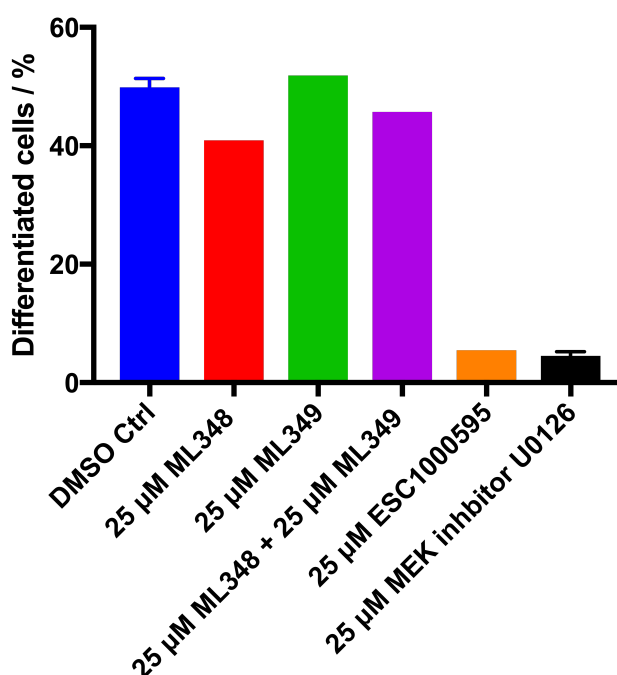


Figure 6.40: Percentage of differentiated PC12 cells with and without APT1/2 inhibitors. Cells were fixed, stained and counted (100 cells) after 10 days of NGF stimulation in presence or absence of APT1/2 inhibitors or the control MEK1/2 inhibitor U0126. Treatment with ML348 (APT1 inhibitor) or ML349 (APT2 inhibitor) or both shows no significant effect on the neuronal differentiation, whereas the new APT2 specific inhibitor ESC1000595 has the same strong inhibitory effect as the control MEK1/2 inhibitor U0126.

Figure 6.40 shows that the APT1 specific inhibitor ML348 as well as the APT2 specific inhibitor ML349 or a combination of both has no significant effect on the neuronal differentiation, whereas upon treatment with the new compound ESC1000595 the neuronal differentiation is strongly reduced to a similar level as with the MEK1/2 inhibitor U0126. The PC12 cells look healthy after the 10-day assay (i.e. they are attached to the surface and show no apoptosis), so that a toxic effect which can lead to dead cells that look like undifferentiated cells can be excluded. In addition, a toxicity test using MDCK-F3 cells was performed at the COMAS (Compound Management and Screening Center, Dortmund), with up to 10 µM of the ESC1000595 inhibitor. A minimal toxic effect was detected only after incubation for more than 24 hours, i.e. the cells became roundish, but still showed no signs of apoptosis.

Thus, surprisingly, only ESC1000595 strongly inhibited the PC12 differentiation, but not the other APT specific inhibitors ML348 and ML349, both alone and in combination. Since all three inhibitors have K_i values in the low nanomolar range, tight binding to APT would be expected, and at least ML349 should show a similar effect as ESC1000595 via inhibition of APT2. This result could possibly be caused by the different membrane penetration ability of the molecules into PC12 cells: it was observed that ML348 and ML349, in contrast to ESC1000595, formed aggregates and even crystals in the growth medium of the PC12 cells, even after sonication (example pictures of the precipitated inhibitors are shown in the appendix in Figure A.3). Consistent with that observation.

for ML348 and ML349 a maximum solubility of $\leq 12.5 \mu\text{M}$ in cell growth medium at room temperature has been determined by Vujic *et al.* [82]. But, as shown in table 6.4 above, the calculated logP and solubility values for ESC1000595 indicate that is even more hydrophobic than ML348 and ML349, so that this inhibitor might even be sequestered to the cell membranes instead of forming aggregates in the medium. Accordingly, the prediction values for the cell permeability are also the highest for ESC1000595. Under the assumption that APT is enriched at the plasma membranes, it might even be possible for APT to directly access the membrane-bound ESC100595.

However, also Vujic *et al.* found that ML348 and ML349 have no or only a small effect on the phosphorylation levels of the N-Ras downstream kinases ERK and Akt [82]. Since ML348 and ML349 showed bioactivity in HEK293T cells at $1 \mu\text{M}$ and $3 \mu\text{M}$ concentration [73], Vujic *et al.* concluded that these inhibitors indeed did not have an effect on the N-Ras pathway, in line with their siRNA studies, where they (at least partially) knocked down APT1, APT2 or both [82]. This would also be consistent with the results from the PC12 assay.

One hypothesis would be that ESC1000595, in contrast to ML348 and ML349, could also target other proteins in the cell which leads to the reduced neuronal differentiation. Therefore a second assay was performed using transiently transfected H-Ras proteins to investigate if the mode of action of ESC1000595 really involves Ras.

As mentioned above, it was shown that NGF also stimulates the PI3K/Akt pathway that can lead to the neuronal differentiation of the PC12 cells [75]. To verify if APT inhibition directly affects the H-Ras mediated signaling, the neuronal differentiation was induced by a transiently transfected, constitutively active H-RasG12VmCitrine construct as described in [74]. The plasmid was a kind gift from Philippe Bastiaens, Systemic Cell Biology Max Planck Institute for Molecular Physiology, Dortmund, Germany. Here, the MAP kinase pathway is directly triggered by the constitutively active, palmitoylatable H-Ras and does not take the indirect route via the NGF stimulation of the TrkA receptor, thus avoiding the possible PI3K/Akt pathway induced differentiation. An example picture of a differentiated cells induced by fluorescent H-RasG12VmCitrine is shown in Figure 6.41.

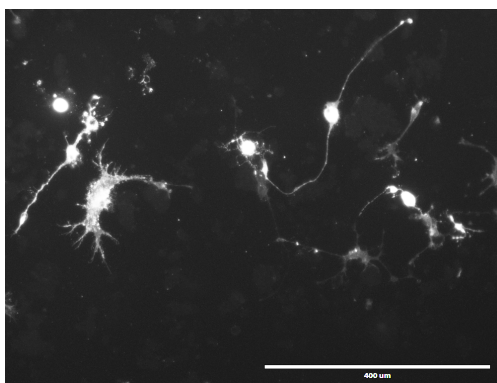


Figure 6.41: Fluorescent image of PC12 cell differentiation, 48 h after transfection with (palmitoylatable) H-RasG12VmCitrine.

PC12 cells were transfected with the HRasG12VmCitrine plasmid using the LTX2000 transfection reagent (Thermo Fisher) according to the manufacturer's protocol). The medium containing the inhibitors was changed after 4 hours and the effect of 25 μ M ESC1000595 or the control MEK1/2 inhibitor U0126 on the neuronal differentiation was analyzed after 48 hours. This differentiation is faster compared to the NGF stimulated one, because of the overexpression and thus the high cellular concentration of the constitutively active Ras, so that the cell receives a higher number of differentiation signals. The mCitrine fluorescence was used to visualize the cell shape. The results are shown in Figure 6.42.

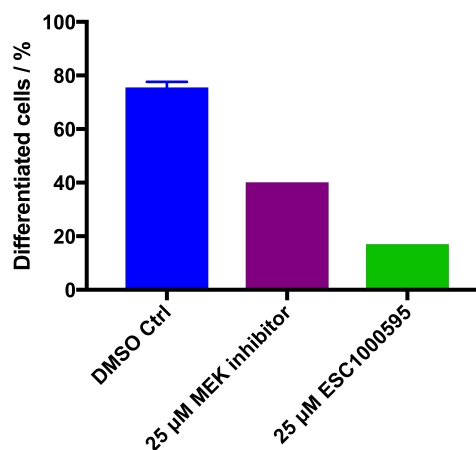


Figure 6.42: Percentage of PC12 cells with neurite outgrowth after transfection with a plasmid containing the constitutively active HRasG12V, with and without inhibitors. Cells were transiently transfected with the HRasG12VmCitrine vector and the neuronal outgrowth was investigated after 48 h in presence or absence of the ESC1000595 APT2 inhibitor or the control MEK1/2 inhibitor U0126. 100 cells were counted. Treatment with ESC1000595 has a slightly stronger effect on the neuronal differentiation than the MEK1/2 inhibitor U0126.

Figure 6.42 indicates that ESC1000595 strongly reduces the neuronal differentiation of the PC12 cells that is triggered by the constitutively active HRasG12V, similar to the MEK1/2 inhibitor U0126. This result corroborates the previous assay and would be consistent with a reduced HRasG12V downstream signal due to APT inhibition. Again, the cells look viable and healthy after 48 hours so that a toxic effect of the transfection or the inhibitors is unlikely.

In summary, the PC12 neuronal differentiation assay was used to investigate the effect of APT1 and APT2 inhibitors *in vivo*. It was shown that the new ESC1000595 has a significant inhibitory effect on the neuronal differentiation of the PC12 cells, in contrast to ML348, ML349 or both together. This unexpected result could be on the one hand caused e.g. by a lower membrane penetration ability of ML348 and ML349, or by their poor solubility in the medium and therefore a reduced concentration of the inhibitors in the cell. On the other hand, the higher lipophilicity of ESC1000595 could lead to either better membrane permeability or even to sequestration and enrichment of this inhibitor in the plasma membrane, where it could possibly directly inhibit APT2.

Furthermore, it was shown that the inhibition of APT2 with ESC1000595 directly influences the H-Ras mediated signaling by reducing the differentiating effect of transfected H-RasG12V in PC12 cells. Thus, it seems plausible that the differentiation of the PC12 cells is prevented by ESC1000595 because of the reduced Ras-mediated downstream signal from the plasma membrane due to APT2 inhibition and subsequent Ras mislocalization from the plasma membrane to the inner cell membranes.

As a conclusion, the new compound ESC1000595 is quite promising, and in addition, it is a modifiable precursor, which can be further improved by the addition of functional groups to enhance the APT2 inhibition.

6.7 *In vivo* localization of APT

6.7.1 Localization of APT in HeLa cells

Multiple studies focused on the *in vivo* localization of both human APT isoforms: Kong *et al.* reported that the palmitoylation of mammalian APT1/2 at Cys2 allows APTs to be enriched on the plasma membrane [33]. Additionally, Vartak *et al.* reported that there are two fractions of APTs in the cell: On one hand a soluble cytosolic, unpalmitoylated APT that can potentially depalmitoylate its substrates on all membranes in the cell, and on the other hand a palmitoylated and Golgi-localized APT. Furthermore, an APT1/2 mutant (C2S) which can not be palmitoylated was found to be randomly distributed in the cytosol [34]. These studies were performed in canine MDCK cells.

Investigation of APT localization in mammalian cells in this study was performed in HeLa cells: HeLa cells were transfected with either a palmitoylatable hAPT1-mCitrine construct or the unpalmitoylatable hAPT1-mCitrine C2S mutant. A control experiment was conducted with just mCitrine. GalT-mTagBFP (mTagBFP is a variant of TagRFP [83]) was used as a Golgi marker [34], since GalT (1,4-galactosyltransferase) is unambiguously located to the *trans*-Golgi membranes and the *trans*-Golgi network [84]. The plasmids were a kind gift from Philippe Bastiaens, Systemic Cell Biology Max Planck Institute for Molecular Physiology, Dortmund, Germany.

Figure 6.43 illustrates that hAPT1 is enriched at the Golgi region (upper row), whereas the unpalmitoylatable hAPT1 C2S mutant is clearly localized in the cytosol. These results are consistent with the findings of Vartak *et al.* [34]. They reported a Golgi localization for the palmitoylatable hAPT1 and a cytosolic distribution for the C2S mutant. In contrast to the detected colocalization of APT and GalT in MDCK cells by Vartak, in HeLa cells APT does not colocalize completely with the Golgi marker GalT, but only a rough similar localization.

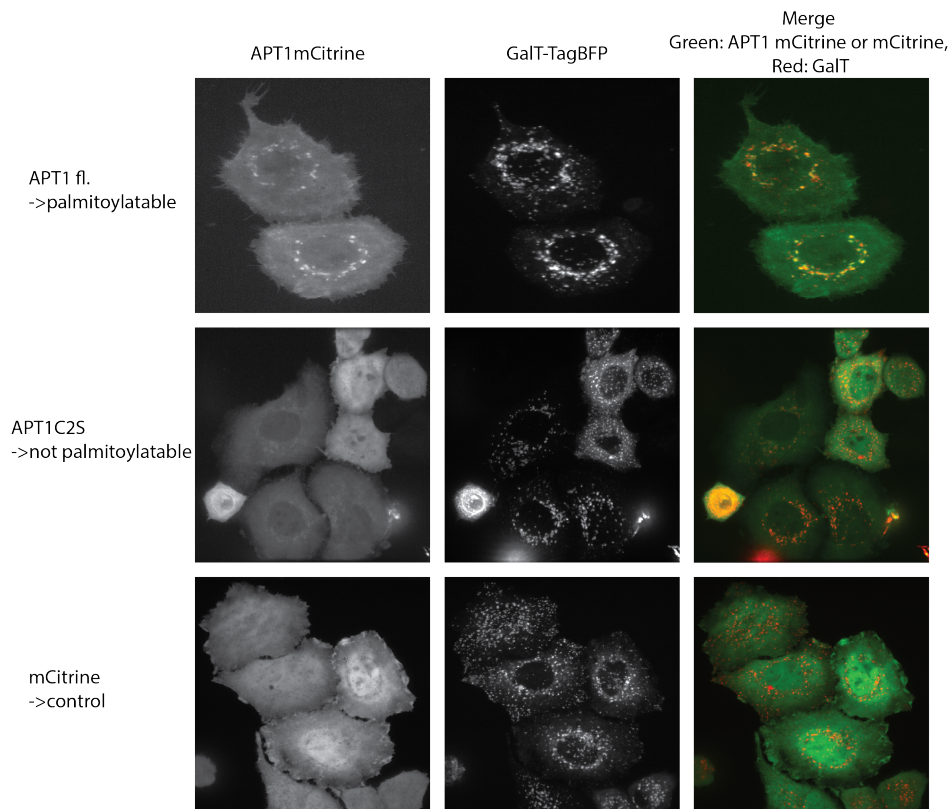


Figure 6.43: hAPT1 localizes to the Golgi region in HeLa cells. Cells were transfected (top row) with hAPT1-mCitrine wt, hAPT1 C2S-mCitrine (middle row) and mCitrine (bottom row). GalT-mTagBFP was used as a Golgi marker. The similar localization of hAPT1-mCitrine and GalT-mTagBFP suggests that hAPT1 localises to the Golgi apparatus.

mCitrine is cytosolically distributed, but in some cells it seems to be slightly enriched in at least some nuclei, due to a passive transport of the 26.9 kDa protein into the nucleus by the nuclear pore complex [85].

These results indicate that *in vivo* the palmitoylation at Cys2, which serves as membrane anchor, leads to APT's binding to membranes, especially at the Golgi region. Kong *et al.* postulated a plasma membrane localization for APT [33] but this was not confirmed in this experiment. APTs only possess a single palmitoylation site and lacking a permanent, irreversible membrane anchor, like prenylation or N-myristoylation, which ensures a permanent membrane localization. The membrane affinity with just one palmitoylation site is relatively weak and Vartak *et al.* postulated that its life time is too short to survive the secretory pathway to the plasma membrane [34]. Upon Vartak's results that APT is enriched at the Golgi, which can be confirmed in this experiment, they suggested a smaller acylation cycle for APT between the cytosol and the Golgi [34]. Although APT shows an auto-depalmitoylation activity, the dynamic palmitoylation of APT1/2 creates a negative feedback on the APT activity at the Golgi, inhibiting this auto-depalmitoylation of APT, which ensures a steady state Golgi-cytosol localization [34].

6.7.2 Localization of electroporated hAPTmCherry proteins in HeLa cells

Electroporation is a relatively novel method to transfect cells from higher organisms [86]. It is a physical transfection method that uses electrical pulses to create temporary pores in the plasma membrane. Substances (for example nucleic acids or proteins) can penetrate into the cell through these pores [87], [88], [86].

Here, electroporation was used to directly deliver recombinant APT proteins into living cells. Full length palmitoylatable hAPT1mCherry or hAPT2mCherry was electroporated into HeLa cells that are transiently transfected with APT1/2-mCitrine proteins, to investigate if the cell is able to palmitoylate these recombinant proteins and if these proteins then localize similarly to the transiently transfected APT1/2mCitrine proteins, which are used as a reference. As a negative control the unpalmitoylatable APT1/2n' (N-terminal shortened version of the proteins lacking the first five amino acids) and just mCherry was used, respectively.

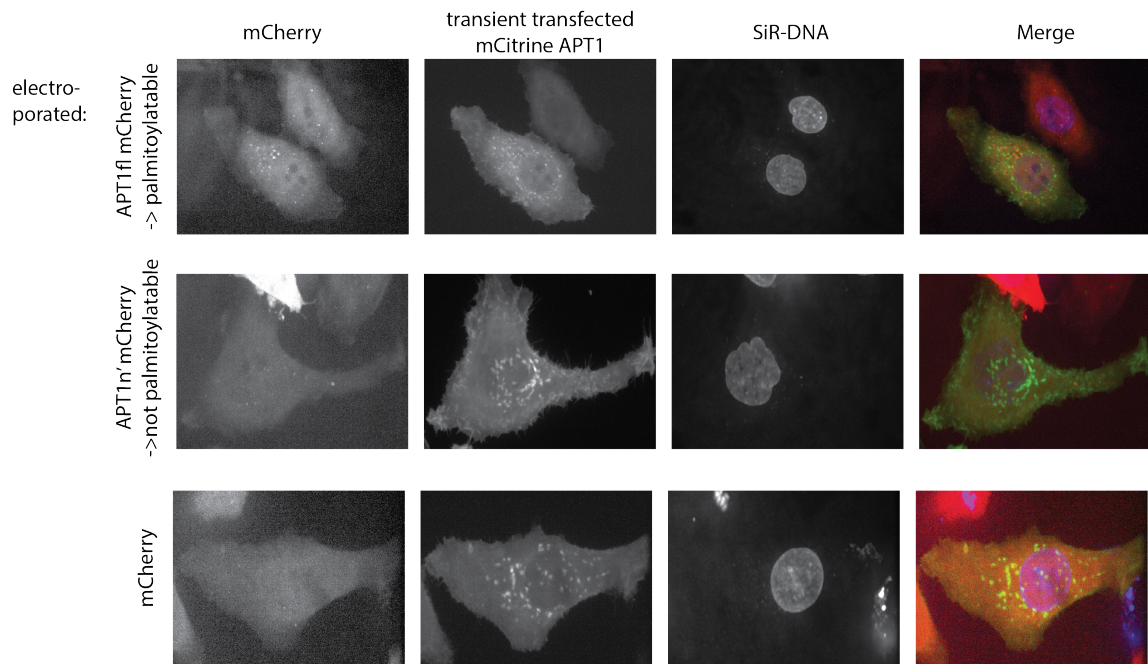
Figure 6.44 displays that full length hAPT1/2 proteins locate in a way similar to the transiently transfected hAPT1/2mCitrine reference (upper rows). Thus it seems likely that HeLa cells are able to palmitoylate the recombinant hAPT1/2 proteins. These palmitoylated APTs can localize to the Golgi, similar as the transiently transfected APT-mCitrine proteins.

An issue of the electroporation compared to other transfection methods is the difficulty in controlling its efficiency [89] and the unknown resulting protein concentration in the cell. For example, there are just a few dots which could be endosomes detectable for the electroporated proteins compared to the transiently transfected proteins, so it seems that the protein concentration after electroporation is much lower. Thus it remains unclear how much protein could be palmitoylated or how much protein is perhaps degraded by the cells. To investigate if the electroporated proteins are targeted for degradation via endocytic pathways, markers like the Ras-related protein 5A (Rab5) (early endosomes) or the Lysosome-associated membrane protein 1 (Lamp1) (late endosomes) could be used as shown in [90].

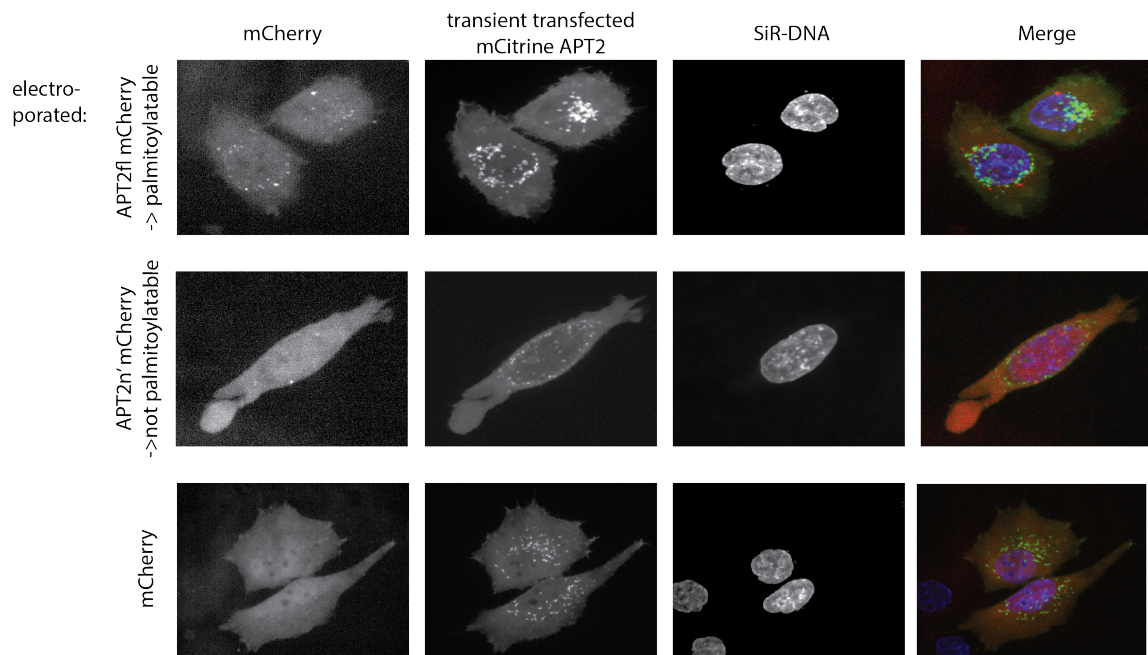
Furthermore, the middle rows show that the shortened unpalmitoylatable proteins hAPT1/2n'-mCherry localize randomly in the cytosol. As expected, the electroporated control protein mCherry shows no specific localization. Thus, also the electroporation experiment indicates that hAPTs need a membrane anchor for a membrane localization in the cell. The same results can be achieved by an experiment without the transiently transfected APT, which is shown in Figure A.4. Thus the localization of the electroporated proteins is not influenced by the transfected APT proteins.

In summary, investigation of APT's *in vivo* localization (transient transfection and electroporation), in HeLa cells show that hAPT1 as well as hAPT2 are localized at or in proximity of the Golgi apparatus if they can be palmitoylated at Cys2. If the proteins lack the Cys2 residue they are distributed in the cytosol. So it seems likely that the proteins need a membrane anchor for a specific localization in the cells. These results confirm the observations in the GUV vesicle studies (section 6.4) that non-palmitoylated APTs do not localize to membranes.

Kong *et al.* postulated a plasma membrane localization for APT [33] but this was not confirmed either by transfection or electroporation experiment in HeLa cells.



(a) Electroporation with hAPT1 proteins.



(b) Electroporation with hAPT2 proteins.

Figure 6.44: Electroporation of APT1/2mCherry proteins into HeLa cells. Cells were transiently transfected with hAPT1/2mCitrine as a reference and then (after 5 hours) electroporated either with the recombinant palmitoylatable full length Apt1/2mCherry protein (top row), recombinant unpalmitoylatable n' versions (N-terminal shortened version of the proteins lacking the first five amino acids) of hAPT1/2mCherry (middle row) or recombinant mCherry (bottom row). SiR-DNA (Spirochrome) was used to stain the nucleus. Both the full length hAPT1mCherry and hAPT2mCherry localize similar to the reference, i.e. the transiently transfected hAPT1/2mCitrine protein, indicating that the cell is able to palmitoylate the recombinant proteins which can then bind to the Golgi (similar Golgi pattern as shown for the Golgi marker GalT in Figure 6.43). The unpalmitoylatable recombinant hAPT1/2mCherry proteins show no significant membrane localization and are distributed in the cytosol. Again the control protein mCherry shows cytoplasmic localization.

6.8 APT's function in mitosis

6.8.1 *In vivo* localization of APT during mitosis

The cell cycle, in which an eukaryotic cell is duplicated, is a fundamental biological process, where replicated chromosomes are separated into two new nuclei in the daughter cells. APT's depalmitoylation activity was reported to have an effect on the asymmetric partitioning of the cell fate determinants Numb and β -catenin [47], but the exact role/function of APT in mitosis is still unknown. As shown by Vartak [34] and in section 6.7.1, APT in interphase is located at or close to the Golgi. During mitosis the Golgi breaks down and becomes reassembled after cell division as described in [51]: In prophase, the Golgi ribbon stretches around the nuclear envelope. In prometaphase, the Golgi is separated into fragments, followed by a partial or complete dispersal of the Golgi in metaphase. Subsequently, the reassembly of the Golgi starts in the telophase with the reappearance of small fragments. Finally, in cytokinesis, the fragments coalesce into a complete new Golgi in the daughter cells [51]. To investigate how APT localises during mitosis, a mitotic gallery for the different steps of the cell cycle was created (Figure 6.45).

Figure 6.45 displays different stages of the cell cycle for HeLa mCherryH2B cells that are transiently transfected with hAPT1 or hAPT2. GalT-mTagBFP was used as a Golgi marker. Similar to the interphase, hAPT1 as well as hAPT2 are still located at the Golgi in prophase. During prometaphase, metaphase and anaphase both proteins are distributed in the cytosol and not located to the Golgi anymore. As mentioned before, the Golgi disassembles during mitosis, but there are still a few Golgi pieces visible (e.g. in metaphase, Figure 6.45 middle row), to which APT is not colocalized at this stage of the cell cycle. In telophase, both human APT isoforms are significantly enriched at the midbody and partially at the plasma membrane. Finally, in cytokinesis hAPT1 and hAPT2 return to their usual Golgi localization. These findings are in agreement with the localization of hAPT1 in asymmetric cell division as shown by Stypulkowski *et al.* in U2 OS cells [47]. They showed an asymmetric plasma membrane localization of hAPT1 in metaphase and early anaphase, and also the significant enrichment of hAPT1 at the midbody in telophase. The result corroborates that hAPT1 and hAPT2 are not located at the Golgi during mitosis. So it seems likely that in mitosis APTs could have a different function, e.g. by depalmitoylating other proteins than in interphase, possibly regulated by the change in localization.

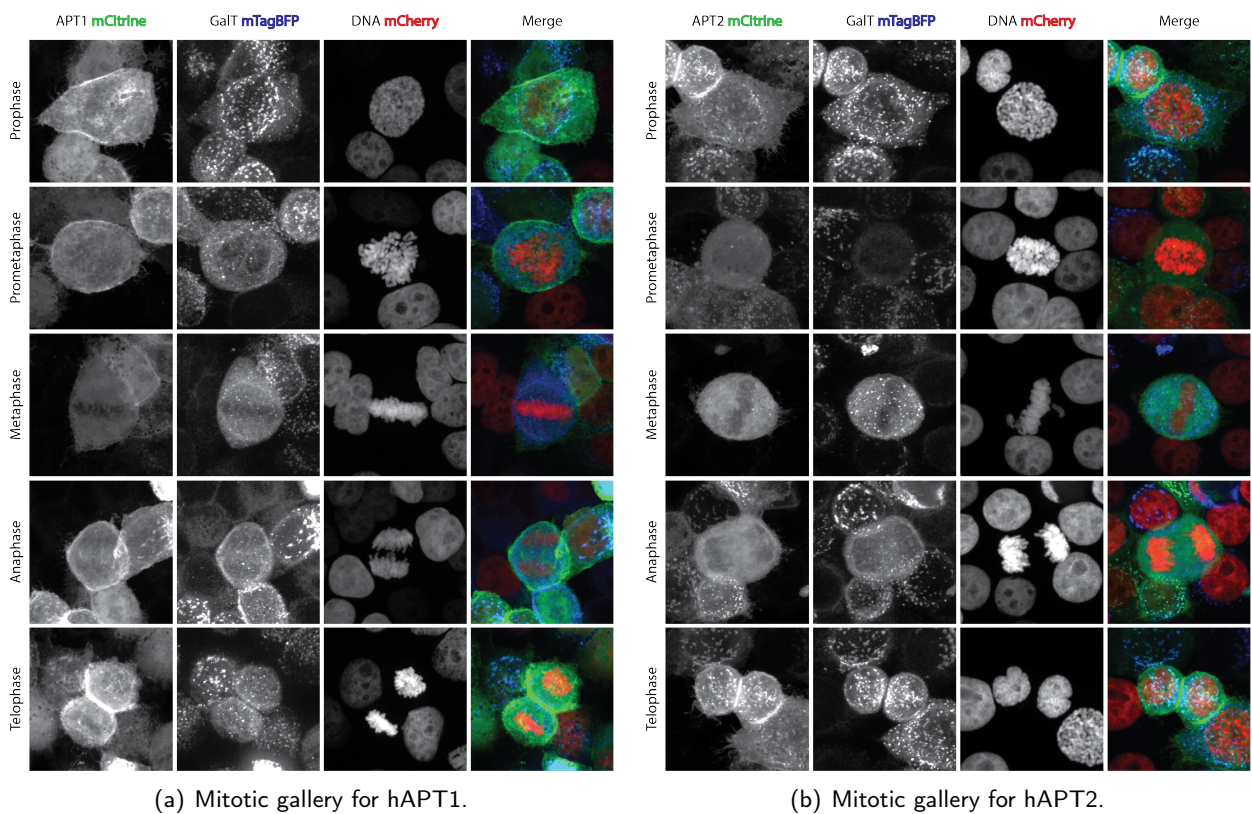


Figure 6.45: Mitotic gallery depicting localization of human APTs during mitosis. HeLa mCherryH2B cells were transiently transfected with hAPT1/2mCitrine and GalT-mTagBFP. Images were taken at different stages of the cell cycle as indicated on the left. In prophase, hAPT1 as well as hAPT2 are localized at the Golgi. During prometaphase, metaphase and anaphase both proteins are distributed in the cytosol, and in telophase a clear enrichment at the midbody is visible.

6.8.2 Effect of hAPT1/2 inhibition on the mitotic index

The results obtained in section 6.8.1 indicate that localization of hAPT1/2 changes in mitosis compared to interphase. To investigate if absence of hAPT1/2 catalytic activity has an effect on mitosis, the proteins were inhibited with hAPT1/2 specific inhibitors (Figure 6.46), and the mitotic index was calculated and used as a read out for normal mitotic progression. The mitotic index is the ratio of the number of (synchronized) cells undergoing mitosis to the number of cells in interphase [91]. For each experiment 500 cells were counted and classified according to their mitotic state (interphase, prophase, metaphase or anaphase) and finally, the ratio of mitotic cells to interphasic cells was calculated as the sum of pro-, meta-, and anaphase cells divided by the number of interphasic cells.

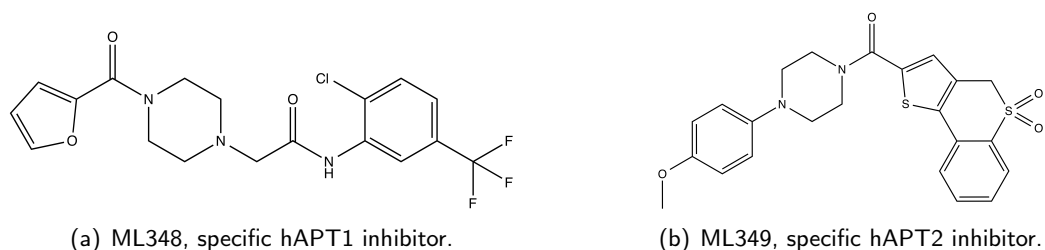


Figure 6.46: Specific hAPT inhibitors.

In detail, HeLa cells were synchronized in G2 phase by adding 9 μM of the RO3306 inhibitor and waiting for 18 hours. RO3306 is a selective CDK1 (Cyclin-dependent kinase) inhibitor which reversibly arrests the proliferating cells at the G2/M phase transition [92]. After mitotic release, by washing out the RO3306 inhibitor, the cells are entering mitosis [92]. Immediately after the washing step, cells were treated with 25 μM ML348 and 25 μM ML349 (Figure 6.46), or as a control with an equivalent amount of DMSO. Cells which are in pro-, prometa-, meta- or anaphase were counted as mitotic cells. The cell density in presence and absence of the inhibitors is comparable and the cells look healthy in both experiments, leading to the assumption that the inhibitors have no toxicological effect on the cells. Also in this cell assay (as previously found in the PC12 cell assay 6.6) the inhibitors ML348 and ML349 both precipitate in the cell culture medium. Nevertheless, an *in situ* APT inhibition was shown in the literature for both inhibitors in HEK293T cells (detailed information on this assay are in section 6.6) [73], thus it is assumed that a sufficient amount of these inhibitors is available inside the cells.

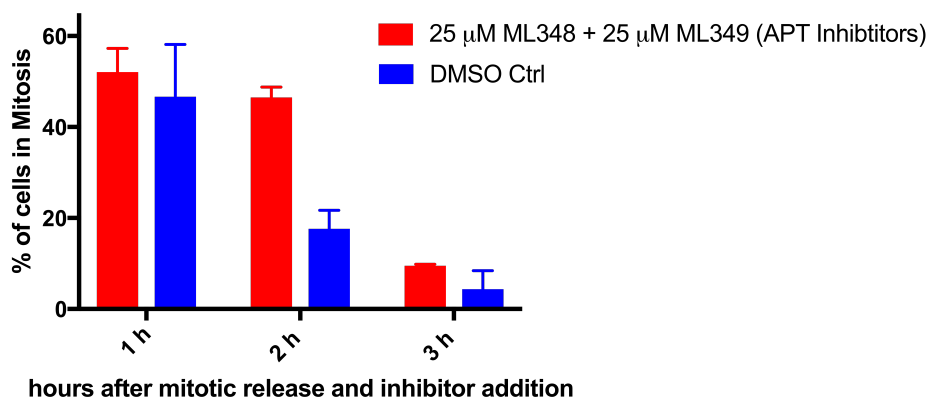


Figure 6.47: Mitotic index after hAPT1/2 inhibition. Cells were synchronized in G2 phase with the RO3306 inhibitor. After mitotic release cells were treated with both 25 μM ML348 and 25 μM ML349 or as a control with DMSO. Cells were fixed at different time points, stained and the mitotic index was calculated. After one hour the cells treated with the inhibitors as well as the control cells have a similar mitotic index of $\sim 50\%$. After two hours the mitotic index for the cells treated with inhibitors ($\sim 50\%$) is approximately twice than the control cells ($\sim 18\%$). After three hours both cell fraction have a similar mitotic index of $\sim 10\%$.

Figure 6.47 displays the mitotic index at different time points after mitotic release in presence or absence of APT inhibitors. After one hour the cells treated with the inhibitors and the control cells have a similar mitotic index of $\sim 50\%$. After two hours a significantly higher mitotic index is visible for the cells that are treated with APT1/2 inhibitors. Thus, more cells are in mitosis at this point of time compared to the control sample, indicating that cells which are treated with the APT inhibitors spend a longer time in mitosis. So either hAPT1/2 are required for a proper cell cycle or the inhibitors somehow disturb mitosis by other unknown effects.

After three hours, both cell batches (treated and untreated ones), have a similar mitotic index of $\sim 10\%$. In all experiments, in presence or absence of the inhibitor, the cells look healthy and the chromosomes (stained with DAPI) look similar in all cells. Thus there were no chromosome segregation defects visible.

To prove that the effect is triggered by hAPT1/2 inhibition, a rescue experiment could be performed. For this, cells could be transfected with the wild type proteins or with mutants that are unable to bind the inhibitor. Suitable mutants were described by Stefan Baumeister [30]. If the mutants would show no significant change in the mitotic index, the differences must be caused by the inhibition of hAPT1/2.

In summary, there are indications that hAPT1/2 could play a role in mitosis. hAPT1 as well as hAPT2 are located in the cytosol during early mitosis. In telophase and cytokinesis, APT1 and APT2 are enriched at the midbody. It could be possible that the enrichment of palmitoylated proteins at the midbody and part of the plasma membrane (e.g. $G_{i\alpha}$ proteins as shown in [93]) triggers a recruitment of APT to the midbody. Apparently, the inhibition of APT's leads to an increase of the mitotic index due to an extension of the time spent in mitosis. These findings might hint at an unknown function of APT in mitosis. One hypothesis would be that this could be caused by APT interaction with the palmitoylated protein Cdc42, as described previously [47]. Cdc42 belongs to the family of small GTPases and has numerous functions in the cell like mediation of polarized processes or remodeling the actin and microtubule cytoskeleton networks (needed for directed cell migration). Additionally, it was shown that Cdc42 has a function in asymmetric cell division [47]. So it could be possible that the interaction of APT and Cdc42 influences the dynamics in mitosis. With help of further experiments e.g. mass spectrometry (pull down MS), it could be possible to identify the interaction partners of hAPT1/2 in mitosis. Also, it would be interesting to investigate the effect of the specific inhibitors on the localization of APTs *in vivo*.

7 Discussion

In 1988, two Acyl Protein Thioesterases (APT) were described in higher organisms for the first time and characterized as lysophospholipases (LYPLA1 and LYPLA2) in a mouse macrophage-like P388D1 cell line [20]. Both enzymes were found to hydrolyze a range of lysophospholipids and other long-chain mono-acyl glycerol esters. Later it was shown that APTs prefer palmitoylated proteins as substrates, like H-Ras or the $G\alpha$ subunit, thus the proteins were subsequently renamed to Acyl Protein Thioesterases [23]. Both enzymes can efficiently depalmitoylate proteins *in vitro* and were shown to regulate S-palmitoylation and trafficking of peripheral membrane proteins in cells (like e.g. $G\alpha$ [22]). It was demonstrated that the inhibition of APT with the inhibitor Palmostatin M can disturb the acylation cycle of the proto-oncogene Ras, which leads to a weaker Ras-mediated signaling in cancer cells, thus making APT a potential anti-cancer target.

APT itself undergoes a dynamic palmitoylation at Cys2 to achieve membrane localization. To date, the effect of membranes on APT and its targets and the mechanism by which the physiological membrane environment influences APT activity still remains unclear. Additionally, it is still unknown how APT gets access to its membrane-bound substrates. One theory is that APT itself can extract and depalmitoylate the palmitoylated proteins, another possibility is that there are "helper" proteins required to extract the membrane bound substrates. For instance FKBP12 was described as a cofactor in Ras depalmitoylation [58].

This thesis provides new insights into the way how and if APT can depalmitoylate a membrane bound substrate using a variety of methods. An *in vitro* FRET system was established using artificial vesicles. Additionally, the membrane localization of palmitoylated APT was analyzed *in vitro* on vesicles and *in vivo* with different transfection methods (transient transfection and electroporation) in cells. Besides investigations of APT at membranes, an assay for physiological substrates was implemented. Furthermore, two known inhibitors and a new APT2 specific inhibitor was tested on its *in vivo* activity in a PC12 differentiation assay. Finally, *in vivo* imaging of cell was used to examine the localization of APT and the effect of its inhibition during mitosis.

7.1 Development of an assay for physiological APT substrates

Until today, several types of assays to investigate APTs activity on artificial substrates are known. Those substrates change their fluorescence or absorbance features after hydrolysis by APTs. Issues for these assays are that these substrates are non-physiological, they are usually oxo-esters (in contrast to thioesters) and they are often difficult to solubilize, so that detergents like CHAPS

or Triton are required. Thus an assay for the turnover of natural substrates was implemented in this thesis, using firstly a DTNB assay that turned out to be unsuitable, as well as an ESI-MS approach.

To detect the free thiol group, produced by APT-catalyzed hydrolysis of thioesters, a DTNB (5,5-dithiobis(2-nitrobenzoic acid)) assay was considered (section 5.2.6), using Acetyl-CoA as a test substrate [55]. Bonner *et al.* showed that the DTNB assay was suitable for the Fatty Acyl Thioesterase I from *E. coli* [54]. Upon hAPT1 hydrolysis a free thiol group on the CoA is formed. This free thiol group can be attacked by DTNB, resulting in one TNB (5-thio-2-nitrobenzoic acid) molecule bound to the thiol, whereas the other "free" TNB molecule gives an absorption signal at 412 nm.

Surprisingly, no hydrolysis of Acetyl-CoA was observed and no significant increase of the absorption was detectable in this assay (see figure 6.4). Thus, hAPT1 seems to be inactive in presence of DTNB. Based on these results it was analyzed how DTNB can inhibit hAPT1. It was shown by ESI-MS measurements that DTNB can modify hAPT1's five cysteines, although only two (Cys168 and Cys206) are solvent exposed, indicating a low stability of the APT fold. Three of those cysteine modifications must lead to an unfolding of the protein, since they are buried in the protein core, resulting in the catalytically inactive hAPT1. To avoid these modifications, a mutant where the cysteines have been replaced by serines could be used.

Interestingly, a more detailed investigation using a combination of the established OPTS assay [30] and an ESI-MS measurement revealed that at stoichiometric DTNB concentrations no cysteine modification was detectable, but hAPT1 was still inactive. It was determined that DTNB can function as a non-covalent APT inhibitor with a K_i of ~ 350 nM. Comparing the DTNB structure with the known hAPT1 inhibitor ML348, there are some common structural features, like the partially negatively charged residues on the benzene rings, or the linker region in the center of the molecules. These similarities suggest the possibility that DTNB can bind into the binding pocket of hAPT1 (figure 7.1). Crystallization trials resulted in either no crystals with high concentrations of DTNB, or relatively weak diffracting crystals. Lowering the DTNB concentration to 0.75 mM in the crystallization setup yielded in nicely diffracting crystals with an hAPT1 mutant (Δ M60 S114C C186S C206S). A weak density in this structure could perhaps correspond to a low occupancy DTNB molecule. Docking into this weak density yielded in a reasonably-looking conformation (Figure 7.1). It often occurs in co-crystal structures of APTs with ligands that even tightly binding ligands disappear from the binding site during crystallization due to rearrangement of the lid-loop, due to crystal packing forces and/ or changes induced by the conditions in the crystallization buffer. To sum it up, the DTNB assay was unsuitable to monitor APT activity on natural substrates, but a possible new lead compound for a hAPT1 inhibitor was discovered.

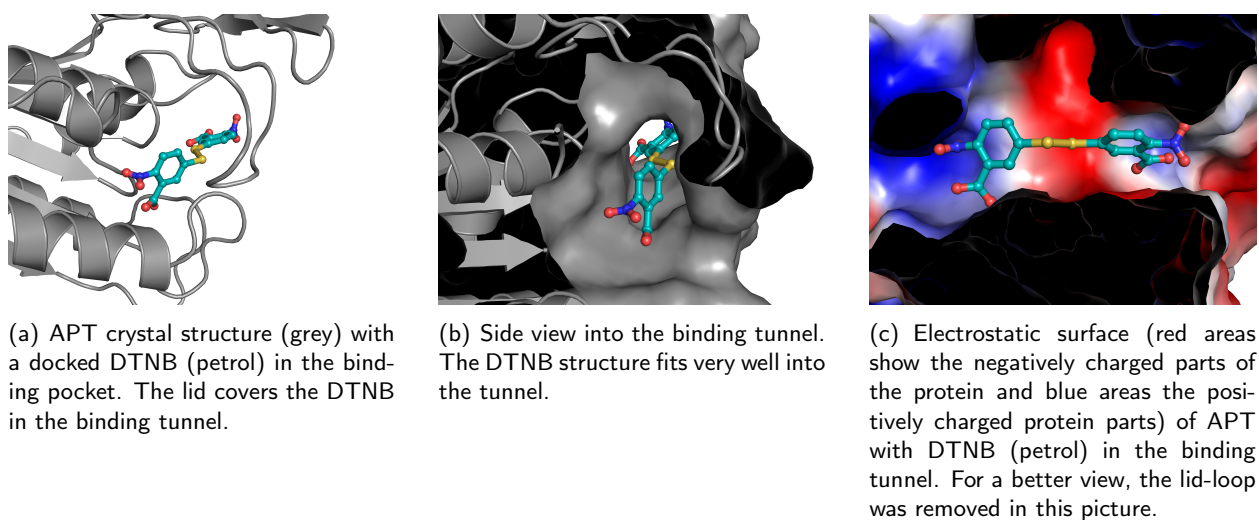


Figure 7.1: APT structure with DTNB in the binding pocket. DTNB fits nicely into APT's binding tunnel. A weak electron density that could correspond to a partially occupied DTNB molecule was detectable, thus the DTNB molecule was docked into the binding tunnel.

Due to the DTNB inhibition and/ or denaturation of APT, another assay was used to investigate APT's activity on a natural substrate. For this, an ESI-MS approach was applied to analyze APT's activity on lysophospholipids and phospholipids, and for comparing the activity on a palmitoylated nonapeptide corresponding to the N-terminus of hAPT1. In this assay, the decrease of the substrate and the increase of the product was monitored. Lyso-palmitoylphosphocholine (lyso-PPC) was chosen as a substrate to investigate the lyso-phospholipase activity of hAPT, and as a second substrate di-palmitoylphosphocholine (DPPC) was used, to analyze if hAPTs are able to hydrolyze lipids that are utilized as model membranes. The establishment of this assay was challenging, due to the poor solubility of the phospholipids in aqueous solutions, but finally the turnover rates could be determined. Both, hAPT1 and hAPT2, have a k_{cat} of $\sim 1.5 \cdot 10^{-4} \text{ s}^{-1}$ for lyso-PPC and show no turnover of DPPC. This value is quite slow, compared to the hydrolysis rate of other natural substrates, e.g. a palmitoylated peptide, as described in the next section. One reason for the slow or lacking turnover rates of lyso-PPC and DPPC could be the poor solubility of the phospholipids, but those results indicate that APT is clearly not a lipase, because lipases are often activated by micelles and usually show eight orders magnitude higher k_{cat} values in the range of $1 \cdot 10^4 \text{ s}^{-1}$ on phospholipids [57].

Summarizing these results, DTNB was found to be a possible new APT inhibitor. In contrast to the DTNB assay the ESI-MS analysis is a suitable method for monitoring the APT activity on natural substrates. With this assay it was shown that (lyso-) phospholipids are hydrolyzed by APTs very slowly, and that APT is not activated by micelles like lipases, the only other class of enzymes that can cleave long-chain fatty acid esters.

7.2 APT's activity on palmitoylated peptides in presence or absence of model membranes

The ESI-MS method above described was also applied for the investigation of APT activity on a palmitoylated peptide. The used nonapeptide represents the N-terminal sequence of hAPT1 and is palmitoylated on the cysteine at position two and is also fluorescein-labeled at a C-terminal lysine for further fluorescence measurements. The ESI-MS analysis (in figure 6.13) displays that both, hAPT1 as well as hAPT2, have a similar catalytic activity on the palmitoylated N-terminal hAPT1 peptide with an estimated k_{cat} of $\sim 27 \text{ s}^{-1}$. This turnover rate is 4-5 orders of magnitude higher compared to the (lyso-)phospholipids. In contrast to the postulated theory that hAPT2 is unable to depalmitoylate hAPT1 (from *in vivo* observations) [33], these results indicate that hAPT2 is indeed capable of depalmitoylating the N-terminus of hAPT1.

The Bastiaens group showed in 2010 that the cytosolic APT depalmitoylates its substrates on all membranes in the cell [14]. But it still remains unclear how APT can get access to the membrane bound substrates. Possible mechanisms are that APT can extract the substrates from the membrane, or that other cofactors are necessary for the membrane extraction. As an example, Ahearn *et al.* showed that FKBP12 can present palmitoylated H-Ras and N-Ras to APT and thus accelerate the hydrolysis rate [58].

To investigate the mechanism of how APT can depalmitoylate a membrane bound substrate, a FRET-based assay with a FITC-labeled palmitoylated N-terminal hAPT1 nonapeptide and rhodamine labeled DOPC vesicles as model membrane was used. It was demonstrated that the peptide can bind to the vesicles and that catalytically active hAPTs can release the peptide from the membrane (figure 6.23) with an apparent k_{cat} value for both human APT isoforms of 0.1 s^{-1} under non-saturating conditions, to allow the measurement of the fast reaction in a plate reader. Thus, both APTs are able to depalmitoylate the vesicle-bound peptide at a similar rate. Compared to the turnover rate in solution ($\sim 27 \text{ s}^{-1}$), the reaction velocity on the membrane bound substrate is much slower. This can be caused either by the non-saturating conditions or by the dissociation of peptide from membrane being the rate-limiting step. The dissociation rate of the peptide from the vesicles was measured as $\sim 0.5 \text{ s}^{-1}$. Typical dissociation rates of mono-palmitoylated peptides are in the range of 0.69-6.9 molecules per second [61]. To investigate if the non-saturating conditions are rate limiting, a fast kinetic measurement of peptide hydrolysis at vesicles with higher enzyme concentration (figure 6.24) was performed, with a resulting k_{cat} of $\sim 0.5 \text{ s}^{-1}$ for both APTs. Thus, the increase of the enzyme concentration did not accelerate the hydrolysis, above the limit of the spontaneous dissociation rate of the peptide, leading to the conclusion that hAPT1 as well as hAPT2 can not actively extract the peptide from the membrane. It seems likely that APT is "waiting" for the peptide outside of the membrane and depalmitoylates it in solution. A scheme of the proposed depalmitoylation process of the membrane bound substrate is shown in figure 7.2. This result would indicate that the hydrolysis of palmitoylated proteins by APT *in vivo* is quite slow. Thus, co-factors such as FKBP12 have to be taken into consideration since they are supposed to accelerate the depalmitoylation to a physiologically relevant speed.

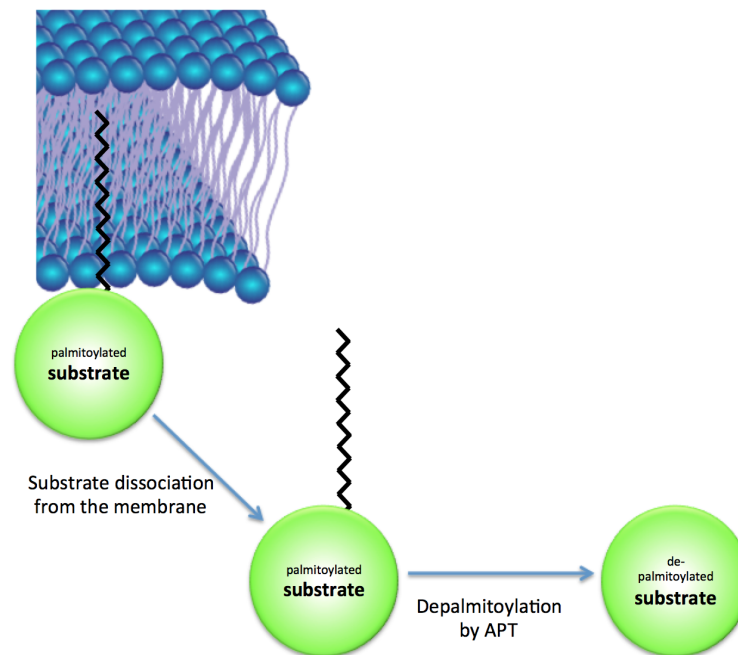


Figure 7.2: Scheme how APT depalmitoylates its membrane bound substrates. The palmitoylated substrate dissociates from the membrane and gets depalmitoylated by APT in the solution/cytosol.

To directly visualize the membrane association of the palmitoylated peptides and their depalmitoylation by APT, the palmitoylated N-terminal hAPT1 peptide was bound to giant unilamellar DOPC vesicles (GUV) (figure 6.35). The setup of the microscopy assay was not straightforward, since GUV are quite flexible, e.g. vesicle fusion takes place and, some vesicles shrink over time. Thus, the quantification of the experiments is challenging, and this assay serves more as a qualitative assay. Nevertheless, this assay proves the membrane localization of the test substrates, and it was directly visible that both hAPT1 and hAPT2 can depalmitoylate a membrane bound peptide that corresponds to the nine N-terminal residues of hAPT1. Furthermore, this assay can reveal potential problems with substrate aggregation, which is also directly observable.

To investigate the APT activity on a longer peptide, a mono-palmitoylated FITC labeled peptide representing the 24 residues of the C-terminus of H-Ras was used in the same FRET and microscopy experiments. Unfortunately the FRET signal was quite weak perhaps due to self-quenching of the FITC when the peptide forms aggregates or micelles. Indeed, aggregates of the peptide were visible in the microscope as bright fluorescent spheres. Another problem might have been the high mobility of the fluorophore: An FP experiment performed by Stefan Baumeister with the same peptide was unsuccessful probably because of the peptide's "propeller effect" [30]. The visualization in the microscope confirms that the H-Ras peptide binds strongly to the vesicle membranes. Fortunately, it could be shown in the FRET assay by monitoring the FITC-fluorescence

intensity changes, that the peptide can indeed bind to the vesicles, and that both hAPT1 and hAPT2 are able to efficiently depalmitoylate the membrane bound peptide. The estimated k_{cat} values are 3-5 times faster than for the hAPT1 nonapeptide (0.37 s^{-1} vs. 0.11 s^{-1} for hAPT1 and 0.6 s^{-1} vs. 0.12 s^{-1} for hAPT2), and again, hAPT2 seems to be slightly more efficient. The difference is more pronounced for the Ras peptide which might be due to the fact that for this longer peptide interactions outside of the binding tunnel are expected, which might influence the affinity and the cleavage efficiency.

After investigation of APT's activity on peptides, the next step was the analysis of APT's activity on a full length palmitoylated protein. A sortase mediated ligation was used successfully to synthesize a full length palmitoylated H-Ras protein. This protein can be used in the future for the ESI-MS measurements as well as for the FRET and microscopy experiments to analyze if the full length protein changes the depalmitoylation mechanism and/ or the efficiency.

Summarizing these results, it was shown that hAPT1 and hAPT2 can depalmitoylate a membrane bound substrate, but they are not actively extracting it from the membrane. hAPT2 seems to be slightly more efficient than hAPT1.

7.3 Investigation of APT's membrane affinity *in vitro* and *in vivo*

In 1998 Duncan and Gilman reported that APT was found to be a cytosolic enzyme in yeast cells [23]. Additionally, Kong *et al.* showed that human APT1/2 are palmitoylated and enriched on the plasma membrane in a canonical acylation cycle, bringing APT closer to their membrane bound substrates and enhancing their activity on the substrates [33]. Additionally, Vartak *et al.* postulated that the cytosolic APT depalmitoylates its substrates on all cell membranes, which is in good agreement with the results discussed in section 7.2, and that a significant fraction of APT is enriched at the Golgi apparatus [34]. In contrast to other lipid-cleaving proteins, APT has a N-terminal lipidation site where it can get reversibly palmitoylated. APT possesses no irreversible lipidation like S-prenylation or N-myristoylation to ensure a permanent membrane localization. The membrane affinity with just one palmitoylation is quite weak and Vartak *et al.* postulated that its life time is too short to survive the secretory pathway to the plasma membrane. Thus they suggested a more local acylation cycle for APT between the cytosol and the Golgi. The auto-depalmitoylation of APT1/2 would create a negative feedback on the APT activity at the Golgi, thus preventing the complete auto-depalmitoylation of APT, ensuring a steady state Golgi localization [34].

In this thesis it was shown by transfection of fluorescently labeled APT constructs into mammalian cells, that hAPT1 is located mainly at the Golgi and not to the plasma membrane. Thus the results by Vartak *et al.* [34] are in accordance with the results of this thesis.

Besides the commonly used transfection techniques, the relatively new electroporation method was used to deliver recombinant APTs into mammalian cells. Providentially, the cells were able to

palmitoylate hAPT1 as well as hAPT2, and those proteins were enriched to the Golgi regions. Another question was if APTs can localize to membranes even without being palmitoylated, since pronounced hydrophobic patches can be found on the surface of both hAPT1 and hAPT2, indicating a membrane affinity of the enzyme. A server for the prediction of the orientation of proteins in membranes ("<http://opm.phar.umich.edu/server.php>") indeed predicted an membrane insertion of APT's core domain. This prediction was not confirmed since it was shown that these hydrophobic patches are insufficient to enrich APT to neutral or negatively charged giant unilamellar vesicles. Instead, a membrane anchor is needed to achieve a membrane localization of APT as could be shown by using His-tagged APT and Ni-NTA-lipid containing vesicles.

Summarizing the activity and the localization studies, APT needs a membrane anchor like its N-terminal palmitoyl modification to localize to membranes. Furthermore, APT does not actively extract its substrates from the membrane, but it is able to depalmitoylate APT- and H-Ras peptides efficiently since their dissociation rates are relatively fast, corresponding to a half-life of the palmitoylated peptides at the membrane of approximately 1 second ($\ln 2/k_{\text{diss}}$). The depalmitoylation activity is expected to be much slower if the natural substrates had a higher membrane affinity, e.g. by a second palmitoyl group like it is present in H-Ras, or by an additional prenyl modification like H-Ras and N-Ras. The dynamical Golgi enrichment of APT ensures a steady state distribution of cytosolic and Golgi-bound APTs.

7.4 *In vivo* effects of APT inhibition

7.4.1 PC12 cell neuronal differentiation assay to investigate the efficiency of new APT inhibitors

The research on APT inhibitors was intensified after Dekker *et al.* showed in 2010 that APT inhibition with palmostatin affects Ras localization and signaling [15]. Also, 2-bromopalmitate was used to inhibit both APT isoforms [30]. Although these inhibitors are able to inhibit APT1 and APT2, they are very unspecific and it was shown that especially the covalent inhibitor Palmostatin has a high number of off-targets [37]. Thus new isoform-specific APT inhibitors were desirable. In 2012, Adibekian *et al.* described two isoform specific piperazine amide-based APT inhibitors, ML348 and ML349 [73]. These inhibitors have been used *in vitro* and *in vivo*, however, the research for more specific ones with higher affinities continues. The European Lead Factory (ELF), a collaborative public-private partnership between the European Screening Centre (ESC), the European Federation of Pharmaceutical Industries and Associations (EFPIA), small and medium-sized enterprises (SMEs) as well as public institutions, shared their facilities to investigate a new hAPT2 inhibitor. They found a potential inhibitor with a K_i of 170 nM out of 500,000 compounds, named ESC1000595. This compound shows less *in vitro* inhibition activity than ML349, when compared in the same assay (OPTS assay), but it can serve as a precursor scaffold that can be modified with

additional functional groups to enhance the APT2 inhibition. This lead compound ESC1000595 was used in *in vitro* studies [30] and was in this work analyzed for its *in vivo* activity in a PC12 cell neuronal differentiation assay. Here, PC12 cells can be stimulated with Neuronal growth factor (NGF), triggering differentiation into neuronal cells, and leading to the growth of long neurites. NGF can stimulate the kinase receptor type 1 (TrkA) which in turn activates the Ras/ERK downstream pathway. With an active APT, Ras is mainly located at the plasma membrane where it can mediate this downstream pathway. If APT is inhibited, it is unable to prevent Ras' mislocalizations on internal membranes, leading to the absence of Ras from the plasma membrane. In contrast to the ML348 and ML349 inhibitors, the new APT2 inhibitor ESC100595 was able to suppress the growth of the neurites. ESC1000595 shows a similar efficiency as the commonly used MEK1/2 inhibitor U0126. From these results it can be concluded that ESC100595 has an effect on APT inhibition in an *in vivo* assay, whereas the old ML349 inhibitor, even when applied together with the hAPT1 inhibitor ML348, has no significant influence on the neuronal differentiation of the cells. This could be due to a lower concentration in the cell, caused by either a lower membrane penetration ability or the poor solubility in the medium, or by a weaker binding to APT2 in the cell, or by a different mechanism of stimulating differentiation. Therefore, it was also investigated whether ESC100595 directly influences the Ras mediated signaling, and does not e.g. influence the PI3K/Akt pathway that also leads to neurite outgrowth, and the neuronal differentiation was induced by expressing of a constitutively active HRasG12V. Also in this case the ESC100595 inhibitor strongly reduced the neurite outgrowth, leading to the conclusion that the new ESC1000595 inhibitor directly influences the H-Ras dependent neurite outgrowth. In the future it should be verified that this effect is indeed due to APT2 inhibition, e.g. by employing APT mutants that are unable to bind the inhibitor and thus could rescue the inhibition effect. The new ESC100595 compound seems to be an interesting APT2 inhibitor as shown in the *in vitro* studies and in the cellular *in vivo* assay. The fact that ESC1000595 is a modifiable precursor and shows such a strong effect on the Ras mediated signaling is quite promising, and further improvement by the addition of functional groups could enhance the APT2 inhibition.

7.4.2 The effect of APT inhibition on the mitotic index

Recently it was reported that interactions of APT1 with the Rho family GTPase CDC42 promote the asymmetric partitioning of β -catenin and Numb, and, additionally, an asymmetric localization of hAPT1 on the plasma membrane during mitosis was shown [47]. Based on this results it was investigated how hAPT1 is located during mitosis in HeLa cells. In comparison to the interphasic Golgi localization (discussed in section 7.3), it was shown in a mitotic gallery (see figure 6.45) that from prometaphase on APT is not located at the Golgi anymore but cytosolically distributed during mitosis. The Golgi disassembles during mitosis, but this process starts only later (in metaphase), compared to the altered APT localization. In the final mitosis phases, i.e. telophase and cytokinesis, APT is clearly enriched at the midbody and partially at the plasma membrane. It could be possible that the localization of palmitoylated proteins at the midbody, like $G_{i\alpha}$ as shown in [93],

triggers APT's recruitment to the midbody. These different localizations during mitosis could indicate that APT might play a role in mitosis.

To get a first insight if APT is essential for a smooth running mitosis, APTs were inhibited with the two specific inhibitors ML348 (APT1 specific) and ML349 (APT2 specific), and the mitotic index was calculated. For this, the cells were synchronized in G2 phase and after a washout the cells were released to mitosis and 25 μ M of both inhibitors were added. Two hours after the mitotic release the mitotic index for the inhibited cells was significantly higher compared to untreated cells. Thus, the APT-inhibited cells stay longer in mitosis and need more time to finish mitosis than the untreated cells.

The different APT localization in mitosis and the longer mitosis time with inhibited APT support the initial conclusion that APT could have a function in mitosis. Further experiments must be carried out to confirm this, for example mitotic interaction partners could be analyzed by pull downs and mass spectrometry.

A Appendix

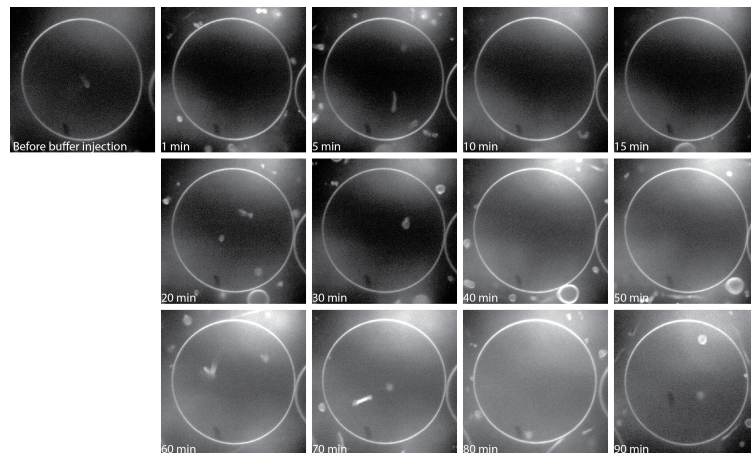


Figure A.1: Bleaching test of DOPC vesicles labeled with rhodamine-phosphoethanolamine-lipids: Time series of rhodamine intensity around the DOPC vesicle of the vesicle where APT2 was added (figure 6.35 b). The intensity in the bleaching experiment stays constant over the measurement time. The measurements were performed in 5 mM Ammoniumcarbonate buffer, pH: 7.4.

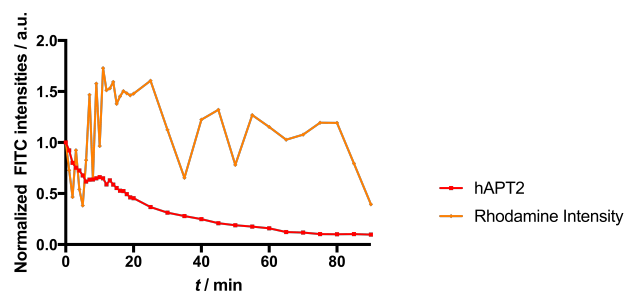


Figure A.2: Integrated and normalized (to the first image) rhodamine intensities of the DOPC vesicles, shown in figure A.1. The calculation is described in section 5.2.3.2. The intensity in this bleaching experiment stays constant over the measurement time.

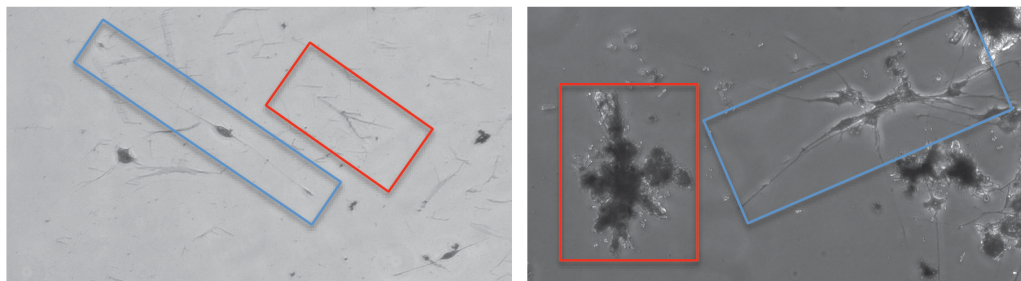


Figure A.3: ML348 (left) and ML349 (right) precipitates in the cell culturing medium. The red boxes show the precipitated inhibitors and the blue boxes are highlighting the differentiated PC12 cells in presence of the inhibitors.

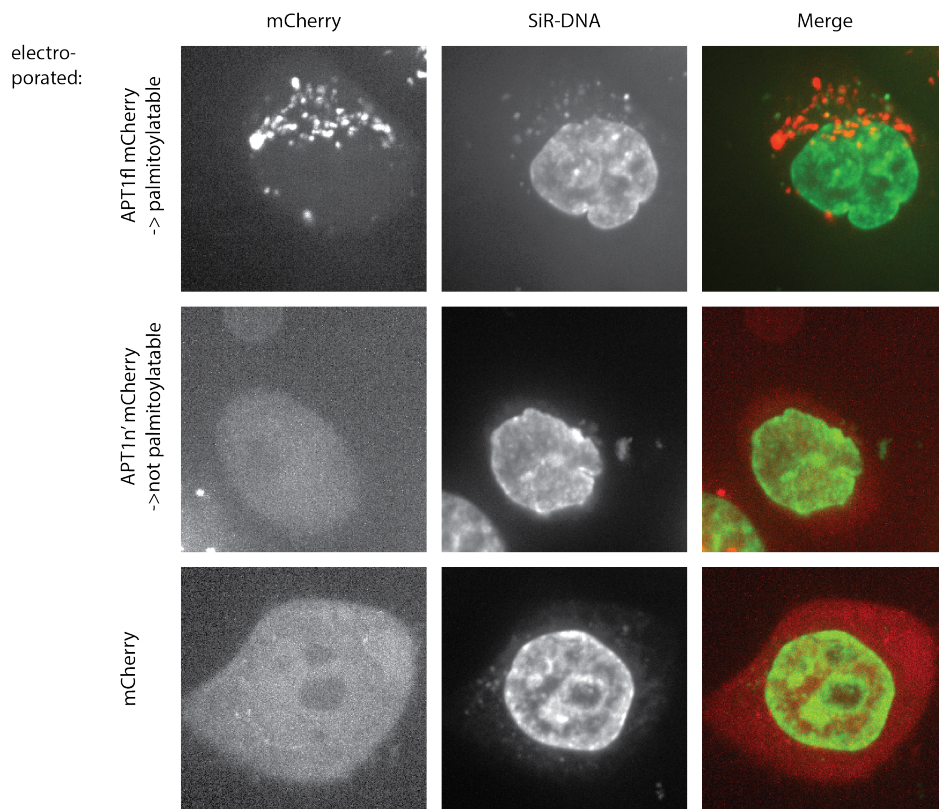


Figure A.4: Electroporation of recombinant APT1mCherry proteins into HeLa cells without a cell compartment marker. Cells were electroporated either with the palmitoylatable full length Apt1mCherry protein (top row), unpalmitoylatable n'versions (N-terminal shortened version of the proteins lacking the first five amino acids) of hAPT1mCherry (middle row) or mCherry (bottom row). SiR-DNA (Spirochrome) was used to stain the nucleus. The results were similar to the one with transiently transfected APTmCitrine (figure 6.44), which was used to show the *in vivo* localization of APT. The full length hAPT1mCherry localizes in dot-like fashion in a perinuclear region, whereas the unpalmitoylatable recombinant hAPT1mCherry protein shows no significant membrane localization and is distributed in the cytosol. The control protein mCherry shows cytoplasmic localization as expected. Thus it is very likely that the electroporated proteins are palmitoylated at their N-terminal cysteine residue which leads either to their aggregation and localization to endosomes, or to a localization at the Golgi.

Table A.1: Crystallographic statistics of the co-crystal structure of 875 μ M hAPT1 Δ M60 S114C C186S C206S with 0.75 mM DTNB. Values for the highest resolution shell are given in parentheses.

Conditions	Qiagen JCSG Core I Suite, well E3	0.2 M Sodium chloride, 0.1 M Na/K phosphate pH6.2 10% PEG 8000
Data collection	Space group	P1
	Wavelength	1.76993 (sulfur wavelength)
	Number of crystals	1
	synchrotron	SLS
	date	16. Feb 2015
	Detector	Pilatus6M
	Mol/AU	2
	a,b, c (Å)	39.9 39.92 68.93
	α, β, γ (°)	85.18 87.09 62.48
	Resolution (Å)	49.26-1.94 (1.99-1.94)*
	R_{sym}	4.9 (11.2)
	$I / \sigma I$	27.6 (13.2)
	CC1/2	92.2 (80.6)
	Completeness (%)	89.7 (70.3)
	Redundancy	6.5 (5.0)
Refinement	Resolution (Å)	35.38-1.94
	No. reflections	23933
	Rwork / Rfree(%)	22.25/26.58
No. atoms	Protein/Ligands	3304
	Water	237
	aver. B (Å ²)	25.60
R.m.s. deviations	Bond lengths (Å)	0.0057
	Bond angles (°)	1.01
Ramachandran	Favored regions (%)	96.79
	outliers	6

Bibliography

- [1] Hong Jiang, Xiaoyu Zhang, Xiao Chen, Pornpun Aramsangtienchai, Zhen Tong, and Hening Lin. Protein lipidation: Occurrence, mechanisms, biological functions, and enabling technologies. *Chemical Reviews*, 118(3):919–988, 2018.
- [2] Alex A Adjei and Manuel Hidalgo. Intracellular signal transduction pathway proteins as targets for cancer therapy. *Journal of Clinical Oncology*, 23(23):5386–5403, 2005.
- [3] Yuko Fukata and Masaki Fukata. Protein palmitoylation in neuronal development and synaptic plasticity. *Nature Reviews Neuroscience*, 11(3):161, 2010.
- [4] Wittinghofer Alfred and Waldmann Herbert. Ras—a molecular switch involved in tumor formation. *Angewandte Chemie International Edition*, 39(23):4192–4214, 2000.
- [5] Johannes L. Bos, Holger Rehmann, and Alfred Wittinghofer. Gefs and gaps: Critical elements in the control of small g proteins. *Cell*, 129(5):865 – 877, 2007.
- [6] Ingrid R. Vetter and Alfred Wittinghofer. The guanine nucleotide-binding switch in three dimensions. *Science*, 294(5545):1299–1304, 2001.
- [7] Krister Wennerberg, Kent L. Rossman, and Channing J. Der. The ras superfamily at a glance. *Journal of Cell Science*, 118(5):843–846, 2005.
- [8] Greg Buhrman, Casey O’Connor, Brandon Zerbe, Bradley M Kearney, Raeanne Napoleon, Elizaveta A Kovrigina, Sandor Vajda, Dima Kozakov, Evgenii L Kovrigin, and Carla Mattos. Analysis of Binding Site Hot Spots on the Surface of Ras GTPase. *Journal of molecular biology*, 413(4):773–789, January 2011.
- [9] John F Hancock. Ras proteins: different signals from different locations. *Nature reviews. Molecular cell biology*, 4:373 –385, 2003.
- [10] Sharon Eisenberg and Yoav I. Henis. Interactions of ras proteins with the plasma membrane and their roles in signaling. *Cellular Signalling*, 20(1):31 – 39, 2008.
- [11] Ian M Ahearn, Kevin Haigis, Dafna Bar-Sagi, and Mark R Philips. Regulating the Regulator: Post-Translational Modification of Ras. *Nature reviews. Molecular cell biology*, 13(1):10.1038/nrm3255, January 2011.
- [12] Luc Brunsveld, Herbert Waldmann, and Daniel Huster. Membrane binding of lipidated ras peptides and proteins — the structural point of view. *Biochimica et Biophysica Acta (BBA) - Biomembranes*, 1788(1):273 – 288, 2009. Lipid Interactions, Domain Formation, and Lateral Structure of Membranes.
- [13] Dekker Frank J., Vartak Nachiket, and Hedberg Christian. *Development of Acyl Protein Thioesterase 1 (APT1) Inhibitor Palmostatin B That Revert Unregulated H/N-Ras Signaling*, chapter 8, pages 123–140. Wiley-Blackwell, 2014.
- [14] Nachiket Vartak and Philippe Bastiaens. Spatial cycles in g-protein crowd control. *The EMBO Journal*, 29(16):2689–2699, 2010.

- [15] Frank J Dekker, Oliver Rocks, Nachiket Vartak, Sascha Menninger, Christian Hedberg, Rengarajan Balamurugan, Stefan Wetzel, Steffen Renner, Marc Gerauer, Beate Schölermann, Marion Rusch, John W Kramer, Daniel Rauh, Geoffrey W Coates, Luc Brunsveld, Philippe I H Bastiaens, and Herbert Waldmann. Small-molecule inhibition of APT1 affects Ras localization and signaling. *Nature Chemical Biology*, 6:449–456, 2010.
- [16] Nagore I. Marín-Ramos, Silvia Ortega-Gutiérrez, and María L. López-Rodríguez. Blocking ras inhibition as an antitumor strategy. *Seminars in Cancer Biology*, 2018.
- [17] Gabriel M Simon and Benjamin F Cravatt. Activity-based Proteomics of Enzyme Superfamilies: Serine Hydrolases as a Case Study. *The Journal of biological chemistry*, 285(15):11051–11055, January 2010.
- [18] Mats Holmquist. Alpha beta-hydrolase fold enzymes structures, functions and mechanisms. *Current Protein and Peptide Science*, 1(2):209–235, 2000.
- [19] Daniel A Bachovchin and Benjamin F Cravatt. The pharmacological landscape and therapeutic potential of serine hydrolases. *Nature Reviews Drug Discovery*, 11:52–68, 2012.
- [20] Y Y Zhang and E A Dennis. Purification and characterization of a lysophospholipase from a macrophage-like cell line p388d1. *Journal of Biological Chemistry*, 263(20):9965–72, 1988.
- [21] Hiroyuki Sugimoto, Shoji Odani, and Satoshi Yamashita. Cloning and expression of cDNA encoding rat liver 60-kDa lysophospholipase containing an asparaginase-like region and ankyrin repeat. *Journal of Biological Chemistry*, 273(20):12536–12542, 1998.
- [22] Gabriele Siegel, Gregor Obernosterer, Roberto Fiore, Martin Oehmen, Silvia Bicker, Mette Christensen, Sharof Khudayberdiev, Philipp F Leuschner, Clara JL Busch, Christina Kane, et al. A functional screen implicates microRNA-138-dependent regulation of the depalmitoylation enzyme apt1 in dendritic spine morphogenesis. *Nature cell biology*, 11(6):705, 2009.
- [23] Joseph A. Duncan and Alfred G. Gilman. A cytoplasmic acyl-protein thioesterase that removes palmitate from G protein α subunits and p21ras. *Journal of Biological Chemistry*, 273(25):15830–15837, 1998.
- [24] Sang Joon Won, Melanie Cheung See Kit, and Brent R. Martin. Protein depalmitoylases. *Critical Reviews in Biochemistry and Molecular Biology*, 53(1):83–98, 2018. PMID: 29239216.
- [25] Takashi Toyoda, Hiroyuki Sugimoto, and Satoshi Yamashita. Sequence, expression in *Escherichia coli*, and characterization of lysophospholipase II. *Biochimica et Biophysica Acta (BBA)-Molecular and Cell Biology of Lipids*, 1437(2):182–193, 1999.
- [26] Joseph D Manna, James A Wepy, Kenneth Hsu, Jae Won Chang, Benjamin F Cravatt, and Lawrence J Marnett. Identification of the major prostaglandin glycerol ester hydrolase in human cancer cells. *Journal of Biological Chemistry*, pages jbc–M114, 2014.
- [27] Joseph A Duncan and Alfred G Gilman. Characterization of *Saccharomyces cerevisiae* acyl-protein thioesterase 1, the enzyme responsible for G protein α subunit deacylation in vivo. *Journal of Biological Chemistry*, 277(35):31740–31752, 2002.
- [28] Deborah C Yeh, Joseph A Duncan, Satoshi Yamashita, and Thomas Michel. Depalmitoylation of endothelial nitric-oxide synthase by acyl-protein thioesterase 1 is potentiated by Ca²⁺-calmodulin. *Journal of Biological Chemistry*, 274(46):33148–33154, 1999.

- [29] Robert Flaumenhaft, Nataliya Rozenvayn, Dian Feng, and Ann M Dvorak. Snap-23 and syntaxin-2 localize to the extracellular surface of the platelet plasma membrane. *Blood*, 110(5):1492–1501, 2007.
- [30] Stefan Baumeister. *Investigation of the properties of Acyl Protein Thioesterases and their role in Ras depalmitoylation*. PhD thesis, Technische Universität Dortmund, 2017.
- [31] Daniel A Bachovchin, Tianyang Ji, Weiwei Li, Gabriel M Simon, Jacqueline L Blankman, Alexander Adibekian, Heather Hoover, Sherry Niessen, and Benjamin F Cravatt. Superfamily-wide portrait of serine hydrolase inhibition achieved by library-versus-library screening. *Proceedings of the National Academy of Sciences*, 107(49):20941–20946, 2010.
- [32] Christian Hedberg, Frank J Dekker, Marion Rusch, Steffen Renner, Stefan Wetzel, Nachiket Vartak, Claas Gerding-Reimers, Robin S Bon, Philippe IH Bastiaens, and Herbert Waldmann. Development of highly potent inhibitors of the ras-targeting human acyl protein thioesterases based on substrate similarity design. *Angewandte Chemie International Edition*, 50(42):9832–9837, 2011.
- [33] Eryan Kong, Shiyong Peng, Goutam Chandra, Chinmoy Sarkar, Zhongjian Zhang, Maria B Bagh, and Anil B Mukherjee. Dynamic palmitoylation links cytosol-membrane shuttling of acyl-protein thioesterase-1 and acyl-protein thioesterase-2 with that of proto-oncogene H-ras product and growth-associated protein-43. *The Journal of biological chemistry*, 288(13):9112–9125, March 2013.
- [34] Nachiket Vartak, Bjoern Papke, Hernan E Grecco, Lisaweta Rossmannek, Herbert Waldmann, Christian Hedberg, and Philippe I H Bastiaens. The autodepalmitoylating activity of APT maintains the spatial organization of palmitoylated membrane proteins. *Biophysical journal*, 106(1):93–105, January 2014.
- [35] Oliver Rocks, Anna Peyker, Martin Kahms, Peter J Vermeer, Carolin Koerner, Maria Lumbierres, Jürgen Kuhlmann, Herbert Waldmann, Alfred Wittinghofer, and Philippe IH Bastiaens. An acylation cycle regulates localization and activity of palmitoylated ras isoforms. *Science*, 307(5716):1746–1752, 2005.
- [36] Patrick Deck, Dirk Pendzialek, Markus Biel, Melanie Wagner, Boriana Popkirova, Björn Ludolph, Goran Kragol, Jürgen Kuhlmann, Athanassios Giannis, and Herbert Waldmann. Development and biological evaluation of acyl protein thioesterase 1 (apt1) inhibitors. *Angewandte Chemie*, 117(31):5055–5060, 2005.
- [37] David Tse Shen Lin and Elizabeth Conibear. Abhd17 proteins are novel protein depalmitoylases that regulate n-ras palmitate turnover and subcellular localization. *Elife*, 4:e11306, 2015.
- [38] Alexander Adibekian, Brent R Martin, Jae Won Chang, Ku-Lung Hsu, Katsunori Tsuboi, Daniel A Bachovchin, Anna E Speers, Steven J Brown, Timothy Spicer, Virneliz Fernandez-Vega, et al. Characterization of a selective, reversible inhibitor of lysophospholipase 2 (lypla2). 2014.
- [39] Alexander Adibekian, Brent R Martin, Jae Won Chang, Ku-Lung Hsu, Katsunori Tsuboi, Daniel A Bachovchin, Anna E Speers, Steven J Brown, Timothy Spicer, Virneliz Fernandez-Vega, et al. Characterization of a selective, reversible inhibitor of lysophospholipase 2 (lypla2). 2014.

- [40] Alexander Adibekian, Brent R Martin, Anna E Speers, Steven J Brown, Timothy Spicer, Virneliz Fernandez-Vega, Jill Ferguson, Benjamin F Cravatt, Peter Hodder, and Hugh Rosen. Optimization and characterization of a triazole urea dual inhibitor for lysophospholipase 1 (lypla1) and lysophospholipase 2 (lypla2). 2013.
- [41] Sang Joon Won, Joseph D Eschweiler, Jaimeen D Majmudar, Fei San Chong, Sin Ye Hwang, Brandon T Ruotolo, and Brent R Martin. Affinity-based selectivity profiling of an in-class selective competitive inhibitor of acyl protein thioesterase 2. *ACS medicinal chemistry letters*, 8(2):215–220, 2016.
- [42] Yancho Devedjiev, Zbigniew Dauter, Sergey R. Kuznetsov, Teresa L.Z. Jones, and Zygmunt S. Derewenda. Crystal structure of the human acyl protein thioesterase i from a single x-ray data set to 1.5 Å. *Structure*, 8(11):1137 – 1146, 2000.
- [43] Sang Joon Won, Dahvid Davda, Kristin J Labby, Sin Ye Hwang, Rachel Pricer, Jaimeen D Majmudar, Kira A Armacost, Laura A Rodriguez, Christina L Rodriguez, Fei San Chong, et al. Molecular mechanism for isoform-selective inhibition of acyl protein thioesterases 1 and 2 (apt1 and apt2). *ACS chemical biology*, 11(12):3374–3382, 2016.
- [44] Aijun Wang, Raymond A. Deems, and Edward A. Dennis. Cloning, expression, and catalytic mechanism of murine lysophospholipase i. *Journal of Biological Chemistry*, 272(19):12723–12729, 1997.
- [45] A Wang and EA Dennis. Mammalian lysophospholipases. *Biochimica et biophysica acta*, 1439(1):1–16, July 1999.
- [46] Marco Bürger. *Development of a Gfp-Based Assay for the Structural Elucidation of Nuclear Pore Proteins and Biochemical and Structural Investigations of Acyl Protein Thioesterases*. PhD thesis, Universität Osnabrück, 2012.
- [47] Ewa Stypulkowski, Irfan A. Asangani, and Eric S. Witze. The depalmitoylase apt1 directs the asymmetric partitioning of notch and wnt signaling during cell division. *Science Signaling*, 11(511), 2018.
- [48] Clare O'Connor. Cell division: Stages of mitosis. *Nature Education*, 1(1):188, 2008.
- [49] Jane B. Reece, Lisa A. Urry, Michael L. Cain, Steven A. Wasserman, Peter V. Minorsky, and Robert B. Jackson. *Campbell Biology (9th Edition)*. Benjamin Cummings, 9 edition, October 2010.
- [50] Katharina Overlack. *Functional analysis of the interactions of the spindle assembly checkpoint proteins BubR1 and Bub1 at the kinetochore*. PhD thesis, Universität Duisburg-Essen, 2016.
- [51] Nihal Altan-Bonnet, Robert D. Phair, Roman S. Polishchuk, Roberto Weigert, and Jennifer Lippincott-Schwartz. A role for arf1 in mitotic golgi disassembly, chromosome segregation, and cytokinesis. *Proceedings of the National Academy of Sciences*, 100(23):13314–13319, 2003.
- [52] Marco Bürger, Tobias J Zimmermann, Yasumitsu Kondoh, Patricia Stege, Nobumoto Watanabe, Hiroyuki Osada, Herbert Waldmann, and Ingrid R Vetter. Crystal structure of the predicted phospholipase LYPLAL1 reveals unexpected functional plasticity despite close relationship to acyl protein thioesterases. *Journal of Lipid Research*, 53(1):43–50, 2012.

- [53] Holger Gerlach, Vanessa Laumann, Sascha Martens, Christian F W Becker, Roger S Goody, and Matthias Geyer. HIV-1 Nef membrane association depends on charge, curvature, composition and sequence. *Nature Chemical Biology*, 6:46–53, 2010.
- [54] William M. Bonner and Konrad Bloch. Purification and properties of fatty acyl thioesterase i from escherichia coli*. *THE JOURNAL OF BIOLOGICAL CHEMISTRY*, 247(10):3123–3133, 1972.
- [55] Fuyuhiko Tamanoi and David Sigman. *The enzymes, Third Edition*. Academic Press, 2000.
- [56] Xue-Xin Fan, Yan-Feng Zhou, Xiang Liu, Lan-Fen Li, and Xiao-Dong Su. Ellman's reagent in promoting crystallization and structure determination of Anabaena CcbP. *Acta Crystallographica Section F*, 68(Pt 11):1409–1414, 2012.
- [57] Yusaku Matsumoto, Shingo Mineta, Kazutaka Murayama, and Daisuke Sugimori. A novel phospholipase b from streptomyces sp. na684, purification, characterization, gene cloning, extracellular production and prediction of the catalytical residues. *The FEBS Journal*, 280(16):3780–3796, 2013.
- [58] Ian M Ahearn, Frederick D Tsai, Helen Court, Mo Zhou, Benjamin C Jennings, Mahiuddin Ahmed, Nicole Fehrenbacher, Maurine E Linder, and Mark R Philips. FKBP12 Binds to Acylated H-Ras and Promotes Depalmitoylation. *Molecular Cell*, 41(2):173–185, jan 2011.
- [59] Konstantin Gavriljuk, Aymelt Itzen, Roger S Goody, Klaus Gerwert, and Carsten Kötting. Membrane extraction of Rab proteins by GDP dissociation inhibitor characterized using attenuated total reflection infrared spectroscopy. *Proceedings of the National Academy of Sciences of the United States of America*, 110(33):13380–13385, jan 2013.
- [60] Norbert Kučerka, John F. Nagle, Jonathan N. Sachs, Scott E. Feller, Jeremy Pencer, Andrew Jackson, and John Katsaras. Lipid bilayer structure determined by the simultaneous analysis of neutron and x-ray scattering data. *Biophysical Journal*, 95(5):2356 – 2367, 2008.
- [61] Simon Sidney and Thomas McIntosh. *Peptide Lipid Interactions*. Academic Press, pages 377-398, 2002.
- [62] Greg T. Hermanson. Chapter 11 - (strept)avidin–biotin systems. In Greg T. Hermanson, editor, *Bioconjugate Techniques (Third Edition)*, pages 465 – 505. Academic Press, Boston, third edition edition, 2013.
- [63] Salvatore A E Marras, Fred Russell Kramer, and Sanjay Tyagi. Efficiencies of fluorescence resonance energy transfer and contact-mediated quenching in oligonucleotide probes. *Nucleic Acids Research*, 30(21):e122–e122, January 2002.
- [64] M Masuko, S Ohuchi, K Sode, H Ohtani, and A Shimadzu. Fluorescence resonance energy transfer from pyrene to perylene labels for nucleic acid hybridization assays under homogeneous solution conditions. *Nucleic Acids Research*, 28(8):E34–E34, January 2000.
- [65] Nelli Erwin. *Biophysikalische Einblicke in die Wechselwirkungen von lipidierten Signalproteinen mit Membranen und Regulatorproteinen*. PhD thesis, Technische Universität Dortmund, 2018.
- [66] Janine Seeliger. *Biophysikalische Einblicke in die Aggregation des Insel-Amyloid-Polypeptids unter Berücksichtigung seiner physiologischen Umgebung*. PhD thesis, Technische Universität Dortmund, 2013.

- [67] Miglena I. Angelova and Dimiter S. Dimitrov. Liposome electroformation. *Faraday Discuss. Chem. Soc.*, 81:303–311, 1986.
- [68] Toshinori Shimanouchi, Hiroshi Umakoshi, and Ryoichi Kuboi. Growth behavior of giant vesicles using the electroformation method: Effect of proteins on swelling and deformation. *Journal of Colloid and Interface Science*, 394:269 – 276, 2013.
- [69] Aimin Yang, Lei Zhao, and Yao-Wen Wu. *Chemical Synthesis and Biological Function of Lipidated Proteins*, pages 137–182. Springer International Publishing, Cham, 2015.
- [70] Sang Joon Won, Dahvid Davda, Kristin J Labby, Sin Ye Hwang, Rachel Pricer, Jaimeen D Majmudar, Kira A Armacost, Laura A Rodriguez, Christina L Rodriguez, Fei San Chong, Kristopher A Torossian, Jasmine Palakurthi, Edward S Hur, Jennifer L Meagher, Charles L Brooks, Jeanne A Stuckey, and Brent R Martin. Molecular mechanism for isoform-selective inhibition of acyl protein thioesterases 1 and 2 (apt1 and apt2). *ACS chemical biology*, 11(12):3374–3382, 2016.
- [71] Alexander Adibekian, Brent R Martin, Jae Won Chang, Ku-Lung Hsu, Katsunori Tsuboi, Daniel A Bachovchin, Anna E Speers, Steven J Brown, Timothy Spicer, Virneliz Fernandez-Vega, Jill Ferguson, Peter S Hodder, Hugh Rosen, and Benjamin F Cravatt. Confirming Target Engagement for Reversible Inhibitors In Vivo by Kinetically Tuned Activity-Based Probes—Supporting Information. *Journal of the American Chemical Society*, 2012.
- [72] *Journal of Chemical Information and Computer Sciences*, 37:615, 1997.
- [73] Alexander Adibekian, Brent R Martin, Jae Won Chang, Ku-Lung Hsu, Katsunori Tsuboi, Daniel A Bachovchin, Anna E Speers, Steven J Brown, Timothy Spicer, Virneliz Fernandez-Vega, Jill Ferguson, Peter S Hodder, Hugh Rosen, and Benjamin F Cravatt. Confirming Target Engagement for Reversible Inhibitors In Vivo by Kinetically Tuned Activity-Based Probes. *Journal of the American Chemical Society*, 2012.
- [74] Dafna Bar-Sagi and James R. Feramisco. Microinjection of the ras oncogene protein into pc12 cells induces morphological differentiation. *Cell*, 42(3):841 – 848, 1985.
- [75] Xinhui Tian, Rongcai Yue, Huawu Zeng, Honglin Li, Lei Shan, Weiwei He, Yunheng Shen, and Weidong Zhang. Distinctive effect on nerve growth factor-induced PC12 cell neurite outgrowth by two unique neolignan enantiomers from *Illicium merrillianum*. *Scientific Reports*, 5:16982, 2015.
- [76] Syntyche Ling-Sing Seow, Murali Naidu, Pamela David, Kah-Hui Wong, and Vikineswary Sabaratnam. Potentiation of neuritogenic activity of medicinal mushrooms in rat pheochromocytoma cells. *BMC Complementary and Alternative Medicine*, 13(1):157, 2013.
- [77] Tamar Barbakadze, Galina Goloshvili, Nana Narmania, Elene Zhuravliova, and David Mikeladze. Subcellular Distribution of S-Nitrosylated H-Ras in Differentiated and Undifferentiated PC12 Cells during Hypoxia. *Cell Journal (Yakhteh)*, 19(3):443–451, 2017.
- [78] Martin Augsten, Rico Pusch, Christoph Biskup, Knut Rennert, Ute Wittig, Katja Beyer, Alfred Blume, Reinhard Wetzker, Karlheinz Friedrich, and Ignacio Rubio. Live-cell imaging of endogenous ras-gtp illustrates predominant ras activation at the plasma membrane. *EMBO reports*, 7(1):46–51, 2006.
- [79] P Sassone-Corsi, C J Der, and I M Verma. ras-induced neuronal differentiation of pc12 cells: possible involvement of fos and jun. *Molecular and Cellular Biology*, 9(8):3174–3183, 1989.

- [80] Frederick D. Tsai, Mathew S. Lopes, Mo Zhou, Helen Court, Odis Ponce, James J. Fiordalisi, Jessica J. Gierut, Adrienne D. Cox, Kevin M. Haigis, and Mark R. Philips. K-ras4a splice variant is widely expressed in cancer and uses a hybrid membrane-targeting motif. *Proceedings of the National Academy of Sciences*, 112(3):779–784, 2015.
- [81] Patrick Deck, Dirk Pendzialek, Markus Biel, Melanie Wagner, Boriana Popkirova, Björn Ludolph, Goran Kragol, Jürgen Kuhlmann, Athanassios Giannis, and Herbert Waldmann. Development and biological evaluation of acyl protein thioesterase 1 (apt1) inhibitors. *Angewandte Chemie International Edition*, 44(31):4975–4980, 2005.
- [82] Igor Vujic, Martina Sanlorenzo, Rosaura Esteve-Puig, Marin Vujic, Andrew Kwong, Aaron Tsumura, Ryan Murphy, Adrian Moy, Christian Posch, Babak Monshi, Klemens Rappersberger, and Susana Ortiz-Urda. Acyl protein thioesterase 1 and 2 (APT-1, APT-2) inhibitors palmostatin B, ML348 and ML349 have different effects on NRAS mutant melanoma cells. *Oncotarget*, 7(6):7297–7306, January 2016.
- [83] Ekaterina M Merzlyak, Joachim Goedhart, Dmitry Shcherbo, Mariya E Bulina, Aleksandr S Shcheglov, Arkady F Fradkov, Anna Gaintzeva, Konstantin A Lukyanov, Sergey Lukyanov, Theodorus W J Gadella, and Dmitriy M Chudakov. Bright monomeric red fluorescent protein with an extended fluorescence lifetime. *Nature Methods*, 4:555–557, 2007.
- [84] Jason M Mackenzie, Malcolm K Jones, and Edwin G Westaway. Markers for trans-Golgi Membranes and the Intermediate Compartment Localize to Induced Membranes with Distinct Replication Functions in Flavivirus-Infected Cells. *Journal of Virology*, 73(11):9555–9567, 1999.
- [85] Joshi Niraj, Marie-Christine Caron, Karine Drapeau, Stéphanie Bérubé, Laure Guitton-Sert, Yan Coulombe, Anthony M Couturier, and Jean-Yves Masson. The identification of FANCD2 DNA binding domains reveals nuclear localization sequences. *Nucleic Acids Research*, 45(14):8341–8357, 2017.
- [86] ThermoFisher Scientific. Electroporation. <https://www.thermofisher.com/de/de/home/references/gibco-cell-culture-basics/transfection-basics/transfection-methods/electroporation.html>, June 2018.
- [87] Francois-Xavier Theillet, Andres Binolfi, Beata Bekei, Andrea Martorana, Honor May Rose, Marchel Stuver, Silvia Verzini, Dorothea Lorenz, Marleen van Rossum, Daniella Goldfarb, and Philipp Selenko. Structural disorder of monomeric α -synuclein persists in mammalian cells. *Nature*, 530, 2016.
- [88] Dean Clift, Chun So, William A McEwan, Leo C James, and Melina Schuh. Acute and rapid degradation of endogenous proteins by Trim-Away. *Nature Protocols*, 13(10):2149–2175, 2018.
- [89] Mina Wu and Fan Yuan. Membrane binding of plasmid dna and endocytic pathways are involved in electrotransfection of mammalian cells. *PLOS ONE*, 6(6):1–9, 06 2011.
- [90] Ryan L Sontag, Cosmin Mihai, Galya Orr, Alexei Savchenko, Tatiana Skarina, Hong Cui, John R Cort, Joshua N Adkins, and Roslyn N Brown. Electroporation of Functional Bacterial Effectors into Mammalian Cells. *Journal of visualized experiments : JoVE*, (95):52296, January 2015.
- [91] NIH National Cancer Institute. Nci dictionary of cancer terms, mitotic index. <https://www.cancer.gov/publications/dictionaries/cancer-terms/def/mitotic-index>, August 2018.

-
- [92] Lyubomir T Vassilev. Cell cycle synchronization at the g2/m phase border by reversible inhibition of cdk1. *Cell Cycle*, 5(22):2555–2556, 2006. PMID: 17172841.
- [93] Hyeseon Cho and John H. Kehrl. Localization of $g_i\alpha$ proteins in the centrosomes and at the midbody: implication for their role in cell division. *The Journal of Cell Biology*, 178(2):245–255, 2007.

Acknowledgments

First of all I kindly want to thank my thesis advisor Dr. Ingrid Vetter for the possibility to work on this project, the excellent scientific support, discussion and inspiration as well as her continuous guidance within the last years. I would also like to thank Prof. Dr Stefan Raunser for the acceptance to take the responsibility and the time to be the first reviewer of my thesis. And I gratefully thank Prof. Dr Andrea Musacchio for the fruitful discussions in the group meetings, as well as being my second supervisor.

My sincere thanks go to our amazing technician Patricia Stege. Not only for providing us excellent pure purified proteins, but also for the laboratory and non-laboratory support during the years of my PhD project. Furthermore I want to thank my former group members Dr. Arthur Porfetye and Dr. Stefan Baumeister, first of all for the recruitment to the MPI, and the collaborations, discussions and the general help.

A great thank goes to Nelli Erwin for the introduction to the world of model membranes as well as the nice company at the national and international conferences.

A special thank goes to Jens Warmers, Michael Winzker and Martina Wischnewski for their help with the Mass-Spectrometry instruments. Additionally I would like to thank, Elena Reckzeh, Philipp Cromm and Sascha Gentz for the chemical support. I furthermore would like to thank George Holtermann and Matthias Müller for the help with the Stopped-Flow machine and other instruments.

And I thank Stefano Maffini and Divya Singh for the support with the microscope experiments.

A grateful thank goes to the whole Department I, especially Kerstin Killinger, Claudia Breit, Katharina Overlack, Anika Altenfeld, Charlotte Smith, and my lab colleagues Sara Carmignani, Marta Mattuzzio, Julia Wernicke, Alexandra Friese, Satya Pentakota, Valentina Piano, Arsen Petrovic, Jenny Keller and Giuseppe Ciossani. I especially would like to thank Carolin Koerner for the funny and amazing support during my PhD time.

I also would like to thank the PhDNet crew at the MPI Dortmund, to get involved in PhDNet, thanks to the amazing team Lea Kraemer, Michael Winzker, Philine Hagel, Annina Burhop, Birte Siebolds, Elisabeth Hennes, Pascal Lill and Tabea Schneidewind.

A great thank goes to my amazing friends which I was allowed to get to know during my studies, especially Kathrin Louven, Philine Hagel, Franziska Leidreiter, Mirja Mewes, Bernhard Feldhues,

Niklas Schaumann, Johannes Rath, Hanne Petersen, Pedro Braun-Streb and Ramona Buente.

I would also like to thank Frank Wennmohs, Sarah Lehnhausen, Raphael Gasper-Schönenbrücher and Charlotte Smith for corrections and suggestions for this thesis.

I want to thank the mensa crew, for the nice lunches at the mensa, thanks to Julia Wernicke, Arthur Porfetye, Kerstin Killinger, Claudia Breit, Raphael Gasper-Schönenbrücher and David Bier.

Furthermore, I greatly thank the "my little ponys", Kai Walstein, Franziska Müller and especially Annika Take for the funny time in and outside the laboratory.

Finally, I want to thank Holger Ostholt for the lovely support in the last month. And in the end I greatly thank my whole family. Especially my parents Ralf and Gisela as well as my sisters, Friederike and Pauline for being there for me and supporting me the whole time. Thank you!!!

Eidesstattliche Versicherung (Affidavit)

Estel, Kathrin
Name, Vorname
(Surname, first name)

137498
Matrikel-Nr.
(Enrolment number)

Belehrung:

Wer vorsätzlich gegen eine die Täuschung über Prüfungsleistungen betreffende Regelung einer Hochschulprüfungsordnung verstößt, handelt ordnungswidrig. Die Ordnungswidrigkeit kann mit einer Geldbuße von bis zu 50.000,00 € geahndet werden. Zuständige Verwaltungsbehörde für die Verfolgung und Ahndung von Ordnungswidrigkeiten ist der Kanzler/die Kanzlerin der Technischen Universität Dortmund. Im Falle eines mehrfachen oder sonstigen schwerwiegenden Täuschungsversuches kann der Prüfling zudem exmatrikuliert werden, § 63 Abs. 5 Hochschulgesetz NRW.

Die Abgabe einer falschen Versicherung an Eides statt ist strafbar.

Wer vorsätzlich eine falsche Versicherung an Eides statt abgibt, kann mit einer Freiheitsstrafe bis zu drei Jahren oder mit Geldstrafe bestraft werden, § 156 StGB. Die fahrlässige Abgabe einer falschen Versicherung an Eides statt kann mit einer Freiheitsstrafe bis zu einem Jahr oder Geldstrafe bestraft werden, § 161 StGB.

Die oben stehende Belehrung habe ich zur Kenntnis genommen:

Official notification:

Any person who intentionally breaches any regulation of university examination regulations relating to deception in examination performance is acting improperly. This offence can be punished with a fine of up to EUR 50,000.00. The competent administrative authority for the pursuit and prosecution of offences of this type is the chancellor of the TU Dortmund University. In the case of multiple or other serious attempts at deception, the candidate can also be unenrolled, Section 63, paragraph 5 of the Universities Act of North Rhine-Westphalia.

The submission of a false affidavit is punishable.

Any person who intentionally submits a false affidavit can be punished with a prison sentence of up to three years or a fine, Section 156 of the Criminal Code. The negligent submission of a false affidavit can be punished with a prison sentence of up to one year or a fine, Section 161 of the Criminal Code.

I have taken note of the above official notification.

Dortmund,
Ort, Datum
(Place, date)

Unterschrift
(Signature)

Titel der Dissertation:
(Title of the thesis):

Investigation of Acyl ProteinThioesterase activity at the membrane

Ich versichere hiermit an Eides statt, dass ich die vorliegende Dissertation mit dem Titel selbstständig und ohne unzulässige fremde Hilfe angefertigt habe. Ich habe keine anderen als die angegebenen Quellen und Hilfsmittel benutzt sowie wörtliche und sinngemäße Zitate kenntlich gemacht.

Die Arbeit hat in gegenwärtiger oder in einer anderen Fassung weder der TU Dortmund noch einer anderen Hochschule im Zusammenhang mit einer staatlichen oder akademischen Prüfung vorgelegen.

I hereby swear that I have completed the present dissertation independently and without inadmissible external support. I have not used any sources or tools other than those indicated and have identified literal and analogous quotations.

The thesis in its current version or another version has not been presented to the TU Dortmund University or another university in connection with a state or academic examination.*

***Please be aware that solely the German version of the affidavit ("Eidesstattliche Versicherung") for the PhD thesis is the official and legally binding version.**

Dortmund,
Ort, Datum
(Place, date)

Unterschrift
(Signature)